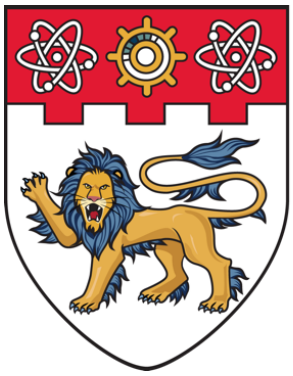

NANYANG TECHNOLOGICAL UNIVERSITY
SINGAPORE

Study of Lanthanides nanocrystals as heterogeneous catalyst

LEE MING DA

School of Chemistry, Chemical Engineering and Biotechnology

2022

Study of Lanthanides nanocrystals as heterogeneous catalyst

LEE MING DA

School of Chemistry, Chemical Engineering and Biotechnology

A thesis submitted to the Nanyang Technological University in partial fulfilment of the requirement for the degree of Master of Science

2022

Statement of Originality

I hereby certify that the work embodied in this thesis is the result of original research done by me except where otherwise stated in this thesis. The thesis work has not been submitted for a degree or professional qualification to any other university or institution. I declare that this thesis is written by myself and is free of plagiarism and of sufficient grammatical clarity to be examined. I confirm that the investigations were conducted in accord with the ethics policies and integrity standards of Nanyang Technological University and that the research data are presented honestly and without prejudice.

11/08/2022
. . . . . .
Date

. . . . . .
Lee Ming Da

*please sign on the water mark area.

Supervisor Declaration Statement

I have reviewed the content and presentation style of this thesis and declare it of sufficient grammatical clarity to be examined. To the best of my knowledge, the thesis is free of plagiarism and the research and writing are those of the candidate's except as acknowledged in the Author Attribution Statement. I confirm that the investigations were conducted in accord with the ethics policies and integrity standards of Nanyang Technological University and that the research data are presented honestly and without prejudice.

11/08/2022

. . . . . .

Date

. . . . . .

Edwin Yeow

*please sign on the water mark area.

Authorship Attribution Statement

Please select one of the following; *delete as appropriate:

(A) This thesis **does not** contain any materials from papers published in peer-reviewed journals or from papers accepted at conferences in which I am listed as an author.

11/08/2022
. . . . . .
Date

. . . . . .
Lee Ming Da

*please sign on the water mark area.

Abstract

This thesis focuses on utilizing lanthanide based nanocrystals for various form of catalysis and evaluating their effectiveness. We have characterized the nanocrystals in this studies in detailed. The nanocrystals synthesized were used in various reactions to show versatility.

Chapter 2 analyses the effectiveness of lanthanide based nanoparticles as a Lewis acid catalyst. YbF_3 nanoparticles in this study were synthesized through the co-precipitation method and characterized using transmission electron microscope (TEM), and x-ray diffraction (XRD). The light to heat efficiency of the crystals were determined. The nanoparticles were used as a photothermal Lewis acid catalyst for the reaction between epoxides and amines obtaining excellent yield. The catalyst showed great results even after being recycling.

In chapter 3, we attempted to utilize chiral ligands with YbF_3 nanocrystals to achieve enantioselectivity which was unsuccessful. We changed our approach into modifying YbF_3 nanocrystals into a chiral catalyst. Which was unsuccessful due to the lack of a chiral environment on the surface of the particle. Which was identified using Spectroscopy methods like Uv-Vis absorption spectroscopy and florescence emission spectroscopy

Acknowledgements

I would like to thank professor Edwin Yeow or accepting me as his student and providing me guidance since my final year as an undergraduate student till my final semester as a post graduate student. I would like to thank him for his patience and kindness towards me during this journey and for all the important lessons that he has imparted to me.

I would like to thank Dr Wu Xiang Yang, Dr Du Qun Chao, Yizhen and Matthew for their help in lab and providing me with fun and laughter during the times in lab.

Finally, I will like to thank my friends and family for their support in during this journey and Edmund for his help.

Table of Contents

Chapter 1: General Introduction

Catalysts plays an important role in chemistry as they are able to increase the rate of a reaction without being consumed during the reaction itself. This allows reactions to be carried out under milder conditions and concurrently activate less reactive precursors in a reaction, thus, improving reaction rates. As only a small amount of catalyst is needed to catalyze a reaction, catalysts are highly efficient and low cost means of improving reaction rates. However, traditional homogenous catalysts are usually neither cost efficient nor sustainable over time due to the need for purification to remove the catalyst. Such purification methods may entail irreversible conversion or decomposition resulting in disposal of the catalyst. This lack of recyclability results in homogenous catalysts often being single-use, leading to increased costs and waste. This creates an urgent need to develop other forms of catalysis that are more environmentally friendly and cost efficient.[1, 2]

Heterogonous catalysts have been of interest in recent times to the pharmaceutical industry as they possess the ability to lower production cost for many chemical compounds due to their unique properties. In particular, heterogeneous catalysts are recyclable, easily separated from the product and are able to do solvent-less reactions.[3] These properties result in heterogeneous catalysts being environmentally friendly. Heterogeneous catalyst can be recovered in many ways such as centrifugation or filtration.

More recently, research has indicated that linking to catalyst to a magnetic adduct enabled the use of an external magnet for recovery of the catalyst. Solvent-less reactions offer many benefits such as lowering cost, reducing toxicity and lessening the harmful impacts on the environment. Some side products are also known to dissolve well in common solvents making it difficult to separate the side products from the desired product after the reaction. In solvent-less reactions, solvent extraction and purification steps can often be skipped or are otherwise greatly simplified, resulting in lower overall costs. Furthermore, many solvents such

as benzene and xylene are toxic to the body causing skin irritation and/or eye irritation. Carcinogenic solvents such as benzene can also result in the development of cancers after prolonged exposure. The elimination of such solvents can improve workplace safety in the chemical industry.

1.1 Lewis acid catalysis

Lewis acid catalyzed reactions are a very unique branch of organic synthesis, as they are able to carry out reactions under milder conditions while offering interesting results. Lewis acid catalysts involve having a metal center acting as an electron acceptor and coordinating to the compound as shown in figure 1. This increases the electron deficiency on the carbon atom and its susceptibility to a nucleophilic attack. A simple example is shown below in figure 1 where benzaldehyde is coordinated by a Lewis acid on the oxygen atom making the carbonyl carbon atom more susceptible to a nucleophilic attack. Thereby, increasing the rate of reaction.

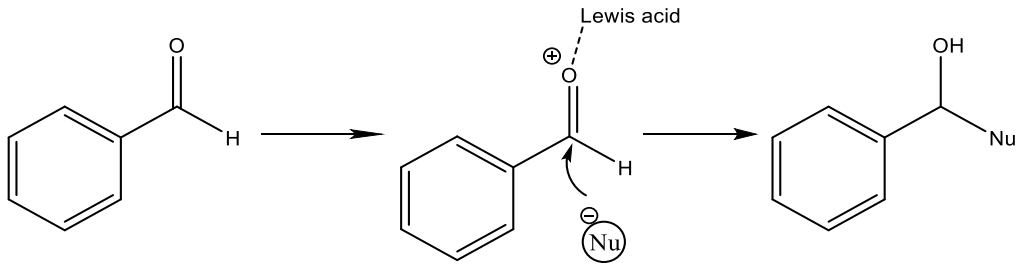

Figure 1: Basic mechanism of a Lewis acid catalysis

1.1.1 Traditional Lewis acid catalysis

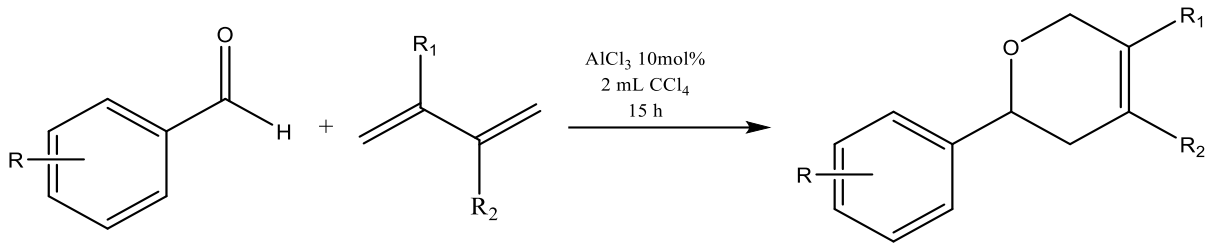

Figure 2: Reaction scheme of a oxa-diels alder reaction between aromatic aldehydes and simple diene

Traditional Lewis acid catalysts such as aluminum chloride ($AlCl_3$), boron trifluoride (BF_3) and titanium chloride ($TiCl_4$) have been used to catalyze many reactions. A study by Daliang Li and co-workers used $AlCl_3$ to catalyst an oxa-Diels alder reaction between aromatic aldehydes like benzaldehydes and simple unactivated dienes as shown in figure 2.[4] In their study, several catalysts such as $RuCl_3.3H_2O$, $NiCl_2.6H_2O$ and $AlCl_3$ were also screened and they found that $AlCl_3$ is most suitable in catalyzing the reaction. . In addition, the researchers also investigated the suitability of several solvents. They compared xylene, benzene, CCl_4 and toluene and found that CCl_4 was the most suitable solvent as it produced the best yield among all the other solvents. This study also screened through many substrates with various functional groups like methoxy, halogens and methyl groups on both the aromatic aldehydes and the diene. They demonstrated that using $AlCl_3$ to catalyze this oxa-diel alder reaction produces reasonable yield under mild conditions while providing good tolerance towards various functional groups. However, $AlCl_3$, like other traditional homogenous catalysts are not cost efficient as they cannot be recovered after the reaction. Therefore, there is a need to develop a heterogeneous Lewis acid catalyst.[4]

1.1.2 Using Lanthanide triflates as a Lewis acid catalyst

Heterogeneous Lewis acid catalysts such as lanthanide salts or triflates have proven to be easily recoverable and reusable without significant loss in their catalytic ability. They are also stable in water making them good candidates for green reactions.[5] Lanthanides have also been shown to be a very effective Lewis acid catalyst due to their high charge of +3.[6] Unlike, traditional Lewis acids such as aluminum and titanium chlorides which are extremely moisture sensitive and cannot be recycled, lanthanide salts and triflates are water stable and are easily recyclable replacements for traditional Lewis acid catalysts.

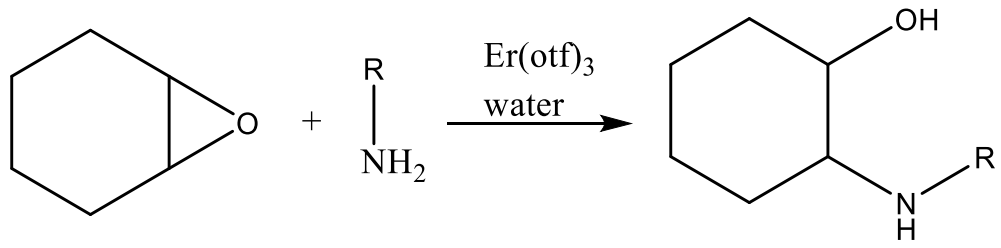

Figure 3: Epoxide ring opening using erbium triflate

An example of utilizing lanthanide salts as heterogeneous catalyst was demonstrated in a study by Antonio Procopio and co-workers.[7] They showed that erbium triflate $Er(otF)_3$ is highly efficient in catalyzing epoxide ring opening reactions by amine in water under mild conditions as shown in figure 3.[7]

Epoxide ring opening by amines yields β-amino alcohols which are used in many industries such as the pharmaceutical, agriculture and cosmetics industries .[8, 9] They play an increasingly critical role in these industries as intermediates to further synthesize compounds of interest.[8, 9] β-amino alcohols are also very important precursors to more complicated and interesting cyclic compounds. Many existing methods of synthesizing β-amino alcohols from epoxides require anhydrous conditions, high catalyst loading or long reaction time. Therefore, a greener and more efficient method is needed to synthesize these β-amino alcohols.

Antonio Procopio and co-workers studied how various epoxides such as cyclohexene oxide, styrene oxide and 2,3-diphenyloxirane react with both aliphatic and aromatic amines.[7] Their study showed that erbium triflate is a powerful catalyst, requiring only 5 mol% to catalyst the reaction. The study used epoxides and amines of various functional groups and demonstrate the versatility of erbium triflate and its tolerance towards many different functional groups in a reaction. Antonio Procopio and co-workers have also recycled the erbium triflate and consistently managed to achieve good yield despite recycling the catalyst up to three times, demonstrating that this catalyst was able to retain its catalytic ability. This shows that lanthanide salts or triflates can help to reduce costs in the pharmaceutical and manufacturing industries in comparision to using traditional Lewis acid catalyst as the traditional catalyst are unable to be recovered after reactions.[7]

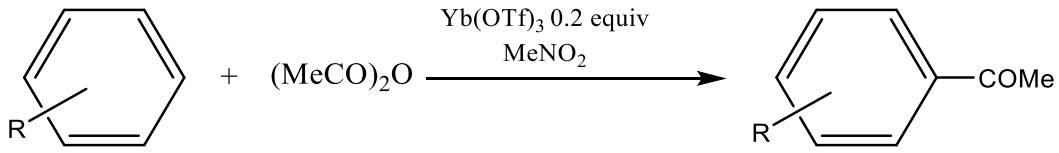

Figure 4: $Yb(OTf)_3$ catalyzed Friedel-Crafts acylation

A study done by Shu Kobayashi and co-workers also explored the use of lanthanide salts as a heterogeneous.[10] They demonstrated the use of ytterbium triflate to catalyze the Fridel-crafts acylation reaction of anisole shown in figure 4. Conventionally, $AlCl_3$ is used as the catalyst for this reaction. However, large amounts of $AlCl_3$ will be required and subsequently destroyed by the aqueous workup after the reaction. Therefore, $Yb(OTf)_3$ was seen as a viable alternative to counter these problems. Firstly, compared to $AlCl_3$, only catalytic amounts of $Yb(OTf)_3$ was needed to catalyze the reaction compared to the stoichiometric amount needed when $AlCl_3$ was used. Secondly, in the study, $Yb(OTf)_3$ was recycled twice and still achieved similar yield. This shows that $Yb(OTf)_3$ can be recycled with no loss to its catalytic ability, making it more sustainable and cost effective than $AlCl_3$. These two properties

reinforces the use of $Yb(OTf)_3$ as a green and cost effective catalyst. However, the substrate scope done in the study was not very extensive. Hence, more effort could be put into this area to expand the library of substrates with various functional groups and explore the functional group tolerance of the catalsyt.[10]

1.1.3 Using photothermal lanthanide based nanoparticles as a Lewis acid catalyst

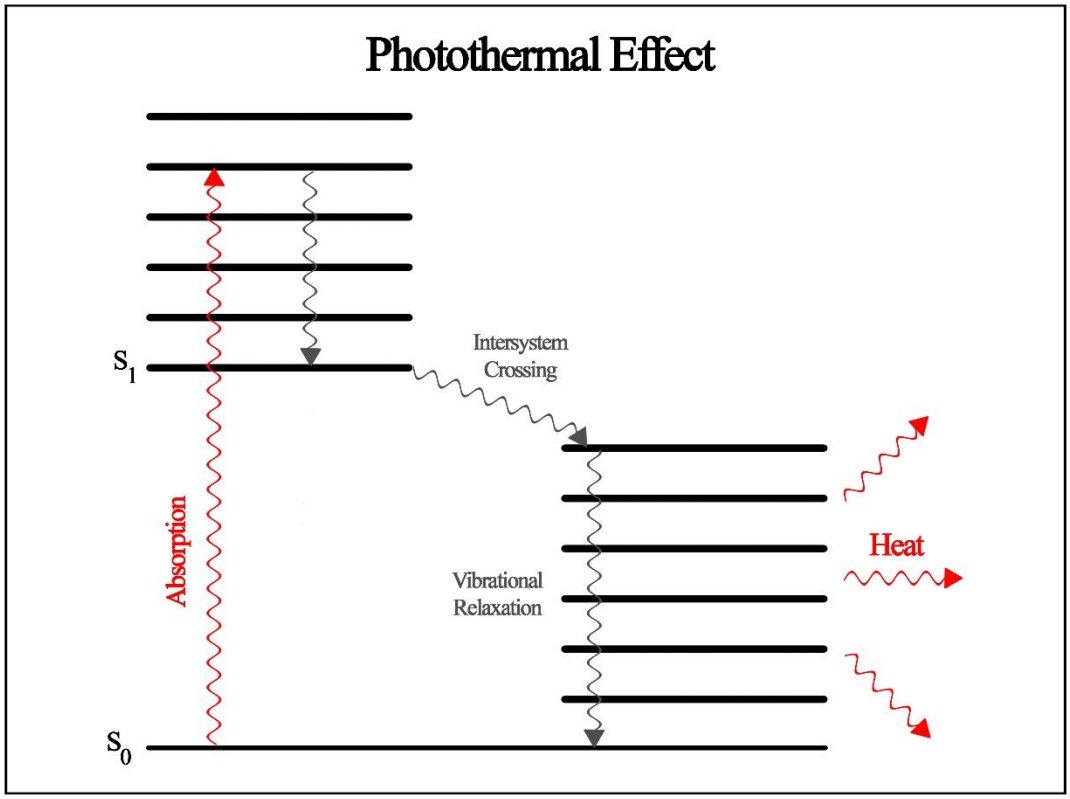

Figure 5: Energy diagram

Lanthanides can be made into nanoparticles that have upconversion and photothermal effects. Upconversion is the phenomenon in which nanoparticles emit light of higher energy compared to the light that was used to excite them. This allows the utilization of near infrared (NIR) light of 808 nm or 980 nm to generate light of higher energy in the UV-visible region. This effect is useful for bio imaging, bio labelling and biosensing.[11] Photothermal effect occurs when the excited lanthanide ions relax via non-radiative pathways when excited by NIR light, which produces heat as seen in figure 5. This is different from the usual relaxation pathway

where there could be both radiative and non-radiative path ways. The lack of radiative pathways will increase the amount of heat being produced. Lanthanide's strong light to heat conversion allows them to be used as a nano thermometer or bifunctional catalyst.[12, 13]

A study by Zhao and co-workers, investigated the mechanism for the photothermal effects of Yb^{3+} ions. Due to the high concentration of Yb^{3+} ions in the nanoparticles, Yb^{3+} ions would be in closer proximity, resulting in a higher probability of cross relaxation between the ions. Subsequently, there would be energy migration to defects and/or surface quenchers which then relaxes through non radiative pathways resulting in heat generated. This relaxation pathway causes the observed photothermal effect.[14]

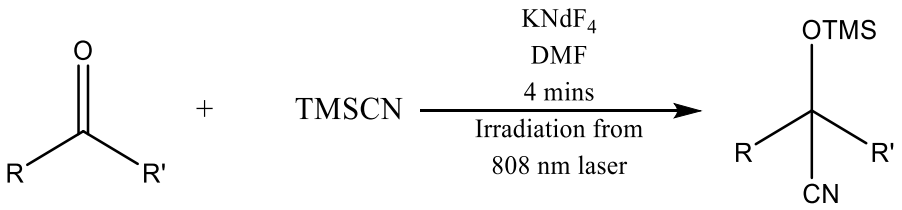

Figure 6:Cyanosilylation reaction of ketones

Our group has recently utilized a nanoscale bifunctional catalyst that makes use of the Lewis acid capability of lanthanides as well as the photothermal effect of the lanthanide nanoparticle.[13] The experiment used $KNdF_4$ and $NaNdF_4$ nanoparticles with an 808 nm laser to catalyze the cyanosilylation reaction between ketones and trimethylsilyl cyanide (TMSCN) and achieved good yields under mild conditions. Reactions between aldehydes and TMSCN are known to be reasonably fast as aldehydes are typically very reactive. Ketones on the other hand, suffer from poorer reactivity compared to aldehydes. Therefore, the photothermal effect from the lanthanide nanoparticles provides heat to drive the reaction forward and increase the rate of reaction. This can be seen from our group's study where complete conversion was achieved exceptionally fast in four minutes. The attempts at recovering the nanoparticles were also very successful, as the $KNdF_4$ nanocrystals were used for 5 reaction cycles under identical

conditions and in each cycle, excellent yield was obtained. This shows that photothermal bifunctional catalysts made from lanthanides are able to activate less reactive substrates and drive harder reactions with the heat arising from the photothermal effect while irradiated with a NIR laser.[13]

The photothermal effect from the nanoparticle is vital for the reaction mentioned above as it drastically increases the rate of reaction. Therefore, allowing the reaction to be completed in only four minutes. This is supported by a study done by Benjamin J. Lear's and co-workers, where they showed that the photothermal effect on the surface of a nanoparticle is beneficial in increasing the rate of reaction.[15] In the study they were investigating the polymerisation of polyurethane films from hexamethylene diisocyanate and diester polyol poly-bis(triethylol) heptanedioate using photothermal effect. In the study, they irradiated gold nanoparticles of 2 nm with a 532 nm pulse laser. The surface plasmon resonance of the gold particles would induce a photothermal effect on the surface of the nanoparticles which would drive the reaction forward. Comparing the rate of reaction using traditional catalyst and the rate of reaction using the photothermal effect from gold nanoparticles, the authors found no significant differences. By comparing, the catalytic ability in terms of per molecule of catalyst vs per nanoparticle, it was found that the gold nanoparticles are 90 times more efficient than the catalyst. Another point to note was that the laser used in the study was a pulse laser and it is understood that the rate of reaction is increased only when the gold nanoparticles are heated due to the irradiation of the laser. Therefore, taking into account of the irradiation time of 2 μs, it was found that the rate of reaction increased by a billion fold. From the study, it is confirmed that by introducing photothermal effect on the surface of nanoparticles the rate of reaction could be increased by many orders of magnitude compared to conventionally used catalyst.[15]

1.2 Chirality and asymmetric reactions

Chirality refers to the 3-dimensional symmetry of a compound. A compound is chiral when it is unable to be super imposed with its mirror reflection by any form of rotations that it goes through. This is observed when two compounds who are mirror images of each other with identical molecular structure but they are unable to be super imposed on each other regardless of any rotation that they go through. Figure 7 provides an example of chirality whereby the molecule on the left is not able to be superimposed on the molecule on the right no matter how many rotations it goes through. These two compounds are known as enantiomers of one another. Enantiomers are known to have similar chemical and physical properties, as well as very similar NMR and IR spectra making it hard to separate and isolate a single desired enantiomer. Therefore, special methods have to be employed to separate the enantiomers. One method is to convert them into diastereomers and make use of their different boiling points to conduct simple distillation to separate them. Another method is to utilize a high performance liquid chromatography instrument (HPLC) equipped with a chiral column that consists of chiral auxiliaries in the stationary phase.[16]

Enantiomers differ in their optical properties. Specifically, the direction that they rotate plane polarized light. Enantiomers will rotate plane polarized light in different directions. For example, the alanine on the left in figure 7 will rotate plan polarized light to the right so it is labelled as dextrorotatory, denoted with a (+). The alanine on the right will rotate plan polarized light to the left and it is labelled as levorotatory denoted with a (-). Through this property, it is possible to identify which enantiomer is the major product after a reaction but it is unable to determine the percentage of the two enantiomers present individually.[16]

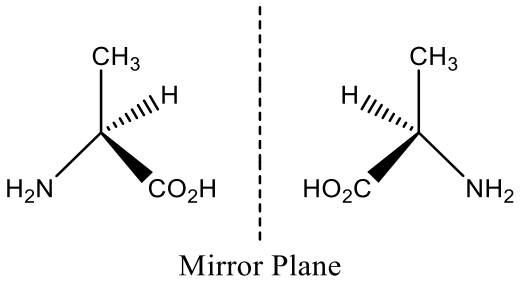

Figure 7: Mirror images of alanine

Chirality is a very important factor in the pharmaceutical industry. Despite identical chemical formula and structure, different enantiomers can have very different effects when consumed and digested in the human body. An example would be the drug thalidomide shown in figure 8 that was sold in the 1950s. Thalidomide was sold as a sedative but was found to be beneficial as a cure for morning sickness among pregnant women. This led to the adoption of thalidomide as a cure for morning sickness in Europe. However, the babies born from these women who had consumed thalidomide suffered from deformities and nerve damage. It was found that because thalidomide was sold as a racemic mixture the presence of (-)-thalidomide enantiomer in the drug caused the deformities in the babies while the (+)-thalidomide did not have such side effects. Since then, it has been necessary to produce drugs that are enantiomerically pure to reduce the possibility of negative side effects that may arise from racemic products. Additionally, it was also more cost effective to synthesis only the active enantiomer, reducing waste and reducing the amount of precursors and catalyst needed to synthesize the compound. Furthermore, it would be safer to produce enantiomerically pure drugs as inactive enantiomer could not be safely absorbed by the body, and may accumulate in the body over time. This may lead to harmful consequences or damage to the body. Therefore, it is preferred to synthesize only the desired enantiomer compound.[16, 17]

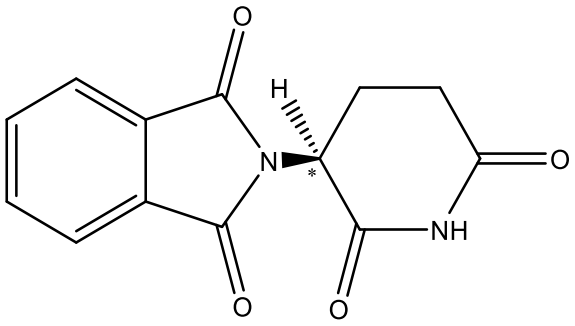

Figure 8: Structure of Thalidomide

1.2.1 Examples of using Lanthanide salts in asymmetric reactions

Since racemic mixtures are undesirable in pharmaceutical industries, methods to synthesize enantiomerically pure compounds through asymmetric synthesis are of critical importance. Lanthanides have previously been demonstrated to be able to catalyze such asymmetric reactions to produce enantiomerically pure compounds. In the work done by Peter M. Smith, the asymmetric addition reaction of TMSCN to benzaldehyde shown in figure 9 using lanthanide chlorides as the catalyst and pybox as the chiral ligand to provide enantioselectivity was demonstrated.[18] In that study the authors screened multiple solvents and found acetonitrile to be the most suitable solvent for the reaction as it yielded the greatest enantiomeric excess for the reaction. They subsequently screened through a variety of lanthanide chlorides like yttrium chloride, ytterbium chloride ($YbCl_3$) and lanthanum chloride and found that $YbCl_3$ gave the greatest enantiomeric excess when used as the catalyst in the asymmetric reaction. Additionally, they found that the enantioselectivity of the reaction was dependent on the ionic radius of the lanthanide ions. Yb^{3+} has the smallest ionic radius and the best enantioselectivity while La^{3+} has the largest ionic radius of the lanthanides that were screened and was found to favor the formation of the other enantiomer that was different from Yb^{3+} ions. Subsequently, comparisons between the isopropyl and phenyl substituted pybox shown in figure 9 revealed that the phenyl substituted pybox was able to give better enantioselectivity possibly due to the greater degree of steric hindrance. [18]

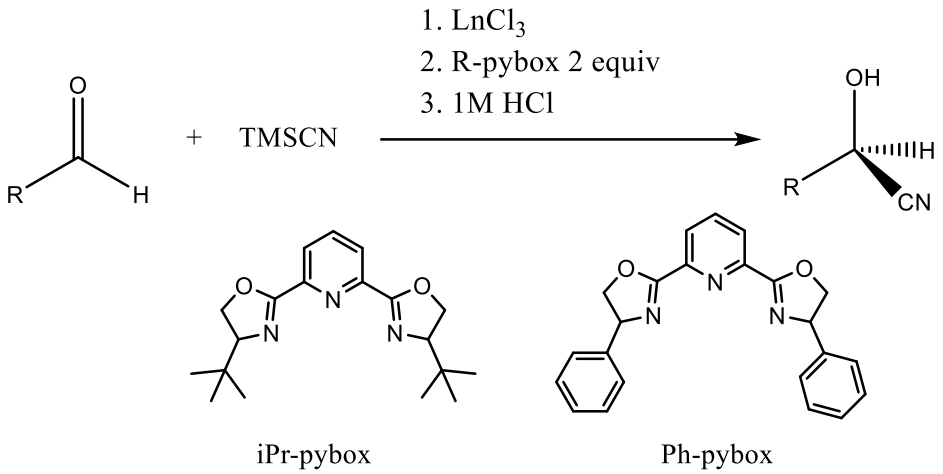

Figure 9: Asymmetric Cyanosilylation of Benzaldehydes with Lanthanide chlorides

1.2.2 Lanthanide salt asymmetric reaction in a micro reactor

In a similar study done by Christina Moberg's and co-workers, the same reaction shown in figure 9, was carried out in a micro reactor which is similar to a flow reactor.[19] The group employed the use of a micro reactor as shown in figure 10 and two standard solutions were prepared. The first contained $YbCl_3$, pybox and benzaldehyde while the other contained only TMSCN, both of which were dissolved in dry acetonitrile. The two standard solutions were then flowed into the reactor through electroosmotic flow, controlled by the voltage applied at inlet A and B (as shown in figure 10). To ensure that the reactions were taking place in the reactor and not at the reservoir at the outlet, the researchers compared the reaction done in the reactor with the reaction done in a round bottom flask. They found that the reaction in the reactor achieved greater yield under similar conditions. Similarly, the yield from the reaction mixture that flowed out directly and those that were left in the outlet reservoir over a period of time were compared and the authors found no significant differences in the yield achieved in both scenarios. Additionally, they were able to achieve high enantiomeric excess using this method.[19] This demonstrates the potential of using lanthanide salts as chiral catalyst in the industry because of its ability to achieve great yield and enantiomeric excess in a micro reactor.

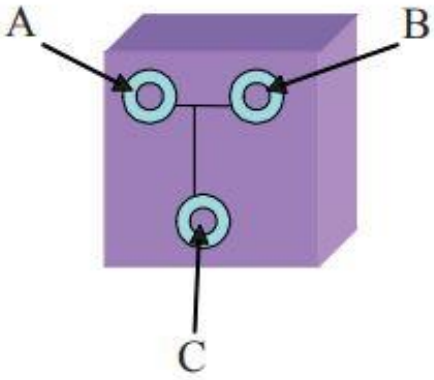

Figure 10: Schematic of the micro reactor consisting of inlets (A and B) and outlet (C).This figure is adapted from reference 19.

1.2.3 Recyclable iron nanoparticle based chiral catalyst for asymmetric reactions

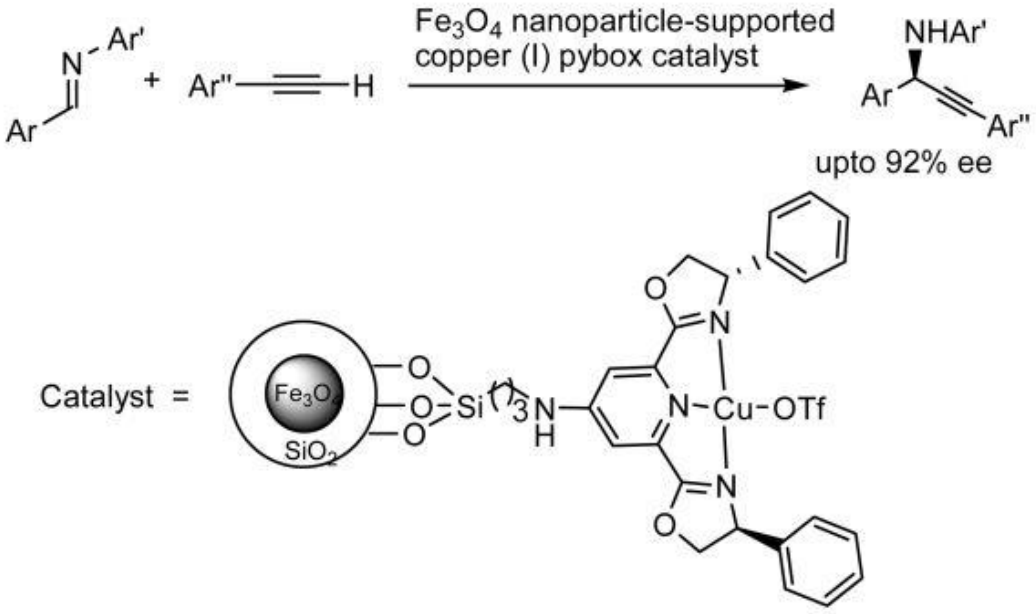

Figure 11: Schematic reaction between imines and terminal alkynes with magnetic chiral catalyst. This figure is adapted from figure 20.

A recent study by Chao Jun Li's and co-workers synthesized a recoverable chiral catalyst that can be used for asymmetric synthesis.[20] In their study, the use of a magnetic iron oxide nanoparticles was employed as an adduct. The nanoparticles were first coated with a layer of silica to protect it, the silica layer was subsequently functionalized with pybox. The

copper catalyst used in the reaction was then coordinated onto the pybox and the catalyst was ready for use as seen in figure 11. In their study, the chiral catalyst was used to catalyze the reaction between imines and aryl alkynes shown in figure 11. The chiral catalyst demonstrated excellent catalytic and enantioselective ability, consistently achieving high yield and enantiomeric excess with differently substituted imines. Furthermore, after every reaction the catalyst could be easily recovered using a magnetic stir bar, dried and then used for subsequent reactions. The catalyst was able to obtain good yield and enantiomeric excess even after multiple reaction cycles demonstrating its ability as a recyclable heterogeneous chiral catalyst.[20]

This study revealed that it is possible to use lanthanide nanoparticles to achieve enantioselectivity. Lanthanide nanoparticles coated with silica have been used for the purpose of bio imaging.[21] Therefore, with a little modification, silica coated lanthanide nanoparticles have the potential to be used as a chiral catalyst in the scenario shown in figure 11, which utilized modified silica nanoparticles for the same enantioselective reaction as shown in Chao Jun Li's group. Additionally, lanthanide nanoparticles also possess the ability to emit light in the visible and UV-region as a catalyst on top of its existing two functions of being a Lewis acid and having photothermal ability which could be beneficial when catalyzing various reactions that require light in the UV or visible light region.

1.3 Aims

In this thesis, we aim to synthesize our own lanthanide nanoparticles to use as a photothermal Lewis acid catalyst for epoxide ring opening reactions. Additionally, we will also modify this lanthanide nanoparticle such that it will be able to act as a chiral catalyst for enantioselective reactions. We chose lanthanide based nanoparticles because it utilizes NIR light which provides advantages over UV/visible light. These advantages are firstly, a deeper penetration into the reaction mixture which ensures that all or most nanoparticles in a reaction mixture are excited. Secondly, most precursors do not absorb light in the NIR region, preventing the precursors from competing with the nanoparticles for the absorption of excitation light. Additionally, this also prevents the photo degradation of the precursors as they do not absorb light in the NIR region.

In chapter 2, we aim to synthesize ytterbium fluoride (YbF_3) nanoparticles and use them as a bifunctional catalyst for the ring opening reaction between epoxides and amines. The catalyst is bifunctional as it has both Lewis acid function and photothermal function. The nanoparticles would be characterized and its photothermal and catalytic properties would be studied.

In chapter 3, we aim to achieve enantioselectivity using the synthesized YbF_3 nanoparticles as chiral catalyst through two methods. Firstly, through the usage of chiral ligands together with the nanoparticle. Secondly, by modifying the nanoparticles by coating it with silica and functionalizing it with pybox to achieve an enantioselective catalyst.

Chapter 2 Using YbF_3 nanocrystals as a photothermal Lewis acid catalyst

Abstract

Lanthanide salts are known to be great Lewis acid catalysts however not many have used lanthanides based nanoparticles as catalysts. This chapter analyses how effective lanthanide based nanoparticles are as a Lewis acid catalyst. YbF_3 nanoparticles in this study were synthesized through the co-precipitation method and characterized using transmission electron microscope (TEM), and x-ray diffraction (XRD). The light to heat efficiency of the nanoparticles was calculated to be 9 %. The nanoparticles were used as a photothermal Lewis acid catalyst for the reaction between epoxides and amines obtaining near quantitative yield. Even after being recycled, excellent yield results were maintained showing great potential as a recyclable catalyst.

2.1 Introduction

Heterogeneous catalyst has been an area of interest for a long time due to its sustainability and cost effective properties especially in this era where resources are limited. In the current industry there has been an increasing preference for heterogeneous catalyst to replace homogenous catalyst. This results in more research being carried out to develop heterogeneous catalyst for the industry. Many studies have shown lanthanides salts to be efficient and sustainable Lewis acid catalyst for many reactions like the cyanosilylation reaction of benzaldehyde and Fidel-crafts reactions. This indicates the huge potential lanthanides has to be used as catalyst to manufacture different products like cosmetics and drugs as they are good Lewis acid catalyst with the ability to be recycled. Earlier in chapter 1 we reported the usage of lanthanide based nanoparticles as Lewis acid catalyst in a cyanosilylation reaction done by our group which can improve the rate of reaction through its photothermal effect in addition to its Lewis acid properties.[13] The importance of photothermal effect is shown in the work done by Benjamin Lear's group which shows that the rate of reaction can be increased by a billion times at the surface of the nanoparticle in the presence of photothermal effect.[15] In this chapter, synthesized YbF_3 based nanoparticles will be used to catalyzed the ring opening reaction of epoxide by amines. YbF_3 nanoparticles discussed in this chapter is synthesized using a co-precipitation method. This method uses high heat to synthesize the required nanoparticles and by controlling the time and temperature we can tune the size of the nanoparticles. The morphology of the YbF_3 nanoparticles will be determined with TEM and the composition and lattices structure are determined with XRD. The efficiency and ability of YbF_3 as photothermal Lewis acid catalyst will also be studied.

2.2 Experimental

2.2.1 Materials and instruments

Cyclohexene oxide, Styrene oxide, Piperidine, Pyrrolidine, Morphline, Aniline, 4-fluoro aniline, 4-chloro aniline, p-Anisidine, Ammonium fluoride, Ytterbium(III) acetate tetrahydrate, Oleic acid, 1-octadecene, o-Xylene (spectrophotometric grade) were purchased from Sigma Aldrich. Methanol (MeOH, HPLC grade) and cyclohexane (HPLC grade) was purchased from Tedia. Ethanol (Analytical reagent grade) was purchased from Macklin. All chemicals were used as received.

Transmission electron microscopy (TEM) images of YbF_3 nanoparticles were recorded using JEM 1400 (JEOL). Nuclear magnetic resonance (NMR) spectroscopy was carried out on an UltraShield 400MHz NMR spectrometer (JEOL). X-ray diffraction (XRD) patterns of nanocrystals were measured using a Bruker D8 Advance XRD diffractometer with Cu Kα radiation. MDL-H-980nm-3W purchased from Changchun New Industries Optoelectronics Technology Co. Ltd

2.2.2 Synthesis of YbF_3 nanocrystals

Synthesis of the nanocrystals is based on a co-precipitation method. Ytterbium(III) acetate tetrahydrate (0.8 mmol) was mixed with oleic acid (6 mL) and 1-octadecene (14 mL) in a 50 mL round-bottom flask under continuous stirring. The mixture was heated to 100 ^{o}C to remove water and oxygen, and further heated to 150 ^{o}C and maintained for 1 h under N2 atmosphere. The mixture was then cooled to room temperature and methanol solution (6 mL) containing NH_4F (2.4 mmol) was added dropwise. The slurry mixture was heated to 50 ^{o}C under N2 flow and maintained for 30 min under N2 atmosphere. Subsequently, the mixture was heated to 100 ^{o}C to remove water and oxygen, and further heated to 290 ^{o}C and maintained under N2 atmosphere for 2 hours. When the solution was cooled to room temperature, the as-

prepared nanocrystals were separated by centrifugation at 7800 rpm, washed with ethanol twice, and re-dispersed in cyclohexane for further characterization.

2.2.3 Solvent transfer of YbF_3 nanocrystal into o-xylene

YbF_3 nanocrystals in cyclohexane (200 µL) and ethanol (1 mL) was added in to a 2 mL centrifuge tube and centrifuge at 13300 rpm for 10 min. The supernatant was discarded and the residue was dispersed into o-xylene.

2.2.4 General procedure of ring opening reaction between epoxide and amines

100 mg of YbF_3 nanocrystals in o-xylene (400 µL), epoxide (0.2 mmol) and amine (0.2 mmol) was added into a 1.5 mL vial and stirred under irradiation of a 980 nm laser (MDL-H-980nm-3W Changchun New Industries Optoelectronics Technology Co. Ltd) for 7 hours. The reaction is then centrifuged at 13300 rpm for 10 min and the supernatant was purified by silica gel column chromatography with Dichloromethane to afford the desired product.

2.2.5 Recycling experiment of YbF_3 nanocrystal

100 mg of YbF_3 nanocrystals in o-xylene (400 µL), epoxide (0.2 mmol) and amine (0.2 mmol) was added into a 1.5 mL vial and stirred under irradiation of a 980 nm laser (MDL-H-980nm-3W Changchun New Industries Optoelectronics Technology Co. Ltd) for 7 hours. The reaction is then centrifuged at 13300 rpm for 10 min and the supernatant was purified by silica gel column chromatography with Dichloromethane to afford the desired product. The residue from the centrifuge was dispersed in 400 µL of o-xylene and used for the same reaction again. This was repeated for 4 times.

2.2.6 Determining photothermal conversion efficiency

The light-to-heat conversion efficiency of nanocrystals in o-xylene was measured using o-xylene solutions (200 μL) of the nanocrystals (~ 81 mg mL^{-1}) in a quartz cuvette. The solution was irradiated with a 980-nm laser (MDL-H-980nm-3W Changchun New Industries Optoelectronics Technology Co. Ltd) at 8.82 W cm^{-2}, and the temperature rise measured with a thermal imaging camera (FLIR Systems, Inc.).

2.3 Results and Discussion

2.3.1 Characterizing of YbF_3 nanocrystals

YbF3 nanocrystals were synthesized using co-precipitation method, To ensure that the composition of the nanoparticles is Yb:F (1:3) the XRD pattern of YbF_3 in figure 12 was examined.

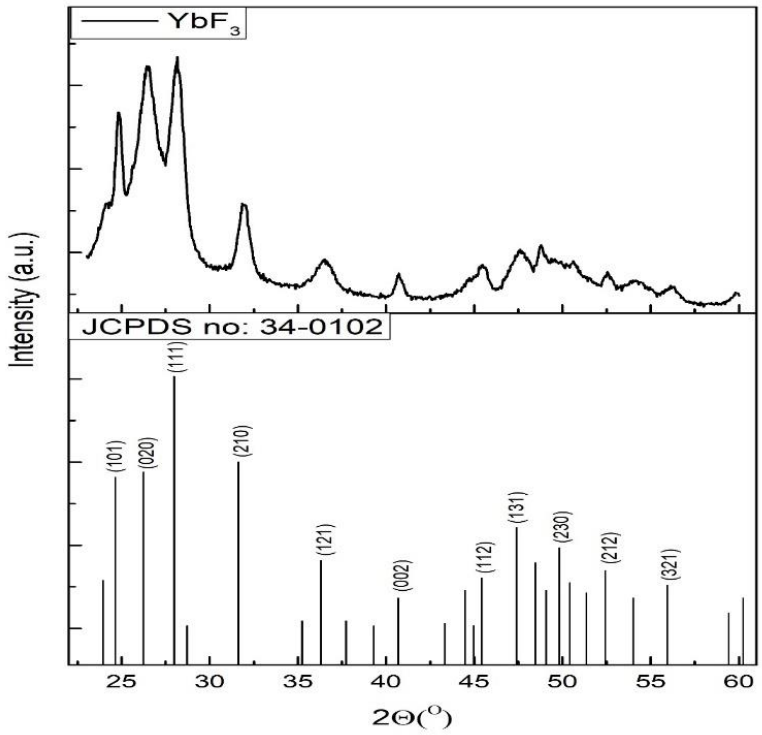

Figure 12: XRD spectrum of YbF_3 nanocrystals, the tope spectrum is the XRD for the synthesized YbF_3 crystals. The bottom spectrum is the reference spectrum for YbF_3 nanocrystals.

The XRD pattern of the synthesized orthorhombic YbF_3 nanocrystals which is the top spectrum shown in figure 12 displays peaks that are well indexed to the standard orthorhombic YbF_3 which is the bottom spectrum in figure 12 with bands at 2 θ = 24.81°, (corresponding to the (101) lattice plane), 26.43° (corresponding to the (020) lattice plane), 28.17° (corresponding

to the (111) lattice plane), 31.84° (corresponding to the (210) lattice plane), 36.50° (corresponding to the (121) lattice plane) and 40.73° (corresponding to the (002) lattice plane).

Through the TEM it is observed that the nanocrystals take on an orthorhombic shape as seen in figure 13. The nanocrystal has an average length of 27.1 ± 4.45 nm, an average width of 23.6 ± 4.60 nm and an average height of 6.60 ± 1.20 nm. The size distribution histogram for each side of the particle can be seen in figure 13 below.

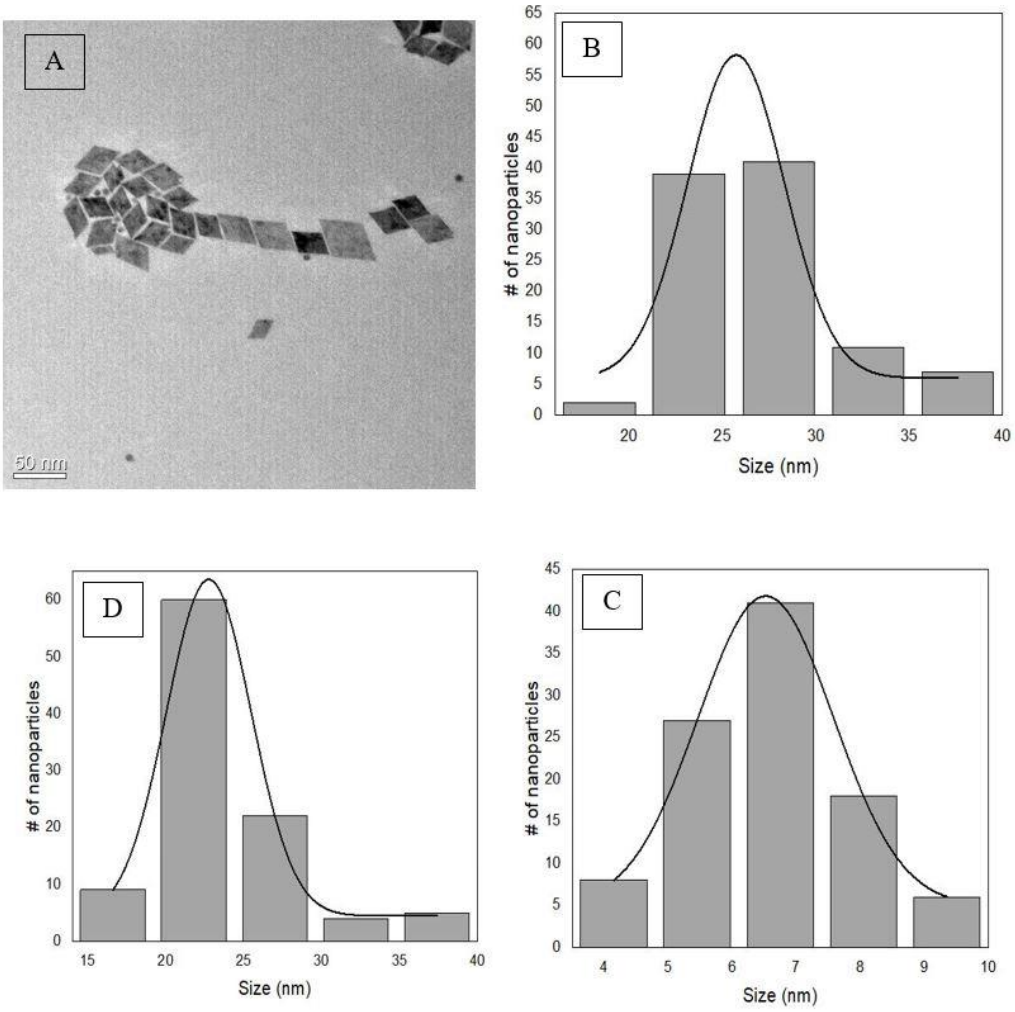

Figure 13: (A) is an image of YbF_3 nanocrystals taken using the TEM. (B), (C) and (D) represent the size distributions of the length, width and height of the orthorhombic nanocrystals, respectively.

The nanocrystal's single unit cell is orthorhombic in shape and the sides are of length a = 0.6216 nm, b = 0.6786 nm and c = 0.4434 nm. Density of YbF_3 = 8.173 g cm^{-3} according to the standard JCPDS card No. 43-0102, d = longest diagonal in the orthorhombic single cell.

Volume of a single unit cell = (a)(b)(c)

$$= 0.187 \text{ nm}^3$$

Given that each YbF_3 nanocrystal has an average Length (L) = 27.14 nm,

Width (W) = 23.57 nm and Height (H) = 6.59 nm.

Volume of a single nanocrystal = (L)(W)(H)

$$= 4215.56 \text{ nm}^3$$

Given that the density of YbF_3 is 8.173 g cm^{-3}.

Mass of one nanocrystal = 4215.56 × 8.173

$$= 3.45 \times 10^{-17} \text{ g}$$

Number of nanocrystals in 1 g of YbF_3 is 2.90×10^{16} particles

To find the amount of Yb^{3+} ion on the surface of the particles we first need to calculate thickness of the outer layer of the nanocrystals. We will assume that the Yb^{3+} will be equally distributed throughout the entire nanocrystals. The thickness of the outer most unit cell layer approximately equals to the longest diagonal, d, in the orthorhombic cell.

$$d = \sqrt{a^2 + b^2 + c^2}$$

$$= \sqrt{0.6216^2 + 0.6786^2 + 0.4434^2}$$

$$= 1.02 \text{ nm}$$

After calculating the value d, taking (H) divided by (d) each nanocrystal is made up of around 6 layers of unit cell and we can use the equation:

$$\frac{N_{surface}}{N_{volume}} = \frac{V_{surface}}{V_{total}} = \frac{(L)(W)(H) - ((L-2d)(W-2d)(H-2d))}{(l)(W)(H)}$$

$$= \frac{4215.56 - (25.10 \times 21.53 \times 4.55)}{4215.56}$$

$$= 41\ \%$$

No. of Yb^{3+} ions on the surface for the YbF_3 nanocrystals is 1.78 mmol g^{-1}

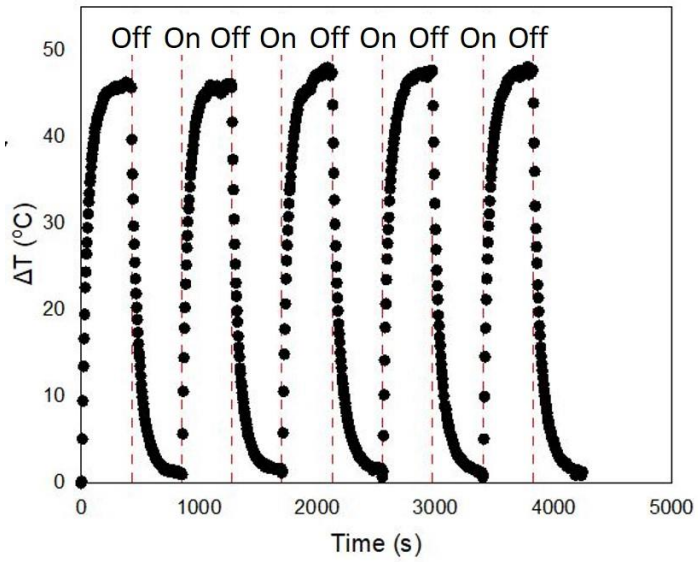

Figure 14 : Heat efficiency graph for YbF3 nanocrystals.

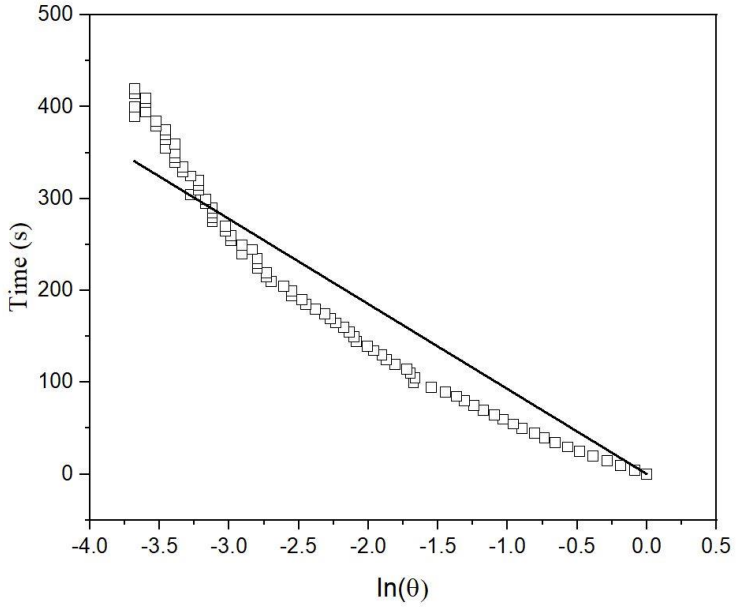

Figure 15 : Cooling curve for YbF_3 nanocrystals

The light to heat efficiency of YbF_3 nanocrystals is determined using the following equation:

$$\eta = \frac{hS(T_{Max} - T_{Surr}) - Q_{Dis}}{I(1 - 10^{-A_{980}})}$$

where h is the heat transfer coefficient, S is the surface area of the container, T_{Max} is the equilibrium temperature which is 69 ^{o}C, T_{Surr} is the ambient temperature of the surroundings which is 21.3 ^{o}C. Q_{Dis} is the energy input by the solvent. *I* is the incident laser power which is measure to be 3.6 W and A_{980} is the absorbance at 980 nm which is measured to be 0.295. Q_{dis} can be calculated by using the following equation:

$$Q_{dis} = \frac{10^3 \times m \times C \times \Delta T}{\mathrm{t}}$$

where m is the mass of the solvent used which is 1.76 x 10^{-4} kg, C is the heat capacity of the solvent which is 1767.64 J/kg K, ΔT is the change in the temperature of the solvent and t is the laser exposure time. When o-xylene is irradiated using 980 nm laser for 420 s, ΔT was 0.9 ^{o}C and Q_{dis} = 0.67 mW. To determine hS a dimensionless driving force temperature θ is defined as:

$$\theta = \frac{T - T_{Surr}}{T_{Max} - T_{Surr}}$$

where T is the temperature at time t. The cooling process after the laser has been turned off can be described by:

$$t = -\tau_s \ln(\theta)$$

The relationship between hS and $\boldsymbol{\tau}_s$ is given by $hS = \frac{mC}{\tau_s}$, where m and C are the mass and heat capacity of the solvent respectively. The cooling curve t vs ln(θ) is plotted in figure 15 to obtain $\boldsymbol{\tau}_s$ = 92. 57. The light to heat efficiency η is found to be 9 %. This photothermal efficiency is considered to be very low because there are studies done with a photothermal efficiency of more than 80 %.[22, 23]

2.3.2 Lewis acid catalysis of epoxide ring opening between cyclohexene oxide with amines

The catalytic ability of the YbF_3 nanocrystals was studied through the reactions between epoxides and amines. In this study, cyclohexene oxide reacted with both aliphatic and aromatic amines in o-xylene

For this reaction, a suitable solvent has to be selected because the reactions will be taking place around 90 to 100 ^oC. The solvent has to fulfil two criteria, firstly, the nanocrystals must be able to disperse in it. Secondly, the solvent has to have a boiling point of above 100 ^oC. The reaction was tested out in toluene first. Toluene met both criteria but as time progresses, toluene started to evaporate and with a smaller amount of toluene in the reaction mixture the solubility of the nanocrystals started decreasing. This resulted in the particles aggregating onto the walls of the vials causing the temperature of the reaction mixture to fluctuate as time proceeds.

o-Xylene was selected due to its high boiling point of 144 ^oC higher than that of toluene. The nanocrystals were also well dispersed in o-xylene. When the reaction was carried out none of the nanocrystals aggregated on to the wall. This allowed for a more stable temperature and also higher catalytic ability by the nanocrystals as it is better dispersed in o-xylene compared to toluene.

Irradiating cyclohexene oxide and amines in the presence of YbF_3 nanocrystals and 980 nm light increased the reaction to 90 ^oC due to photothermal effect. For the reaction more particles were used than in the heat efficiency study to ensure that the temperature is able to increase from 70 ^oC to 90 ^oC. After irradiating for 7 hours, the reaction yielded the β-amino alcohol product **2** in near quantitative amounts (entry 1-7 shown in table 1). This was observed even for electron poor amines that have electron withdrawing substituents (entry 4-7 shown in table 1).

To ensure that the reaction requires both the photothermal and Lewis acid effect in order to proceed, two sets of control experiment under different conditions were conducted. One set of control is conducted when the substrates were added together and stirred at the temperature that the reaction takes place at (i.e. 90 ^{o}C). The second set of control experiment was when the nanocrystals were added in with the substrate and stirred together with no photothermal effect present. From the control experiments no yield was observed for the control experiments (entry 1-7 of table 2). The above results indicate both photothermal effect and Lewis acid are needed for the reaction to proceed.

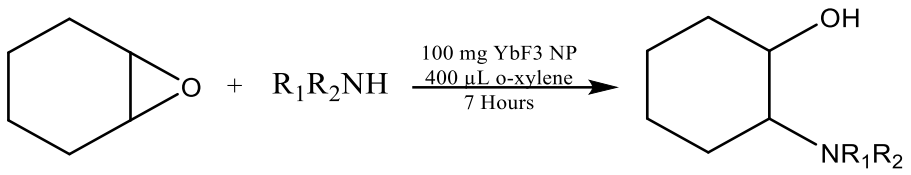

1 **2**

Table 1: Reaction between cyclohexene oxide and amines, the reactions were carried out in 400 µL of o-Xylene under the irradiation of a 980 nm laser to reach the temperature of 90 °C and 100 mg of YbF_3 nanocrystals were used for each reaction. All yield was determined by NMR.

Entry	Amine	Yield (%)
1	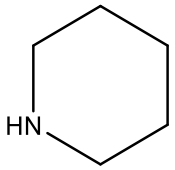	85
2	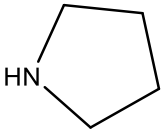	90
3	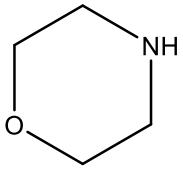	96

4	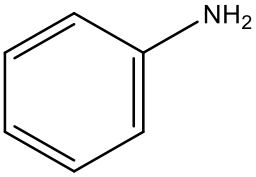	99
5	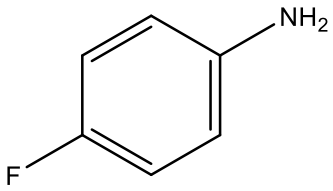	92
6	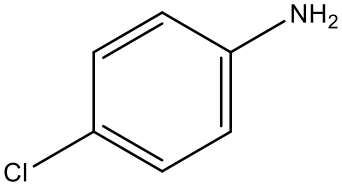	89
7	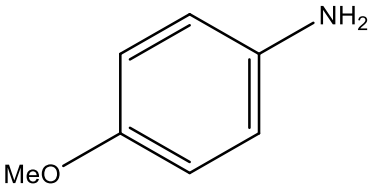	72

a) For NMR spectrum refer to figures S1-S7 in appendix.

Table 2: Control experiment between cyclohexene oxide and amines. All yield was determined by crude NMR.

Entry	Amine	Yield[a] (%)	Yield[b] (%)
1	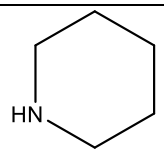	0	0
2	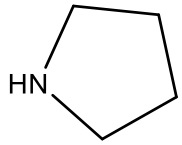	0	0
3	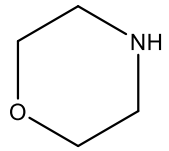	0	0
4	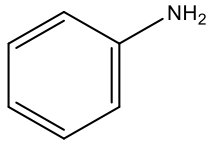	0	0
5	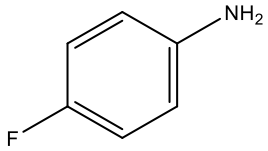	0	0
6	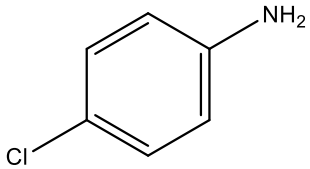	0	0
7	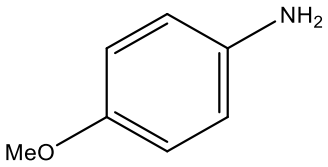	0	0

a) Experiment was carried out in 400 µL of o-xylene, at 90 ºC without the presence of nanocrystals.

b) Experiment was carried out in 400 µL of o-xylene, at room temperature in the presence of 100 mg of YbF_3 nanocrystals.

c) There was no irradiation from 980 nm laser

d) For NMR spectrum refer to figures S8-S21 in appendix.

2.3.3 Lewis acid catalysis of epoxide ring opening between styrene oxide with amines

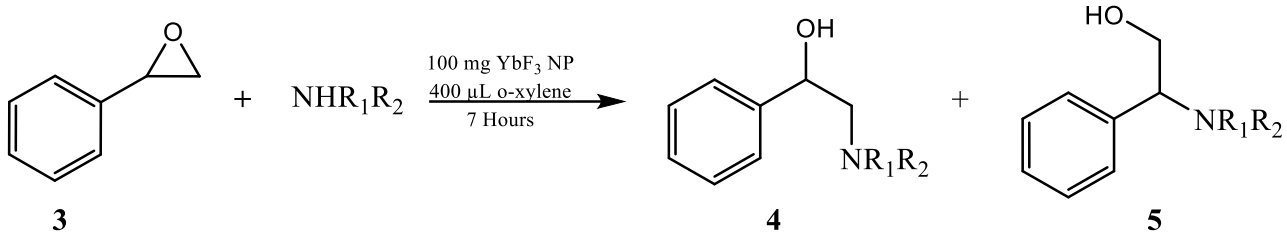

3 **4** **5**

Table 3: Reaction between styrene oxide and amines, the reactions were carried out in 400 µL of o-xylene under the irradiation of a 980nm laser to reach the temperature of 100 ^{o}C and 100 mg of YbF_3 nanocrystals was used for each reaction. Yield was determined using NMR.

Entry	Amine	Yield (%) **4**	Yield (%) **5**
1	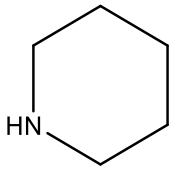	98	0
2	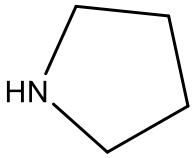	82	0
3	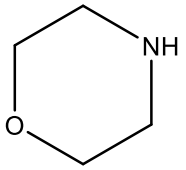	86	0
4	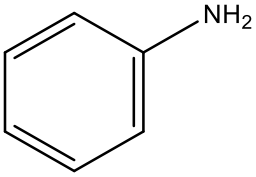	34	65
5	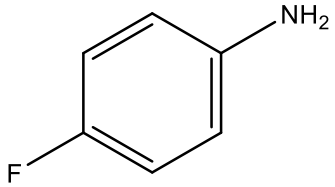	34	65
6	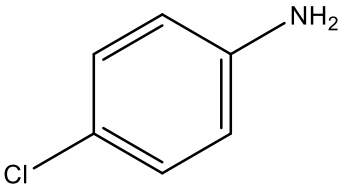	32	62

7	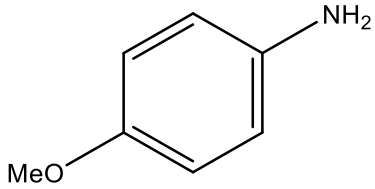	29	62

a) For NMR spectrum refer to figures S22-S28 in appendix

Table 4: Control experiment between styrene oxide and amines. Yield was determined by crude NMR.

Entry	Amine	Yield[a] (%) **4:5**	Yield[b] (%) **4:5**
1	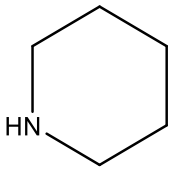	35:0	12:0
2	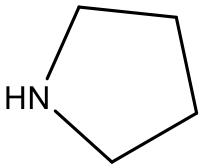	66:0	10:0
3	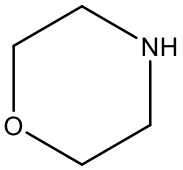	18:0	4:0
4	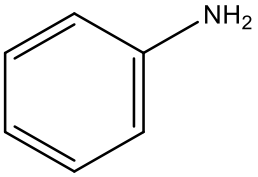	0	0
5	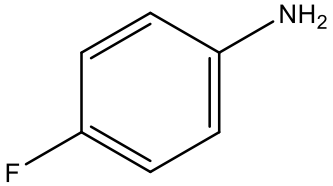	0	0
6	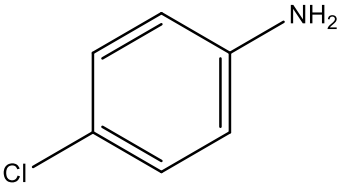	0	0

7	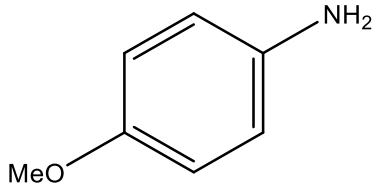	0	0

a) Experiment was carried out in 400 µL of o-xylene, at 100 ^{o}C without the presence of nanocrystals.

b) Experiment was carried in 400 µL of o-xylene, at room temperature in the presence of 100 mg of YbF_3 nanocrystals.

c) There was no irradiation from 980 nm laser

d) For NMR spectrum refer to figures S22-S42 in appendix

The regioselectivity of β-amino alcohols formed from the epoxide ring opening reaction between styrene oxide and amines in the presence of YbF_3 nanocrystals and 980 nm light is studied next. Aliphatic amines gave close to perfect regioselectivity (entry **1-3** in table 3). The aliphatic amines attack the less substituted carbon to give β-amino alcohols **4** in good to excellent yield, indicating that the reaction proceeds via a S_n2 mechanism due to its strong nucleophilicity. Whereas, for aromatic amines two possible products are formed with the major product being β-amino alcohols **5** and the minor product being β-amino alcohols **4** (entry **4-7** in table 3). This indicates that aromatic amines prefer to attack the more substituted carbon. Hence, the reaction most likely follows a S_N1 mechanism whereby a carbo cation is formed to allow the weaker nucleophilic aromatic amine to attack.

For the control experiments in table 4 most of the experiments have little to no yield (entry **1-7** in table 4). Hence, both photothermal effect and Lewis acid will be needed in order for the reaction to proceed.

Another thing to point out is that 100 mg may be a very high catalyst loading as it is double the amount of mols when compare to the precursors. However, using nanocrystals as

catalyst is very different compared to traditional catalyst. Traditional catalyst will fully dissociate in the solvent into individual metal ions but the nanocrystals will not. For nanocrystals not all the Yb^{3+} ions are on the surface of the nanocrystals more than half of the Yb^{3+} ions are inside the nanocrystal lattice structure not participating in the reaction. Additionally, even for the Yb^{3+} that is on the surface of the particle taking part in the reaction as catalysts it is also sterically hindered as part of it is covered in the nanocrystal structure. All these factors reduce the effective collision between the catalyst and the precursors in the reaction. Hence, there is a need for higher catalyst loading to ensure that the reaction proceeds smoothly.

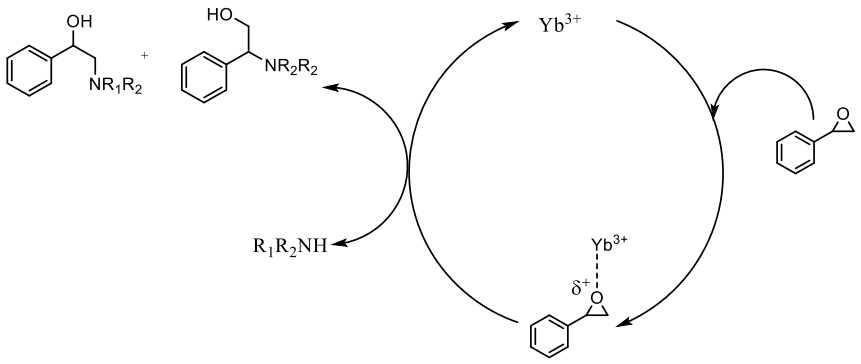

Figure 16: Catalytic cycle showing the mechanism for the ring opening reaction of epoxide with amine catalyzed by YbF3 nanocrystals.

The proposed mechanism for the reaction will be an approach by the nanocrystal first followed by the coordination of the Yb^{3+} ions on the nanocrystal to the oxygen atom on the epoxide as shown in figure 16. This will activate the epoxide making it more susceptible to a nucleophilic attack by the amine seen in figure 16. After the nucleophilic attack by the amine, the β-alcohol product is formed.

2.3.3 Recycling of YbF_3 nanocrystals

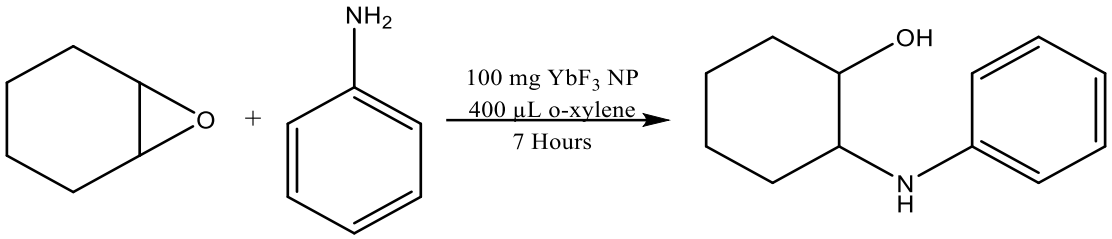

Table 1: Recycling of YbF_3 nanocrystal catalyst, Reaction between cyclohexene oxide and aniline, the reactions were carried out in 400 µL of o-xylene under the irradiation of a 980 nm laser to reach the temperature of 90 ^oC and 100 mg of YbF_3 nanocrystals was used for each reaction.

Entry	No. of Runs	Yield (%)
1	1	85
2	2	99
3	3	99
4	4	99
5	5	99

a) For NMR spectrum refer to figures S43-S47 in appendix

The reaction between cyclohexene oxide and aniline was repeated 5 times. Each time the particles were collected via centrifugation after the reaction, dispersed and used again for the subsequent reaction. After five reactions, near quantitative conversion is still observed as shown in table 5, this shows that even after recycling the nanocrystal for four times there is no decrease in its catalytic abilities. This is a clear indication that YbF_3 nanocrystals are excellent recyclable Lewis acid catalysts that can offer an additional photothermal effect that may be use to drive reactions of unreactive precursors.

2.4 Conclusion

In conclusion, in this chapter we demonstrated the catalytic ability of YbF_3 nanoparticles in catalysing Lewis acid reactions like the ring opening of epoxide with amines. Concurrently from the control experiments we can determine that the additional photothermal effect is beneficial in activating the precursors of the reaction. We also studied the photothermal efficiency of the nanoparticles and characterized them using TEM and XRD. This chapter also showed that lanthanide based nanoparticles provides a more sustainable approach to the environment compared to traditional catalyst as they can be recycled which puts less strain on the environment.

Chapter 3: Utilizing YbF_3 nanocrystals for enantioselective reactions

Abstract

Asymmetric synthesis is extremely important in many industries in order to reduce undesirable side effects arising from the presence of poisonous enantiomers. This need for asymmetric synthesis increases the need for a sustainable way to use chiral ligands instead of them being a one-time use product. Using only chiral ligands with YbF_3 nanocrystals was not effective in achieving enantiomeric pure products. Attempts at synthesizing a chiral catalyst with YbF_3 nanocrystals was unsuccessful due to the lack of chiral ligands on the surface.

3.1 Introduction

In chapter 1, the importance of enantioselective asymmetric reactions was discussed. Due to undesired side effects in drugs and other consumable products, the synthesis of selective enantiomers is favored over the synthesis of other enantiomers. An example will be thalidomide, with one enantiomers while causing birth defects while the other is able to reduce morning sick symptoms in pregnant women with causing birth defects. Another example is Propranol shown in figure 17 .[16] One form of the enantiomer **13** is used for treating heart disease while the other form **14** is a contraceptive. In this scenario, enantiomeric purity is extremely important because patients being treated for heart disease will not be able to conceive if the drug was introduced as a racemic drug. Through these examples, the importance of asymmetric synthesis is shown.

There are many methods to selectively synthesize the desired enantiomers. The most common method will be employing chiral ligands to bind onto metal centers. This causes one face of the catalyst to be hindered restricting the substrate's interaction with the catalyst to only the other face. This selective interaction with the catalyst will form a product of high enantiomeric purity. An example is a study reported by Peter M. Smith's group.[18] They reported an asymmetric synthesis that used lanthanide chloride with Pybox to produce products of high enantiomeric purity. However, such methods do not allow for the recycling of the chiral ligands, leading to high costs and sustainability problems. Therefore, studies on creating enantioselective catalysts that are able to be recycled and reused while not losing its catalytic and enantioselective abilities is increasingly important in this era of limited resources.

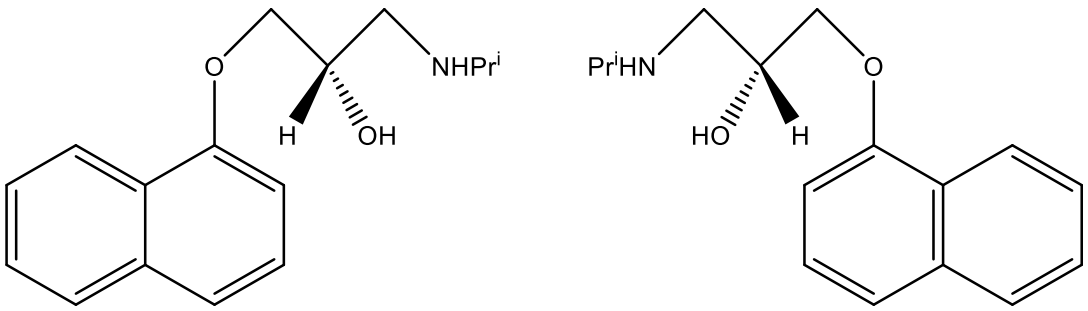

13 **14**

Figure 17: Structure of enantiomers of Propranol.

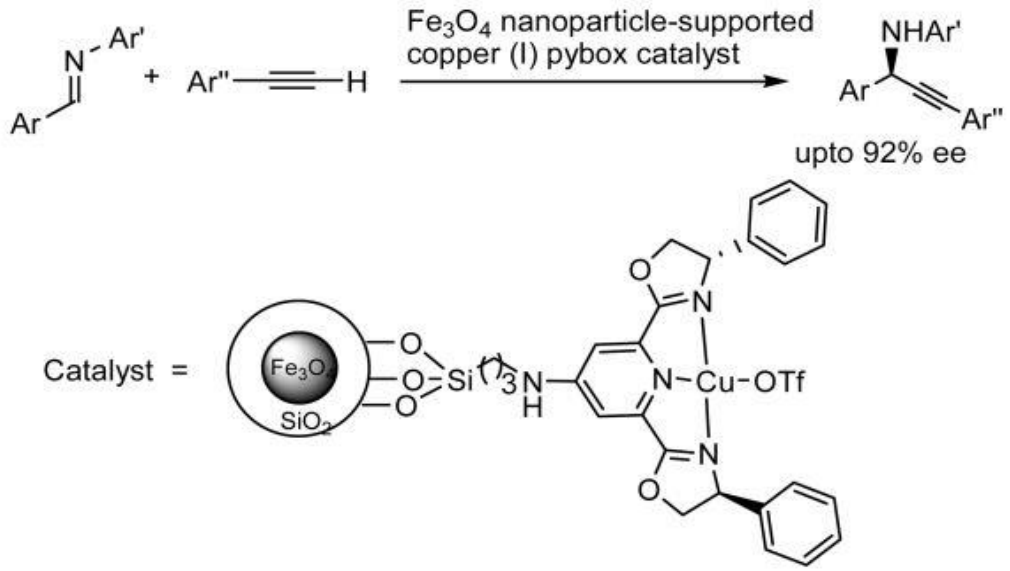

Figure 18: Reaction between alkynes and imines and an image of the pybox supported copper catalyst. This figure was adopted from refrence 20.

A recent study by Chao-Jun Li and co-workers showed a synthesis of a novel enantioselective catalyst that is able to be recycled and reused up to 6 times while retaining its catalytic and enantioselective abilities fully.[20] In the study, they first use iron oxide nanocrystals coated with a layer of silica, then they functionalize the silica outer layer with pybox ligands. The resultant nanocrystal was then use to bind to copper (I) catalyst. The iron oxide nanocrystal is used so that the catalyst can be easily recovered by just using an external magnet after the reaction. Their catalyst was used for an addition reaction between alkynes and imines and after recycling for 6 times the iron nanocrystal catalyst still gave good yield and

enantioselectivity. This shows the possibility of creating a recyclable catalyst that is able to provide enantioselectivity as well.[20]

In this chapter we aim to create a recyclable trifunctional catalyst that is able to have three functions, catalyze the reaction, have enantioselectivity and produce heat for the reaction by using the YbF_3 nanocrystal as a base platform for this catalyst. This will be different from Chao-Jun Li catalyst that only possess one function which is to provide enantioselectivity.

3.2 Experimental

3.2.1 Materials and Instruments

N-Benzylideneaniline, Phenyl acetylene, Copper(I) trifluoromethanesulfonate toluene complex, Potassium carbonate, Ammonium fluoride, Ytterbium(III) acetate tetrahydrate, Oleic acid, 1-octadecene, 1,1'-Bi-2-naphthol, Tripotassium phosphate (K_3PO_4), (3-Aminopropyl) triethoxysilane (AEOS), IGEPAL® CO-520, Tetaethyl orthosilicate and Ph-pybox were purchased from Sigma Aldrich. Methanol (MeOH, HPLC grade) and cyclohexane (HPLC grade) was purchased from Tedia. Trimethylsilyl cyanide (TMSCN, 96%) and Ethanol (Analytical reagent grade) was purchased from Macklin. 2-isopropanol (HPL grade) and Hexane (HPLC grade) were purchased from J.T Baker. Hydrochloric acid was purchased from Honeywell. OD-H and AD-H column were purchased from Daicel Chemical Industries. iPr-pybox, copper bromide (CuBr) and (4S,4'S)-2,2'-(4-Bromopyridine-2,6-diyl)bis(4-isopropyl-4,5-dihydrooxazole) were purchased from ChemScene. Ethylenediaminetetraacetic acid (EDTA) was purchased from Alfa Aesar. All chemicals were used as received.

Transmission electron microscopy (TEM) images of YbF_3 nanocrystals were recorded using JEM 1400 (JEOL). Nuclear magnetic resonance (NMR) spectroscopy was carried out on an Ultra Shield 400MHz NMR spectrometer (JEOL). Enantiomeric excess was determined with a Higher performance liquid chromatography instrument (HPLC, Shimadzu LC-20AD). Uv-Vis absorption spectroscopy is carried out using Shimadzu UV-1800 UV spectrophotometer, Florescence emission spectroscopy is carried out using Shidmazu RF-5301pc Spectrofluorophotometer. Fourier transform infrared (FTIR) was carried out using Shimadzu Irprestige-21 Fourier transform infrared spectrophotometer. MDL-H-980nm-3W was purchased from Changchun New Industries Optoelectronics Technology Co. Ltd

3.2.2 Synthesis of YbF_3 nanocrystals

Synthesis of the nanocrystals is based on a co-precipitation method. Ytterbium(III) acetate tetrahydrate (0.8 mmol) was mixed with oleic acid (6 mL) and 1-octadecene (14 mL) in a 50 mL round-bottom flask under continuous stirring. The mixture was heated to 100 ^{o}C to remove water and oxygen, and further heated to 150 ^{o}C and maintained for 1 h under N2 atmosphere. The mixture was then cooled to room temperature and methanol solution (6 mL) containing NH_4F (2.4 mmol) was added dropwise. The slurry mixture was heated to 50 ^{o}C under N2 flow and maintained for 30 min under N2 atmosphere. Subsequently, the mixture was heated to 100 ^{o}C to remove water and oxygen, and further heated to 290 ^{o}C and maintained under N2 atmosphere for 2 hours. When the solution was cooled to room temperature, the as-prepared nanocrystals were separated by centrifugation at 7800 rpm, washed with ethanol twice, and re-dispersed in cyclohexane for further characterization.

3.2.3 Coating and functionalizing of YbF_3 nanocrystals

YbF_3 nanocrystals in cyclohexane and IGEPAL CO-520 (1.5 mL) was added into a 25 mL round bottomed flask. The reaction mixture is sonicated for 30 min and stirred for 10 min. Ammonia (230 µl) was added and the reaction mixture was stirred for 30 min and sonicated for another 30min. TEOS (135 µl) and stirred overnight. AEOS (100 µl) was added the following day and the reaction mixture is stirred overnight. The nanocrystals were washed with ethanol and deionized water and dispersed in ethanol.

3.2.4 Functionalizing silica surface with pybox

YbF_3 nanocrystals in DMF (4 mL), (4S,4'S)-2,2'-(4-Bromopyridine-2,6-diyl)bis(4-isopropyl-4,5-dihydrooxazole) (0.1 mg), Binol (5.7 mg, 0.02 mmol), CuBr (2.8 mg, 0.02 mmol) and K_3PO_4 (42.4 mg, 0.2 mmol)was added into a 15 mL recovery flask and stirred overnight at

50 ^{o}C under N2. The nanocrystals were then washed with EDTA, DCM and ethanol. They were then dispersed into ethanol.

3.2.5 Coordinating Copper(I) trifluoromethanesulfonate toluene complex to functionalized silica coated nanocrystals

iPr-pybox functionalized silica coated nanocrystals were stirred with Copper(I) trifluoromethanesulfonate toluene complex (0.2 mmol) and DCM (2 mL) overnight. The reaction mixture is then centrifuged for 10 mins at 13300 rpm. The residue is washed with DCM and ethanol. The nanocrystals are then dispersed in DCM.

3.2.6 General procedure for reaction between N-benzylideneaniline and phenyl acetylene

N-benzylideneaniline (0.2 mmol), phenyl acetylene (0.3 mmol), Copper(I) trifluoromethanesulfonate toluene complex (0.02 mmol) and DCM (400 µL) were added into a 1.5 mL vial and stirred overnight at 35 ^{o}C. the reaction mixture was purified by silica gel column chromatography with DCM to afford the desired product

3.2.7 General procedure for reaction N-benzylideneaniline and phenyl acetylene with pybox

N-benzylideneaniline (0.2 mmol), phenyl acetylene (0.3 mmol), Copper(I) trifluoromethanesulfonate toluene complex (0.02 mmol), pybox (0.04 mmol) and DCM (400 µL) were added into a 1.5 mL vial and stirred overnight at 35 ^{o}C. the reaction mixture was purified by silica gel column chromatography with DCM to afford the desired product.

3.2.8 General procedure for reaction between N-benzylideneaniline and phenyl acetylene using YbF_3 as a nano heater

N-benzylideneaniline (0.2 mmol), phenyl acetylene (0.3 mmol), Copper(I) trifluoromethanesulfonate toluene complex (0.02 mmol), YbF_3 nanocrystals and DCM (400

µL) were added into a 1.5 mL vial and stirred overnight under the irradiation of a 980nm laser (MDL-H-980nm-3W Changchun New Industries Optoelectronics Technology Co. Ltd) to 35 ^{o}C. the reaction mixture was purified by silica gel column chromatography with DCM to afford the desired product.

3.2.9 Reacting benzaldehyde with TMSCN

YbF_3 nanocrystals, Ph-pybox (0.04 mmol), benzaldehyde (0.2 mmol), TMSCN (0.8 mmol) and ACN (400 µl) was added into a 1.5 ml vial and stirred overnight. The reaction mixture is quenched with a saturated solution of potassium carbonate and washed with ethyl acetate. The organic layer is dried over magnesium sulphate ($MgSO_4$), filtered and concentrated. The residue is added into a 20 ml vial with 1 M HCL (5 mL) and stirred for 2 hours. Ethyl acetate (5 mL) was added into the reaction mixture and stirred for another 30 min. The organic layer was washed with deionized water, the aqueous layer was washed with ethyl acetate. The combined organic solution is washed with brine, dried with $MgSO_4$, filtered and concentrated. The residue is then purified by silica gel column chromatography with DCM to afford the desired product. Enantiomeric excess was determined with HPLC equipped with a OD-H column

3.3 Results and Discussion

3.3.1 YbF_3 with pybox

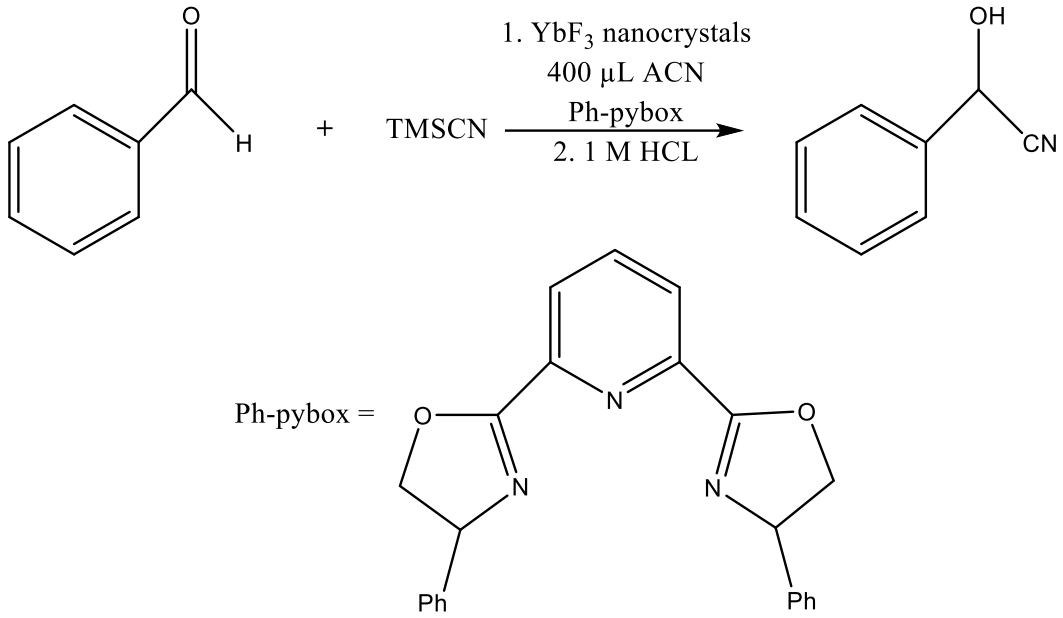

Figure 19: Reaction scheme between Benzaldehyde and TMSCN

In this sub chapter we investigated the possibility of utilizing YbF_3 nanocrystals in enantioselective reactions together with chiral ligands shown in figure 19. The enantioselective reaction between benzaldehyde and TMSCN is a classical Lewis acid driven reaction which has been successfully achieved by lanthanide salts. Enantioselectivity was conferred by ph-pybox and C_2 symmetric ligands.[19, 24]

Our first approach was to react benzaldehyde with TMSCN in the presence of YbF_3 nanocrystals and Ph-pybox in acetonitrile overnight. Then the product for the first step is then stirred in 1 M HCl to give the product shown in figure 19. However, no enantiomeric excess was observed from the HPLC as seen in figure 20 below.

We believe the lack of enantiomeric excess is due to the steric hindrance of the Yb^{3+} ions in the nanocrystal by its lattice structure. This physically prevents the Ph-pybox from coordinating onto the Yb^{3+} ions, hence, failing to induce the chiral environment needed for enantioselectivity. Additionally, defects on the surface of the nanocrystals could prevent coordination of the chiral ligand, hence, no enantiomeric excess was observed.

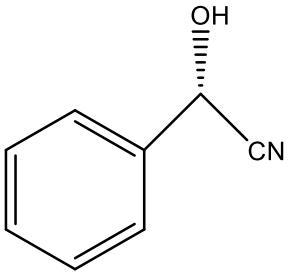

(R)-Mandelonitrile

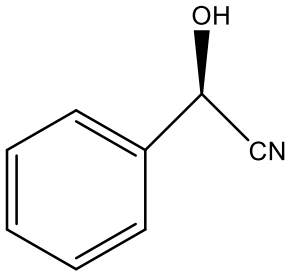

(S)-Mandelonitrile

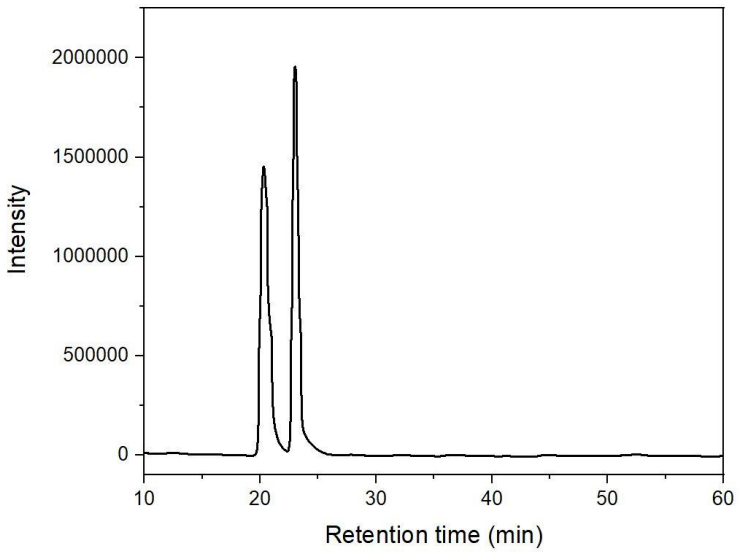

Figure 20: HPLC spectrum for reaction shown in figure 19 using an AD-H column. The first peak belongs to (R)-Mandelonitrile and the second peak belongs to (S)-Mandelonitrile.

3.3.2 YbF_3 nanocrystal as nano heaters

Our second approach was to use the YbF_3 nanocrystals as a nano heater. As mentioned in Chapter 2 using nanocrystals as a nano heater will potentially increase the rate of reaction by many folds which greatly improves the overall yield of the reaction.[15] An additional benefit is the possibility of activating less reactive precursors in the reaction as heat energy could help to increase the amount of effective collisions between substrates leading to an increase in reaction rate. In order for our catalyst to act solely as a nano catalyst, we selected a non- Lewis acid catalyzed reaction to eliminate the possibility of Lewis acid catalysis from occurring in the reaction. Hence, an alkyne-imine coupling reaction shown in figure 21 below was chosen.

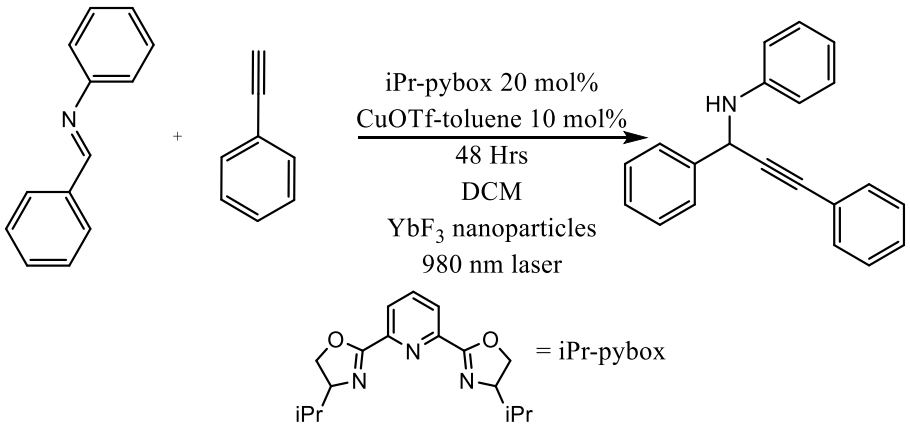

Figure 21:Reaction between alkyne and imine using YbF3 nanocrystals as Nano heaters in the reaction.

Phenyl acetylene and N-Benzylideneaniline was reacted together in the presence of Copper(I) trifluoromethanesulfonate toluene complex and iPr-pybox in DCM.The reaction mixture was heated to 35 ^{o}C by irradiating YbF_3 nanoparticles with a 980 nm laser. This reaction achieved a yield of 60 % was obtained quantified with NMR shown in figures S48 and S49. The reaction has an enantiomeric excess of 60 % derived from the HPLC as shown below in figure 22.

The enantiomeric excess was achieved through to the use of the iPr-pybox ligand. This ligand will first bind strongly to Copper(I) trifluoromethanesulfonate forming a chiral complex.

After which, the sterically hindered ligand will provide a chiral environment for the enantioselective reaction to take place. Thus, favoring the formation of on enantiomer over the other, leading to an enantiomeric excess of one enantiomer.

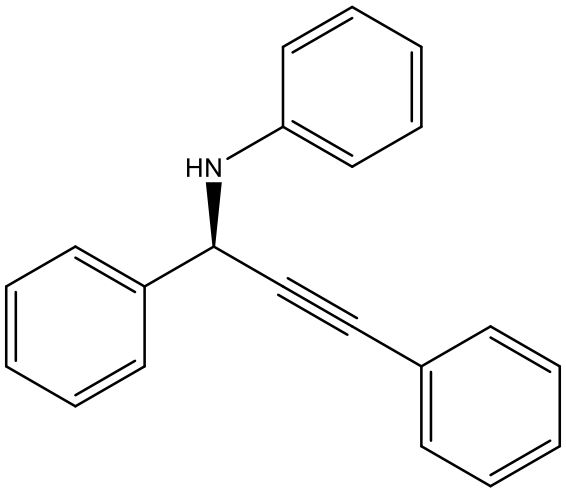

(R)-N-(1,3-diphenyl-prop-2-yn-1-yl)aniline

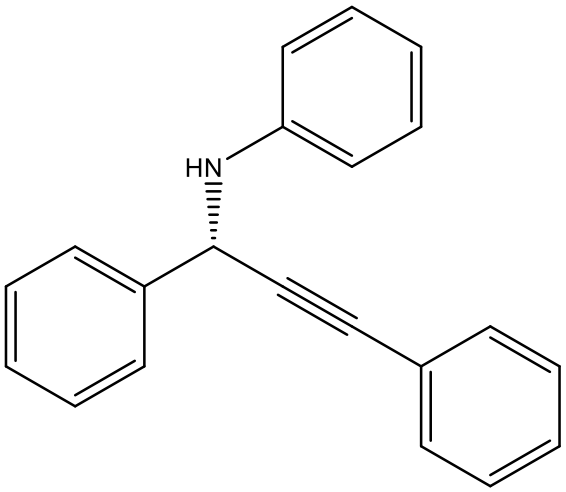

(S)-N-(1,3-diphenyl-prop-2-yn-1-yl)aniline

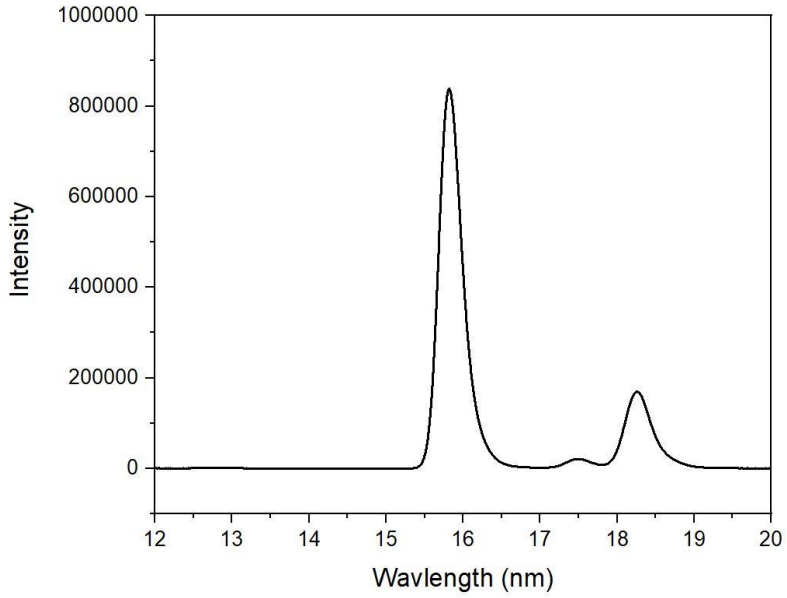

Figure 22: HPLC spectrum of using YbF_3 as nano heaters. The peak with a retention time of 16 mins belong to (R)-N-(1,3-diphenyl-prop-2-yn-1-yl)aniline while the peak with a retention time of 18.4 mins belong to (S)-N-(1,3-diphenyl-prop-2-yn-1-yl)aniline.

3.3.3 Synthesizing a reusable chiral catalyst

Despite the lack of success in the system explained in chapter 3.3.1, which uses YbF_3 nanocrystals together with pybox to drive traditional enantioselective reactions, their role as a nano heater has proven to be successful. Therefore, we decided to modify our catalyst to encompass both functions, a chiral catalyst that could act as a photothermal nano heater.

We attempted a similar approach in the study done by Chao Jun Li's group.[20] We coated our nanocrystals will a layer of silica first to protect the YbF_3 nanocrystals from possible degradation during the reaction. From figure 23 it is evident that the YbF_3 nanocrystals have been coated with a layer of silica coating with an average length of 13.17 ± 1.51 nm and the distribution for the thickness is seen in figure 24.

Subsequently, to functionalize the outer layer of the silica with iPr-pybox it has to be pre-functionalized with NH_2 groups in order for iPr-pybox to be linked on to the outer silica layer. FTIR was use to verify that the outer layer of silica is coated with NH_2 groups and comparisons were made between the before and after spectra in figure 25.

On the black spectrum, the peak at 1600 cm^{-1} shows C=O stretching of carboxylate ions. 1714 cm^{-1} represents– C=O stretching of saturated carboxylic acids and 2924cm^{-1} and 2852cm^{-1} shows C-H stretching of methyl groups. These peaks indicated the presence of oleic acid. After coating and functionalizing the surface with NH_2 groups, peaks are observed at 1635 cm^{-1} indicating N-H bend of primary amines and the large peak at 3421cm^{-1} shows N-H stretching of primary amines. This shows that YbF_3 nanocrystals have been coated and functionalized with NH_2 groups on the surface.

After coating, the surface must be functionalized with iPr-pybox to afford the desired catalyst shown in figure 26.

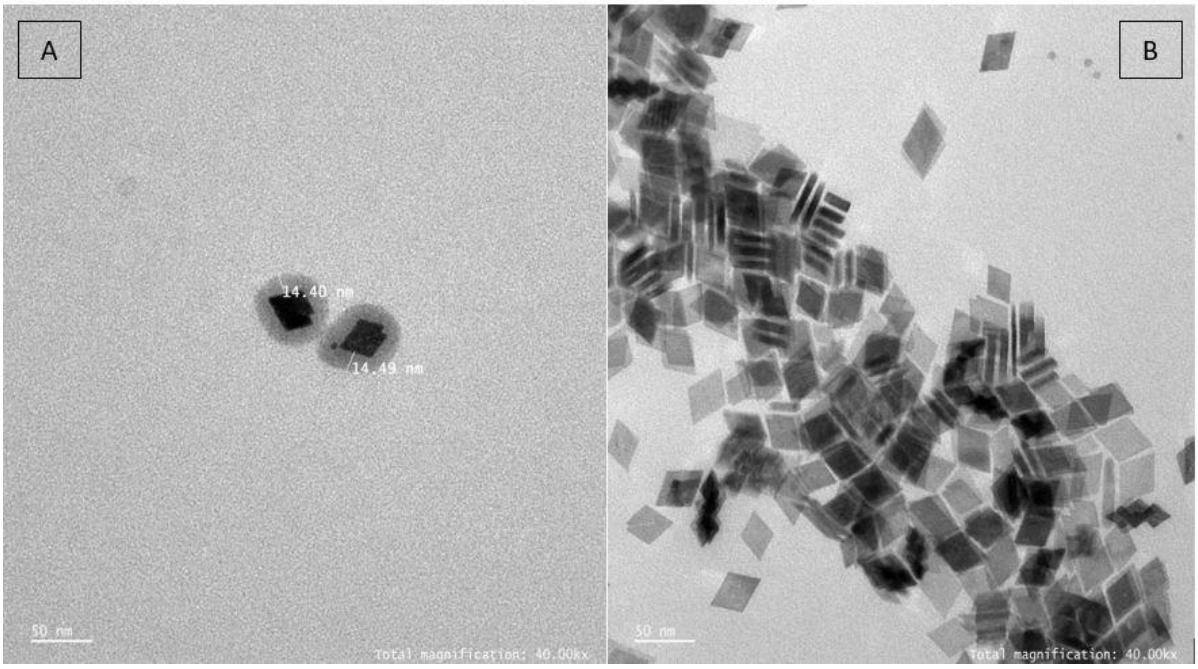

Figure 23: (A) YbF3 nanocrystals after silica coating, (B) YbF3 nanocrystals before silica coating.

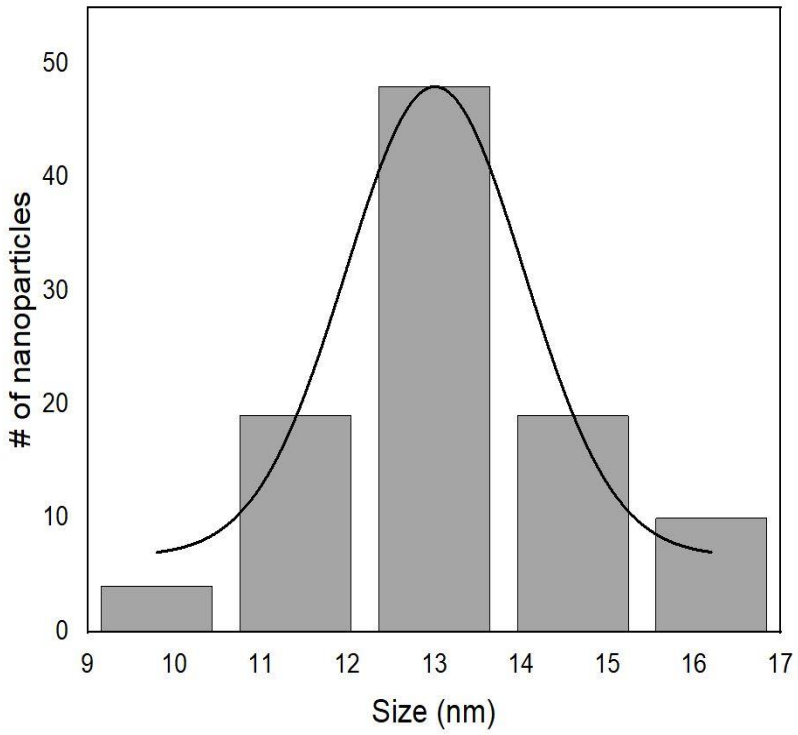

Figure 24: Size distribution for the thickness of Silica coating on nanocrystal.

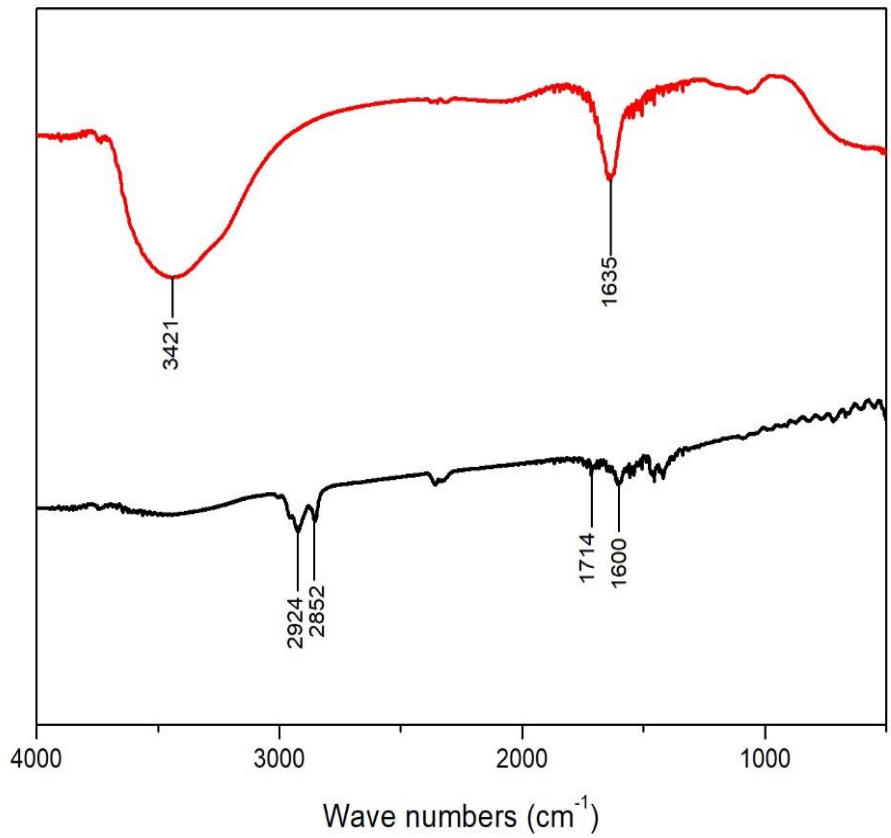

Figure 25: FTIR spectrum of Functionalizing the outer layer of the silica with NH2 groups. (RED) is after coating the YbF_3 nanocrystals with silica and functionalizing the silica layer with NH_2 groups, (**BLACK**) is before functionalizing and silica coating of the YbF_3 nanocrystals.

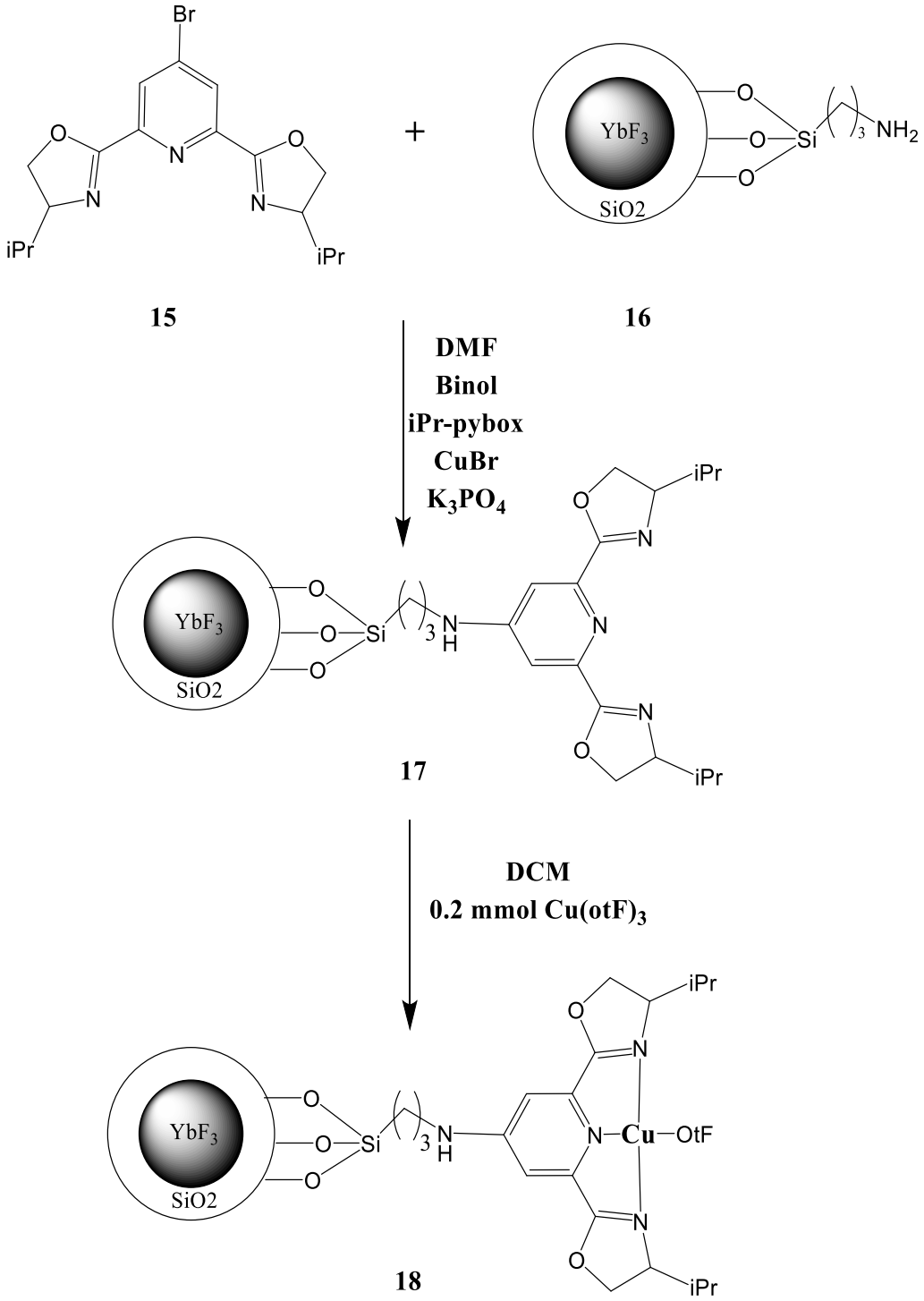

Figure 26: Reaction schematics to obtain desired catalyst (3)

To form the desired catalyst **18** as shown in figure 26, a CuBr/BINOL-catalyzed N-arylation reaction was carried out using commercially available compound **15** seen in figure 26 and nanocrystals **16** that was synthesized earlier. To ensure that the linkage is present and nanocrystal **17** in figure 26 was formed, florescence emission spectroscopy was used to

ascertain the presence of the linkage. Both, the absorption and emission spectrum for iPr-pybox was obtained to use for comparison purposes as shown in figures 27 and 28, respectively.

From figure 29 below, a broad peak at approximately 410 nm is seen in the sample after linkage whilst there is no characteristic peak is seen in the sample prior to linkage. This suggests that that iPr-pybox has indeed linked onto the nanocrystal and forming the desired catalyst nanocrystal **17**. Subsequently, Cu(otF) is coordinated onto nanocrystals **17** to form the chiral catalyst **18**.

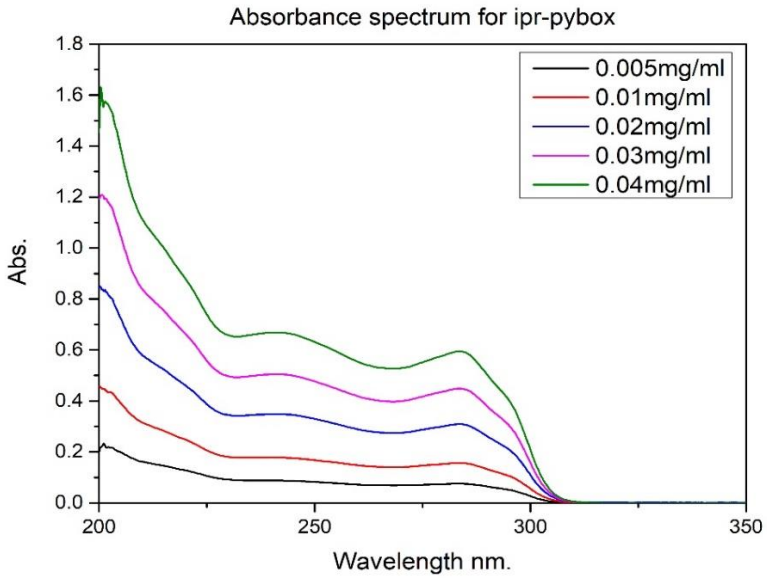

Figure 27: Absorption spectrum of iPr-pybox

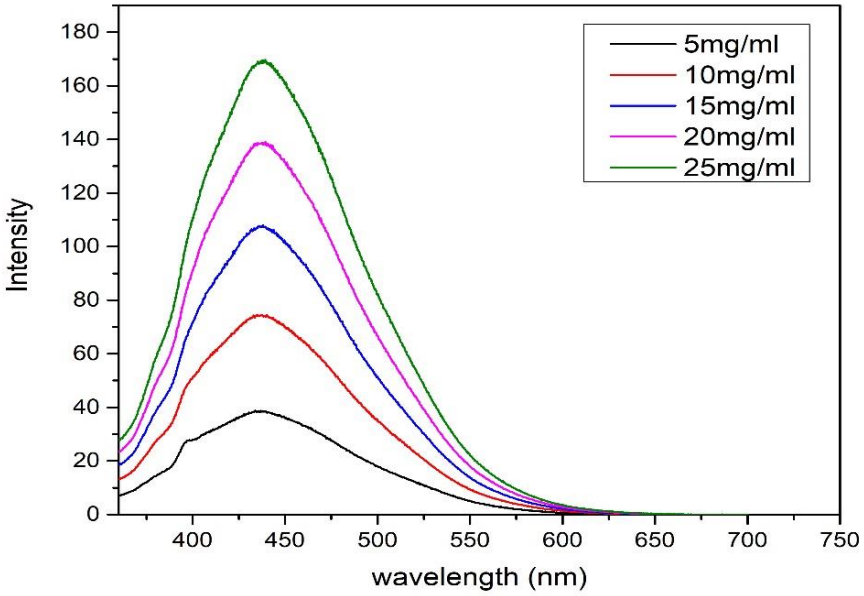

Figure 28: Emission spectrum of iPr-pybox

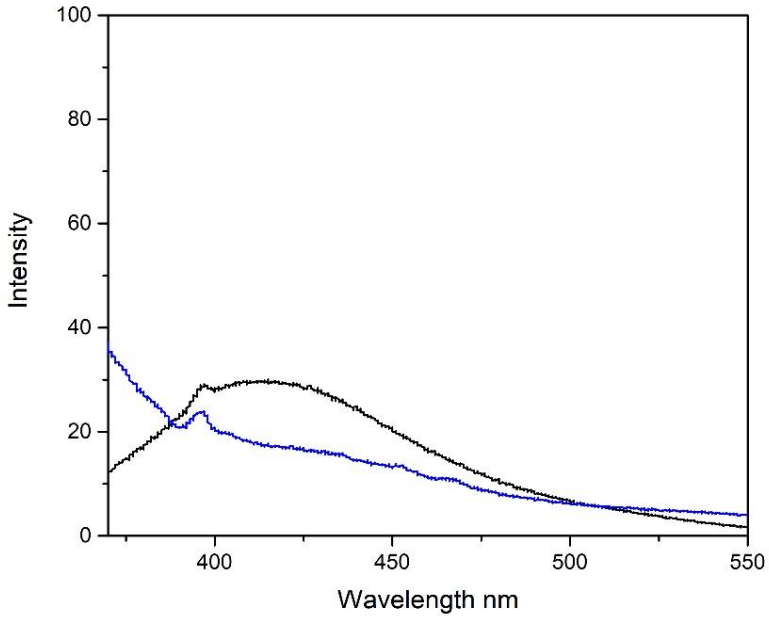

Figure 29: Emission spectrum of before and after the linkage of iPr- Pybox on to the nanocrystals, (BLACK) is after the linkage which belongs to compound 17 in figure 26. and (BLUE) is before the linkage which belongs to compound 16 in figure 26.

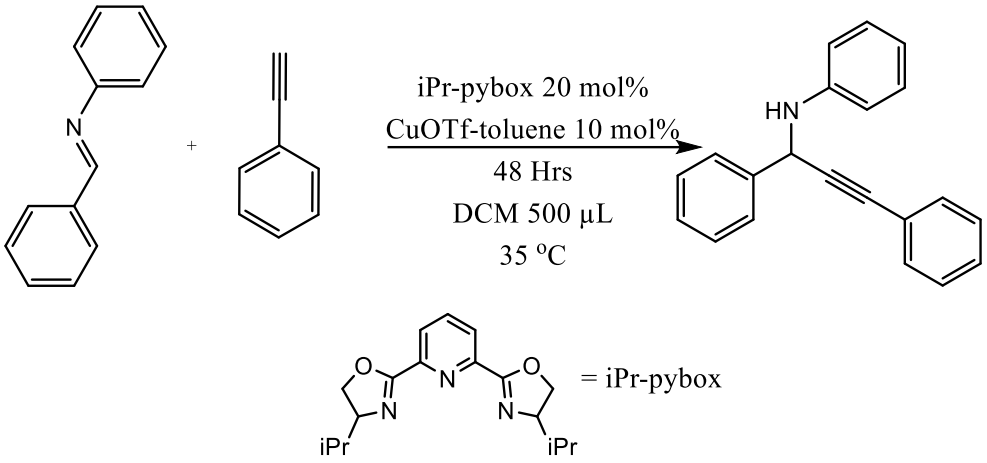

Table 6: Coupling reaction between imine and alkyne at various conditions.

Entry	Yield (%)	EE(%)
1[a]	88	0
2[b]	86	75
3[c]	72	0

a) Reaction was carried out only using 0.02 mmol of CuOTf-toluene

b) Reaction carried out using 0.02 mmol of CuOTf-toluene with 0.02 mmol of iPr-pybox

c) Reaction was carried out using chiral catalyst **18** as shown in figure 26

d) For NMR spectrum refer to figures S50-S52 in appendix.

In general, this reaction between phenyl acetylene and N-Benzylideneaniline was carried out in DCM at 35 °C. However, for Entry 1 and 2 Copper(I) trifluoromethanesulfonate toluene complex was used as the catalyst, in entry 2 iPr-pybox was also used which resulted in enantiomeric excess. For entry 3, the chiral catalyst 18 in figure 26 was used as the catalyst instead of Copper(I) trifluoromethanesulfonate toluene complex and no iPr-pybox was used in entry 3.

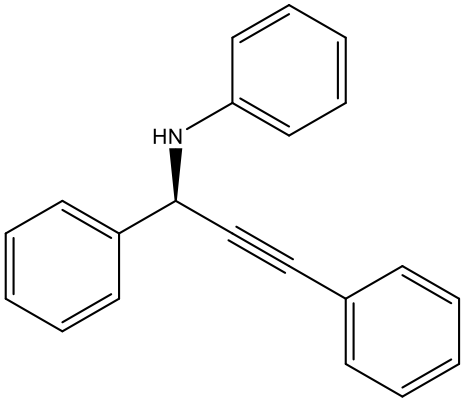

(R)-N-(1,3-diphenyl-prop-2-yn-1-yl)aniline

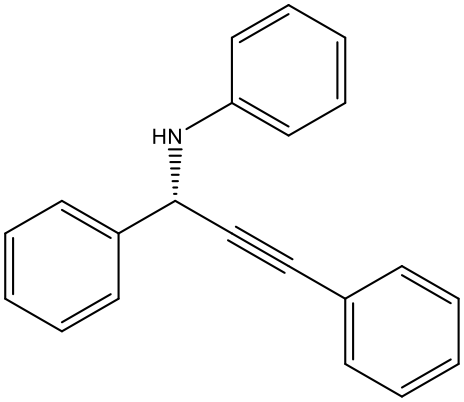

(S)-N-(1,3-diphenyl-prop-2-yn-1-yl)aniline

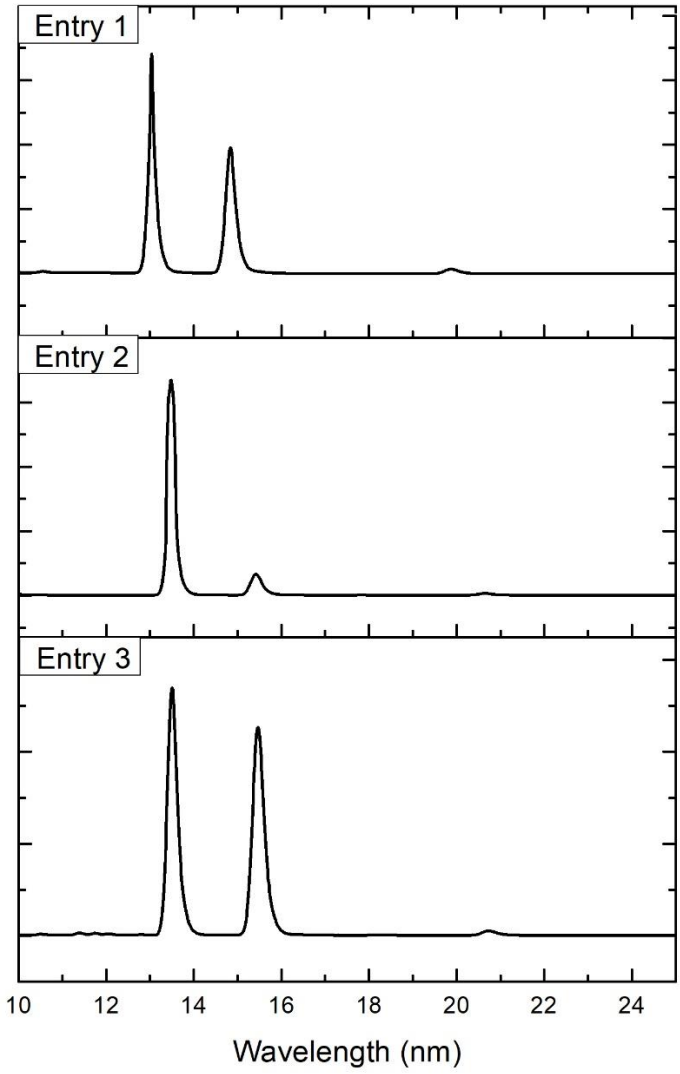

Figure 30: HPLC spectrum for reaction shown in table 6. The peak with retention time of 13.5 mins belong to (R)-N-(1,3-diphenyl-prop-2-yn-1-yl)aniline while the peak with retention time of 15.5 mins belong to (S)-N-(1,3-diphenyl-prop-2-yn-1-yl)aniline.

The reaction that used only Copper(I) trifluoromethanesulfonate toluene complex as a catalyst achieved a yield of 88 % (entry 1 in table 6). The reaction that use Copper(I) trifluoromethanesulfonate toluene complex together with iPr-pybox obtained a yield of 86 % and achieved an enantiomeric excess of 75 % (entry 2 in table 6). From entry 2 in table 6, we know that iPr-pybox is a suitable chiral ligand to induce enantioselectivity for the reaction.

However, although the nano catalyst gave a yield of 72% (entry 3 shown in table 6), no enantiomeric excess was seen as shown in table 6 and figure 30 above. This suggests that the chiral catalyst **18** synthesized lacked the ability to confer enantioselectivity to the reaction.

One plausible hypothesis could be due to a lack of chiral environment, likely attributed by insufficient amount of iPr-pybox on the surface of the silica coated nanocrystals. In order to verify this, we used Uv-Vis absorption spectroscopy to calculate the amount of iPr-pybox participating in the reaction. From figure 31 below, it is found that there is only 0.02 mg of ipr-pybox in the sample. The sample was prepared by diluting 15 µL of YbF_3 linked with iPr-pybox into a 1 mL solution.

Therefore, the amount of iPr-pybox $= \frac{1000}{15} \times\ 0.02 = 1.33$ mg

From the value of 1.33 mg calculated above it is clear that there is not enough iPr-pybox linked onto the YbF_3 nanocrystals. This is because in reactions that was ran 13 mg of iPr-pybox is needed to induce enantioselectivity. Thus, no enantiomeric excess was observed even though there was a yield of 72 %. The reason for the high yield of 72 % could be due to the presence of free Copper(I) trifluoromethanesulfonate that did not coordinate to the iPr-pybox on the nanoparticle. These free Copper(I) trifluoromethanesulfonate are those that could not be washed away when Copper(I) trifluoromethanesulfonate was coordinated to the iPr-pybox that was linked onto the nanocrystal. As a result, these free Copper(I) trifluoromethanesulfonate can catalyst the reaction but do not possess the chiral environment for enantioselectivity. The

absence of enantioselectivity is not exactly due to lack of catalyst but due to the lack of chiral ligands on the surface of the chiral ligand.

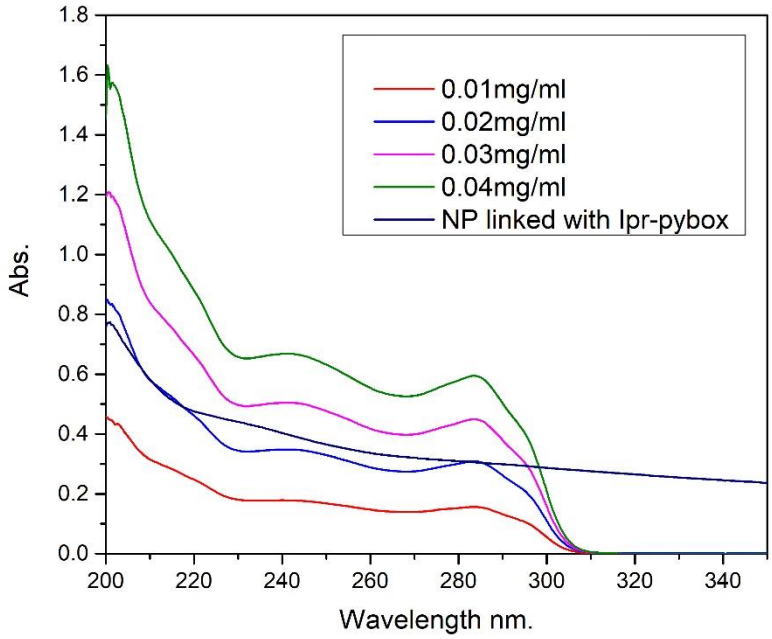

Figure 31: Absorption spectrum of iPr-pybox and YbF3 nanocrystal linked with iPr-pybox

3.4 Conclusion

In conclusion, this chapter has shown that without modifying YbF_3 nanoparticles it is not possible to achieve enantioselectivity even with the use of chiral ligands. This chapter has also show that YbF_3 can be used as a Nano heater in reactions to increase the rate of reaction. Lastly, although we did not manage to achieve enantioselectivity in this chapter but if we manage to link more chiral ligands on the surface of the nanocrystals it will be possible to achieve enantioselectivity.

Chapter 4 Conclusion and future works

4.1 Conclusion

To summarize, this thesis has reported the synthesis of YbF_3 nanocrystals via the co-precipitation method. The synthesized YbF_3 nanocrystals were well characterized with TEM and XRD. Through the ring opening reaction of epoxides with amines catalyzed by the YbF_3 nanocrystals, it's evident that lanthanide based nanocrystals have the ability to be excellent Lewis acid catalysts. Additionally, they are able to provide a bonus photothermal effect which can be used to activate less reactive precursors.

If we manage to develop this series of lanthanide base nanocrystals capabilities as catalyst further it will be extremely beneficial to the society and environment. These nanocrystals can be recycled for many times and no lose its capabilities as a catalyst, this will be a more sustainable way to catalyze reaction and can reduce the harmful impact on environment. Concurrently, these nanocrystal catalyst utilizes NIR light which reactants do not absorb so we can prevent photodegradation of the reactants which leads to a more efficient reaction. With the increase in efficiency it will lead to large cost saving over time in the industry.

The surface modification of these YbF_3 nanocrystals offers the potential for a chiral catalyst that is able to provide both photothermal effect and enantioselectivity. Since we know that we can link chiral ligands onto the surface of the nanocrystals, this means that if we are able to link more than what was presented in the thesis it means that the is a chance to confer enantioselectivity. However, more research has to be carried out to achieve that.

4.2 Future works

Future works on the project outlined in this thesis will be to optimize the surface modification done to the silica coated YbF_3 nanocrystals mentioned in Chapter 3. This will create a stronger chiral environment so that enantiomeric ally pure products can be achieved.

Another possible future work could be the expansion of the library of reactions that lanthanide nanocrystals are capable of. This will explore the tolerance towards various functional groups and other unreactive precursors in reactions catalyzed by lanthanide based nanocrystals.

Appendix

S1. Characterization of Products

s = singlet, d = doublet, t = triplet, m = multiplet these are the abbreviations used in this section.

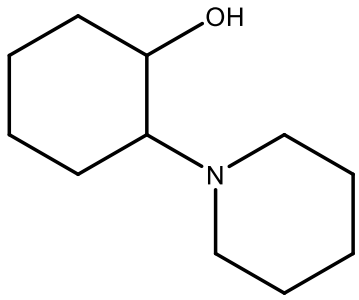

2-(piperidin-1-yl)cyclohexan-1-ol. ^{1}H NMR (400 MHz, Chloroform-d) δ 3.37-3.31 (m, 1H), 2.68-2.63 (m, 2H), 2.31 (bs, 2H), 2.15-2.08 (m, 2H), 1.78-1.74 (m, 2H), 1.70 – 1.67 (m, 1H), 1.62-1.53 (m, 4H), 1.44 (d, J = 8 Hz, 2H), 1.28-1.11 (m, 5H).

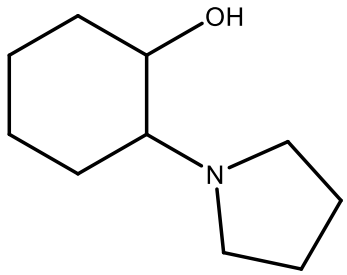

2-(pyrrolidin-1-yl)cyclohexan-1-ol. ^{1}H NMR (400 MHz, Chloroform-d) δ 3.32 (td, J = 8.0, 4.0 Hz, 1H), 2.69-2.64 (m, 2H), 2.55-2.53 (m, 2H), 2.47-2.42 (m, 1H), 2.12-2.08 (m, 1H), 1.77 – 1.69 (m, 7H), 1.29-1.16 (m, 5H)

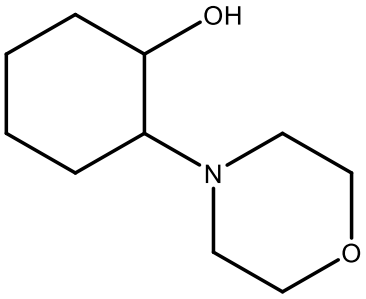

2-morpholinocyclohexan-1-ol. ^{1}H NMR (400 MHz, Chloroform-d) δ 3.75-3.65 (m, 4H), 3.36 (td, J = 8.0, 4.0 Hz, 1H), 2.74-2.68 (m, 2H), 2.44-2.38 (m, 2H), 2.20-2.10 (m, 2H), 1.82-1.77 (m, 2H), 1.71-1.69 (m, 1H),1.29-1.17 (m, 4H)

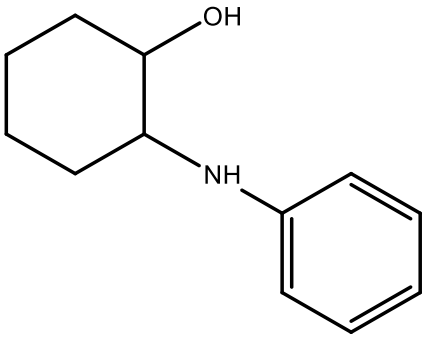

2-(phenylamino)cyclohexan-1-ol. ^{1}H NMR (400 MHz, Chloroform-d) δ 7.18 (t, j=8.0, 2H), 6.76-6.69 (m, 3H), 3.34 (td, J = 12.0, 4.0 Hz, 1H), 3.14 (td, J = 10.0, 4.0 Hz, 1H), 2.14-2.10 (m, 2H), 1.80-1.69 (m, 2H), 1.41-1.25 (m, 4H),1.15-1.00 (m, 1H)

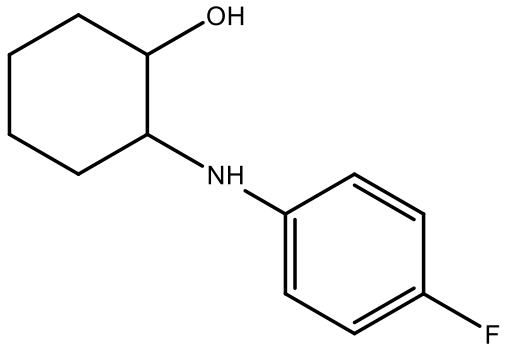

2-((4-fluorophenyl)amino)cyclohexan-1-ol. ^{1}H NMR (400 MHz, Chloroform-d) δ 6.90-6.82 (m, 2H), 6.66-6.59 (m, 2H), 3.34 (td, J = 8.0, 4.0 Hz, 1H), 3.02 (qd, J = 8.0, 4.0 Hz, 1H), 2.13-2.07 (m, 2H), 1.79-1.68 (m, 2H), 1.32-1.24 (m, 3H),1.07-0.98 (m, 1H)

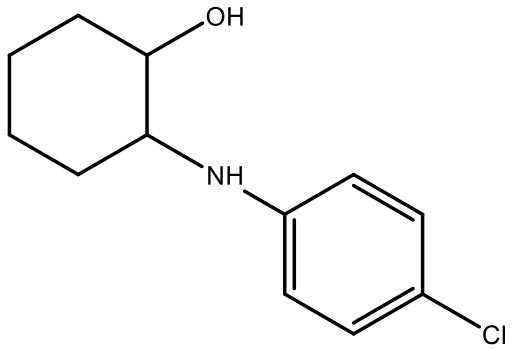

2-((4-chlorophenyl)amino)cyclohexan-1-ol. ^{1}H NMR (400 MHz, Chloroform-d) δ 7.11 (d, j = 8.0 Hz, 2H), 6.61 (d, J = 4.0 Hz, 2H), 3.34 (td, J = 12.0, 4.0 Hz, 1H), 3.07 (qd, J = 8.0, 4.0 Hz, 1H), 2.13-1.99 (m, 2H), 1.79-1.70 (m, 2H), 1.33-1.25 (m, 3H),1.10-0.99 (m, 1H)

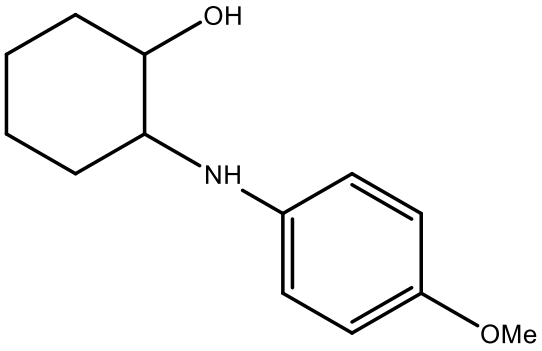

2-((4-methoxyphenyl)amino)cyclohexan-1-ol. ^{1}H NMR (400 MHz, Chloroform-d) δ 6.79-6.64 (m, 4H), 3.74 (s, 3H), 3.33 (td, J = 12.0, 4.0 Hz, 1H), 3.00 (qd, J = 8.0, 4.0 Hz, 1H), 2.14-2.07 (m, 1H), 1.77-1.70 (m, 3H), 1.37-1.24 (m, 3H), 1.06-0.96 (m, 1H)

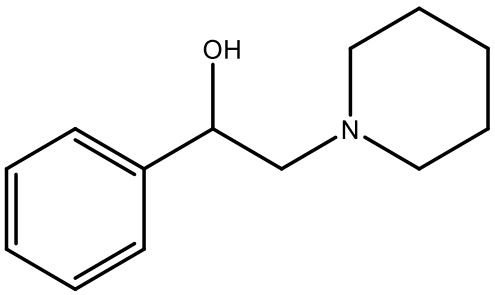

1-phenyl-2-(piperidin-1-yl)ethan-1-ol. ^{1}H NMR (400 MHz, Chloroform-d) δ 7.36-7.33 (m, 5H), 4.70 (dd, J = 12.0, 4.0 Hz, 1H), 2.69 (bs, 2H), 2.50-2.35 (m, 4H), 1.64-1.57 (m, 4H), 1.49-1.45 (m, 2H)

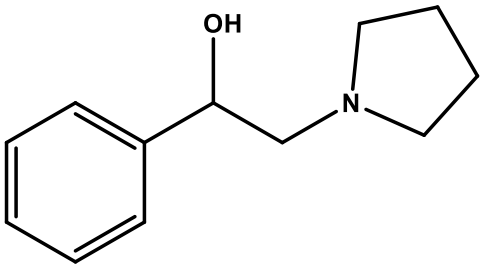

1-phenyl-2-(pyrrolidin-1-yl)ethan-1-ol. ^{1}H NMR (400 MHz, Chloroform-d) δ 7.38-7.31 (m, 5H), 4.69 (dd, J = 12.0, 4.0 Hz, 1H), 2.80-2.74 (m, 3H), 2.55-2.46 (m, 3H), 1.82-1.73 (m, 4H)

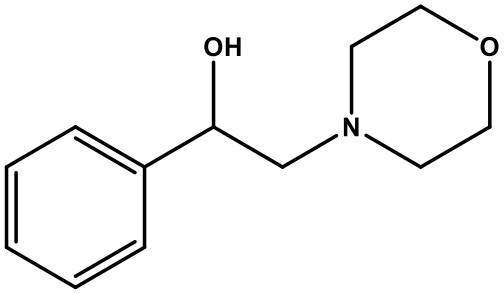

2-morpholino-1-phenylethan-1-ol. ^{1}H NMR (400 MHz, Chloroform-d) δ 7.38-7.27 (m, 5H), 4.76 (dd, J = 12.0, 4.0 Hz, 1H), 3.78-3.70 (m, 4H), 2.75 (bs, 2H), 2.57-2.45 (m, 4H)

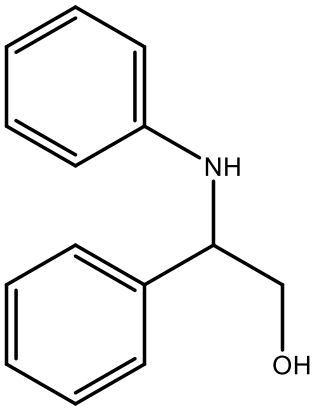

2-phenyl-2-(phenylamino)ethan-1-ol. ^{1}H NMR (400 MHz, Chloroform-d) δ 7.37-7.27 (m, 5H), 7.09 (dd, J = 8.0, 4.0 Hz, 2H), 6.67(tt, J = 8.0, 1.1 Hz, 1H) 6.58-6.55 (m, 2H), 4.51 (dd, j= 4.0, 4.0 Hz, 1H), 3.95 (t,j= 4 Hz, 1H), 3.77 (t, j=10 Hz, 1H)

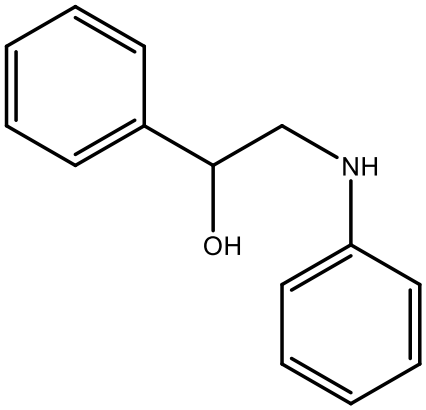

1-phenyl-2-(phenylamino)ethan-1-ol. ^{1}H NMR (400 MHz, Chloroform-d) δ 7.43-7.27 (m, 5H), 7.19 (dd, J = 8.0, 8.0 Hz, 2H), 6.75(tt, J = 4.0, 1.2 Hz, 1H) 6.68 (d, J = 8.0, 2H), 4.92 (dd, J = 8.0, 4.0 Hz, 1H), 3.44 (dd, J = 8.0, 4.0 Hz, 1H), 3.30 (dd, J = 14.0, 12.0 Hz, 1H)

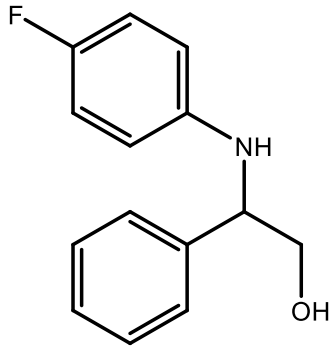

2-((4-fluorophenyl)amino)-2-phenylethan-1-ol. ^{1}H NMR (400 MHz, Chloroform-d) δ 7.35-7.27 (m, 5H), 6.79 (t, J = 10 Hz, 2H), 6.49(dd, J = 8.0, 4.0 Hz, 2H), 4.43 (dd, J = 8.0, 4.0 Hz, 1H), 3.94 (d, J = 8.0 Hz, 1H), 3.73 (dd, j = 12.0, 8.0 Hz, 1H)

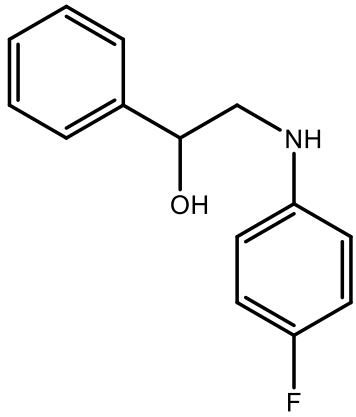

2-((4-fluorophenyl)amino)-1-phenylethan-1-ol. ^{1}H NMR (400 MHz, Chloroform-d) δ 7.40-7.35 (m, 5H), 6.90 (t, J = 10.0 Hz, 2H), 6.62 (dd, J = 12.0 Hz, 4.0, 2H), 4.91 (dd, J = 8.0, 4.0 Hz, 1H), 3.38 (dd, J = 12.0, 4.0 Hz, 1H), 3.26 (dd, J = 12.0, 8.0 Hz, 1H)

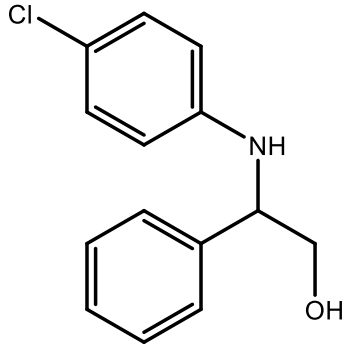

2-((4-chlorophenyl)amino)-2-phenylethan-1-ol. ^{1}H NMR (400 MHz, Chloroform-d) δ 7.34-7.27 (m, 5H), 7.02 (d, J = 12.0 Hz, 2H), 6.47 (d, J = 8.0 Hz, 2H), 4.45 (dd, J = 4.0, 4.0 Hz, 1H), 3.95 (t, J = 6.0 Hz, 1H), 3.76 (bs, 1H)

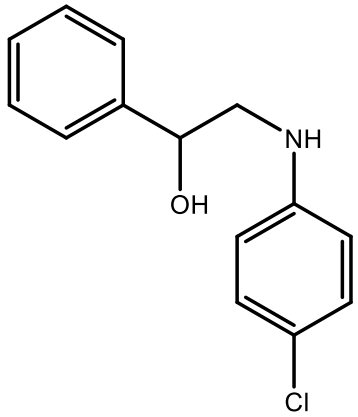

2-((4-chlorophenyl)amino)-1-phenylethan-1-ol. ^{1}H NMR (400 MHz, Chloroform-d) δ 7.40-7.33 (m, 5H), 7.13 (d, J = 8.0 Hz, 2H), 6.58 (d, J = 8.0 Hz, 2H), 4.91 (dd, J = 8.0, 4.0 Hz, 1H), 3.38 (dd J = 16.0, 4.0 Hz, 1H), 3.28 (dd, J = 12.0, 8.0 Hz, 1H)

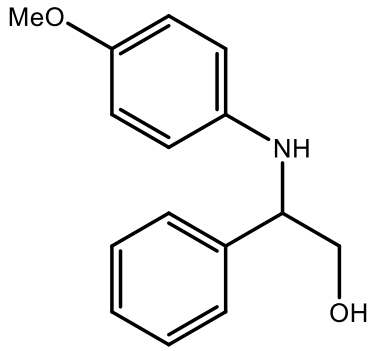

2-((4-methoxyphenyl)amino)-2-phenylethan-1-ol. ^{1}H NMR (400 MHz, Chloroform-d) δ 7.34-7.31 (m, 5H), 6.69 (d, J = 8.0 Hz, 2H), 6.53 (d, J=12.0 Hz, 2H), 4.43 (dd, J = 8.0, 4.0 Hz, 1H), 3.92 (bs, 1H), 3.80 (s, 1H), 3.69 (s, 3H)

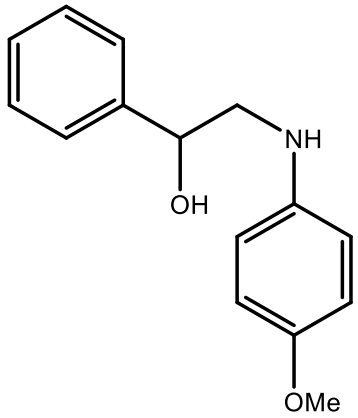

2-((4-methoxyphenyl)amino)-1-phenylethan-1-ol. ^{1}H NMR (400 MHz, Chloroform-d) δ 7.40-7.27 (m, 5H), 6.79 (d, J = 8.0 Hz, 2H), 6.66 (d, J = 12.0 Hz, 2H), 4.9 (dd, J = 8.0, 4.0 Hz, 1H), 3.75 (s, 3H), 3.39 (dd, J = 16.0, 8.0 Hz, 1H), 3.28-3.20 (m, 1H)

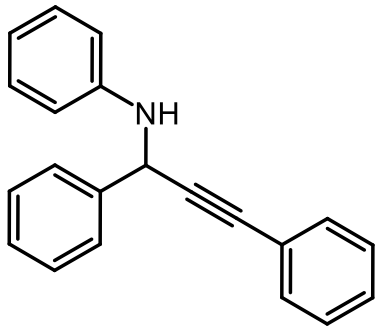

N-(1,3-diphenylprop-2-yn-1-yl)aniline. 1H NMR (400 MHz, Chloroform-d) δ 7.67 (d, J = 8, Hz, 2H), 7.53 (dd, J = 8.0, 1.5 Hz 1H), 7.42-7.40 (m, 4H), 7.36 – 7.34 (m, 1H), 7.29 – 7.25 (m, 2H), 7.23 – 7.19 (m, 2H), 6.80 – 6.77 (m, 3H), 5.50 (s, 1H)

S2. Supplementary NMR spectra

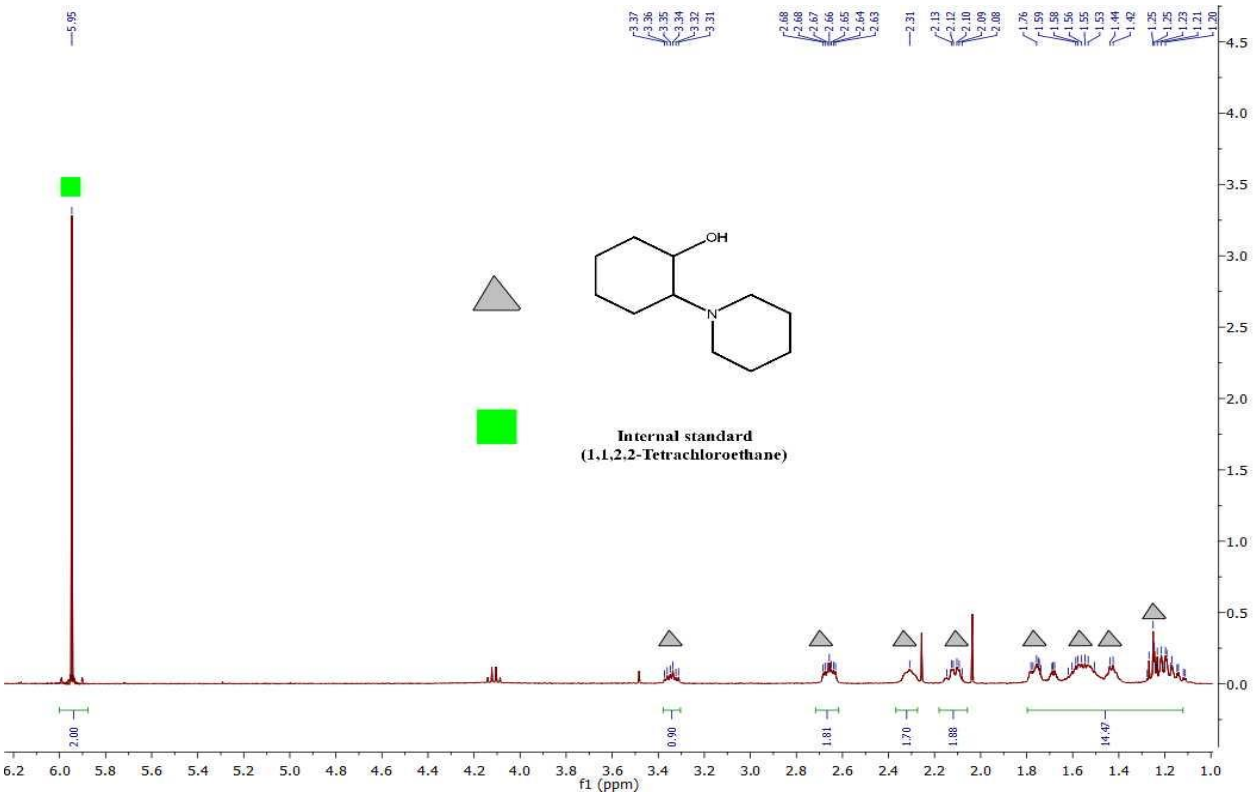

Figure S 1: ^{1}H NMR spectrum for entry 1 in table 1

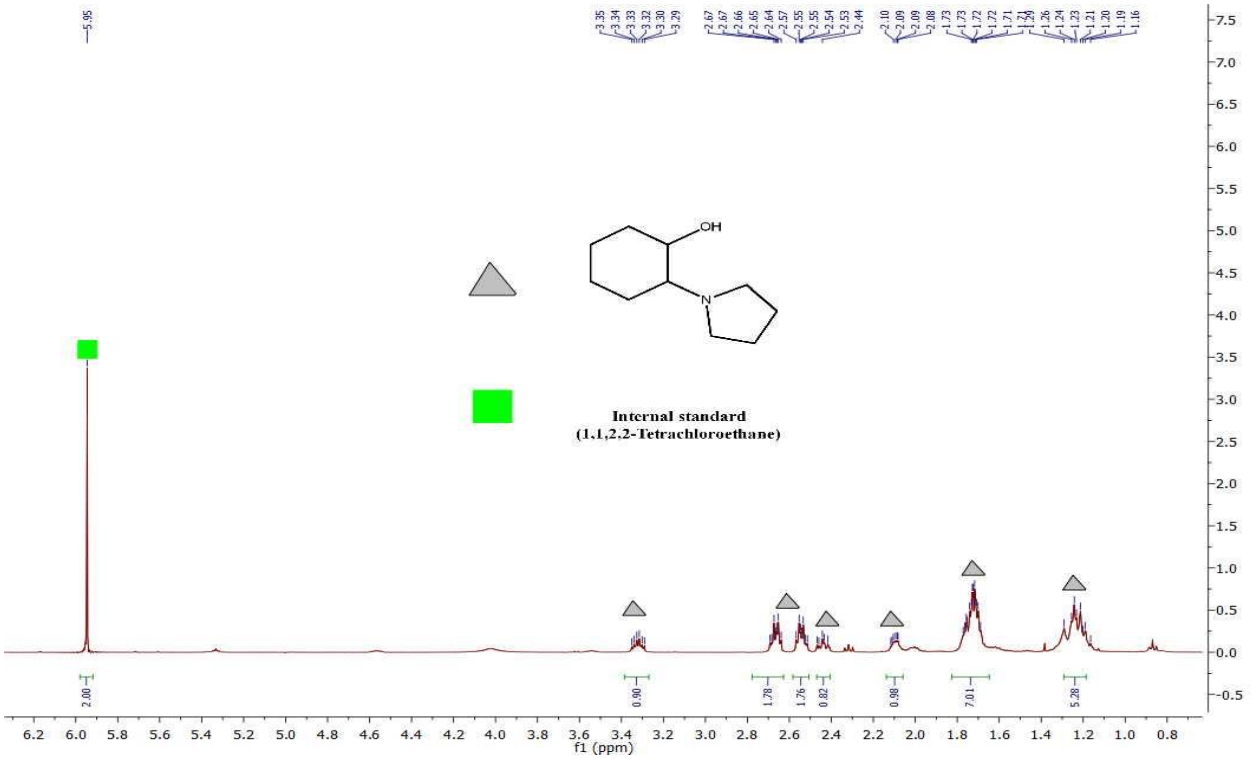

Figure S 2: ^{1}H NMR spectrum for entry 2 in table 1

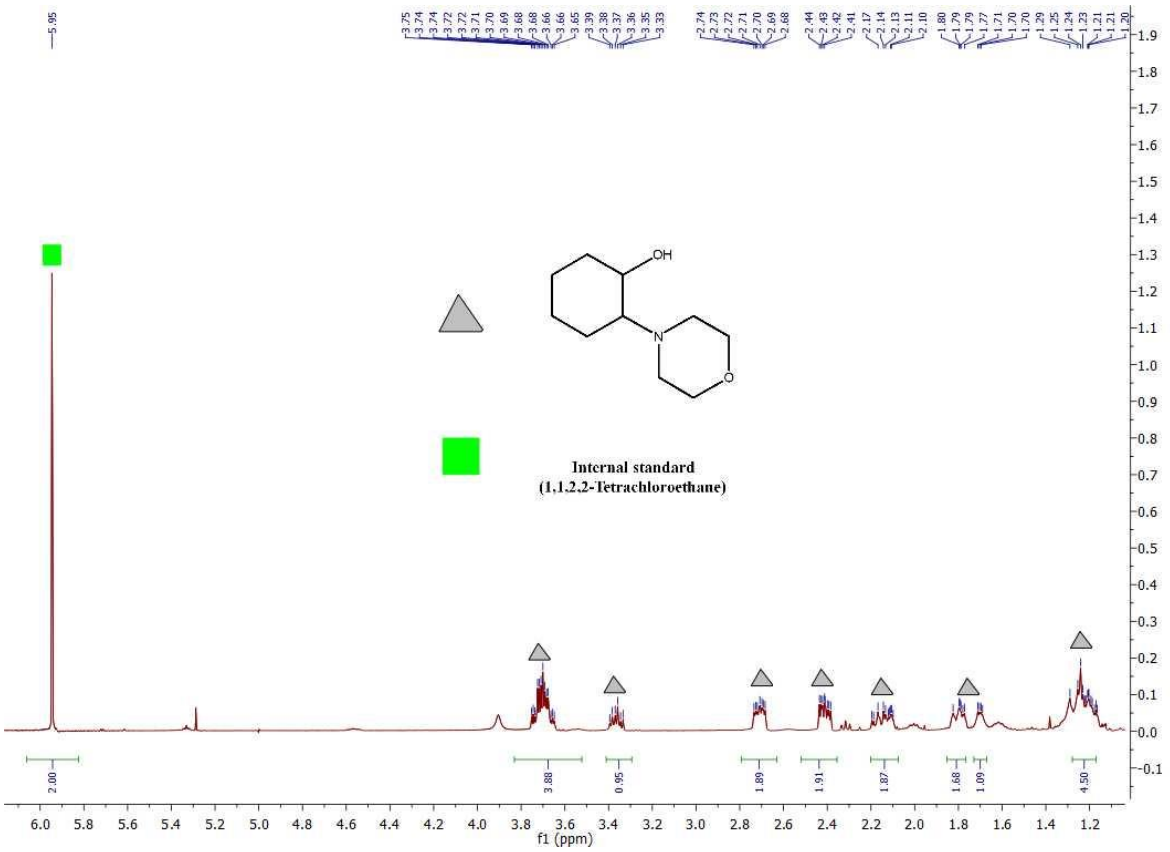

Figure S 3: ^{1}H NMR spectrum for entry 3 in table 1

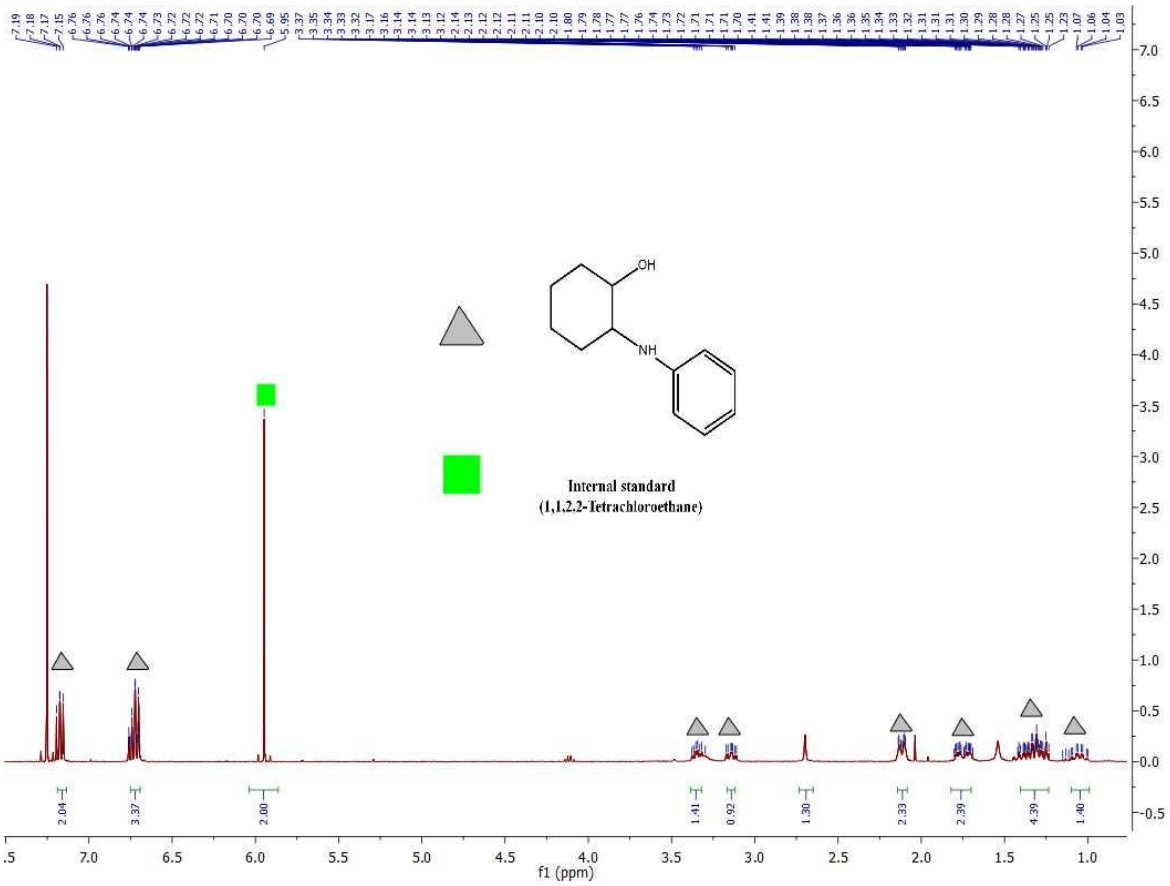

Figure S 4: ^{1}H NMR spectrum for entry 4 in table 1

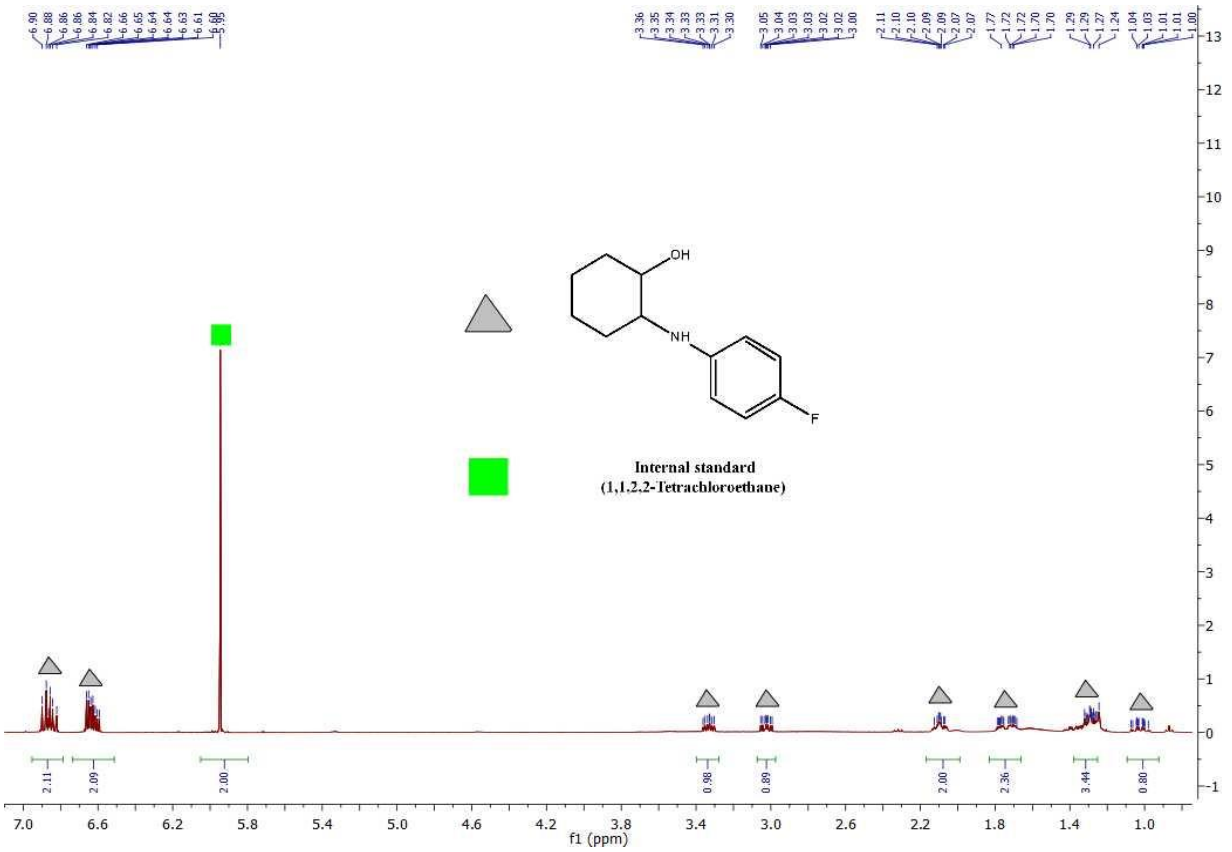

Figure S 5: ^{1}H NMR spectrum for entry 5 in table 1

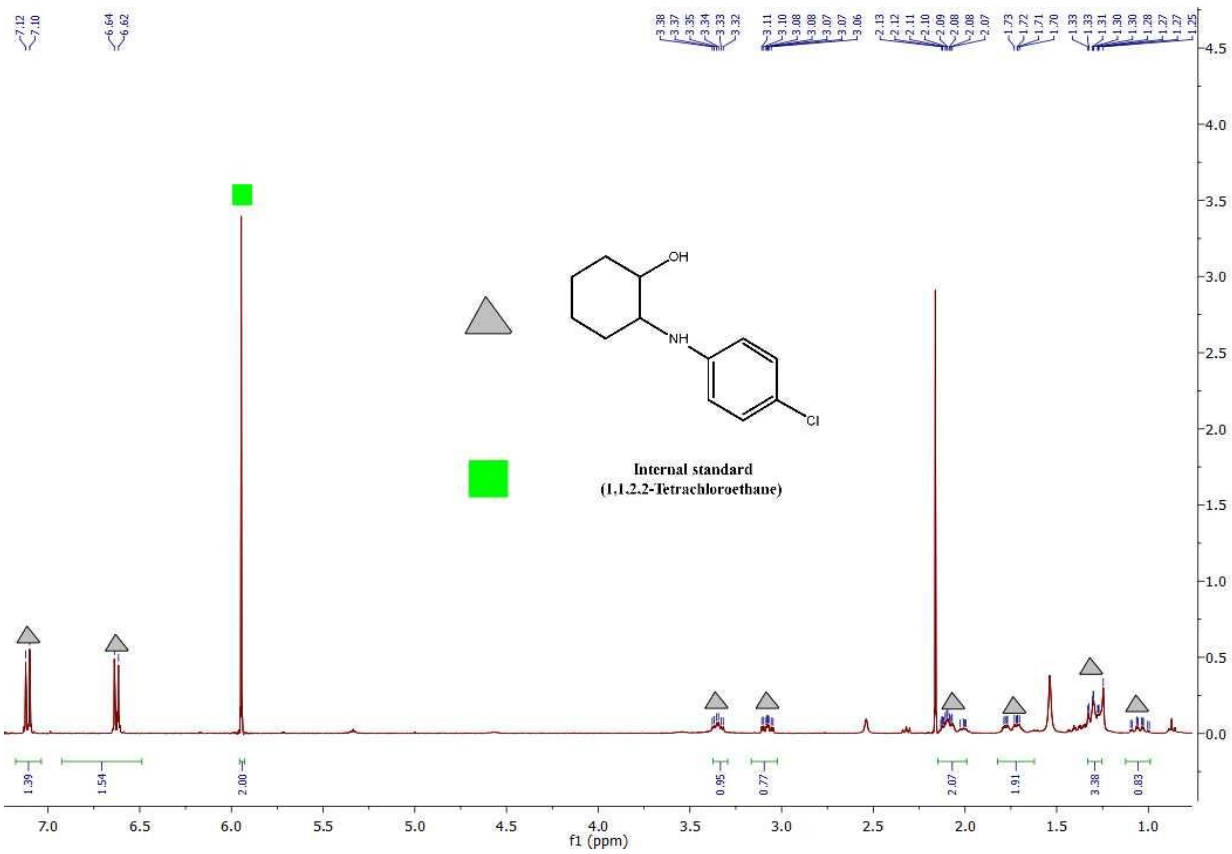

Figure S 6: ^{1}H NMR spectrum for entry 6 in table 1

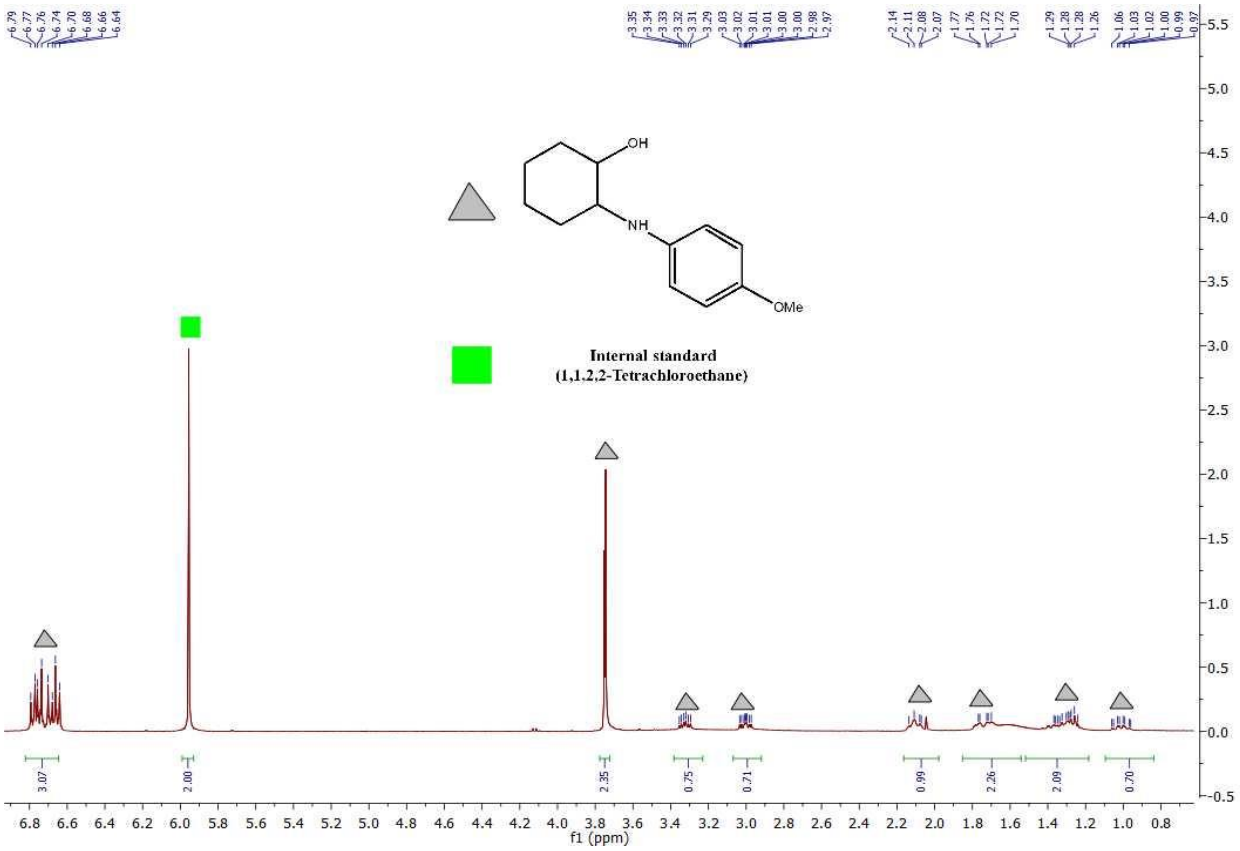

Figure S 7:[1]H NMR spectrum for entry 7 in table 1

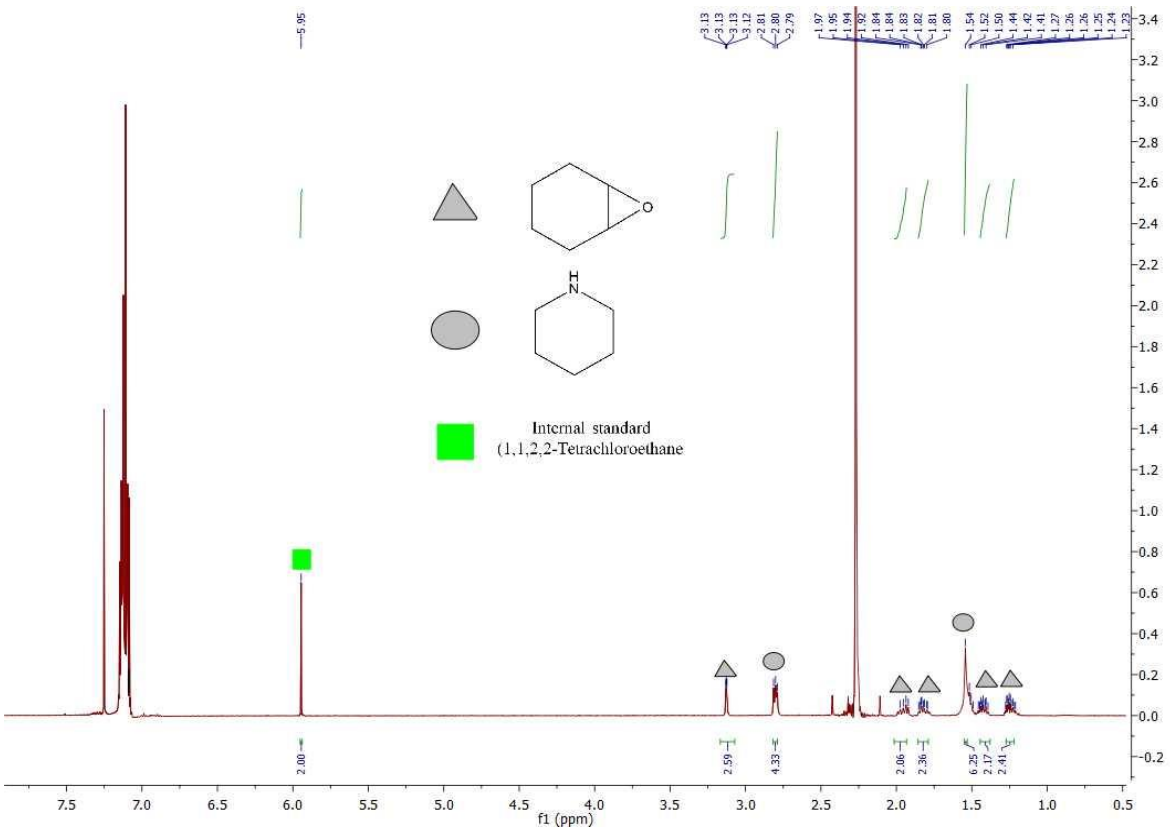

Figure S 8: [1]H NMR spectrum for entry 1[a] in table 2

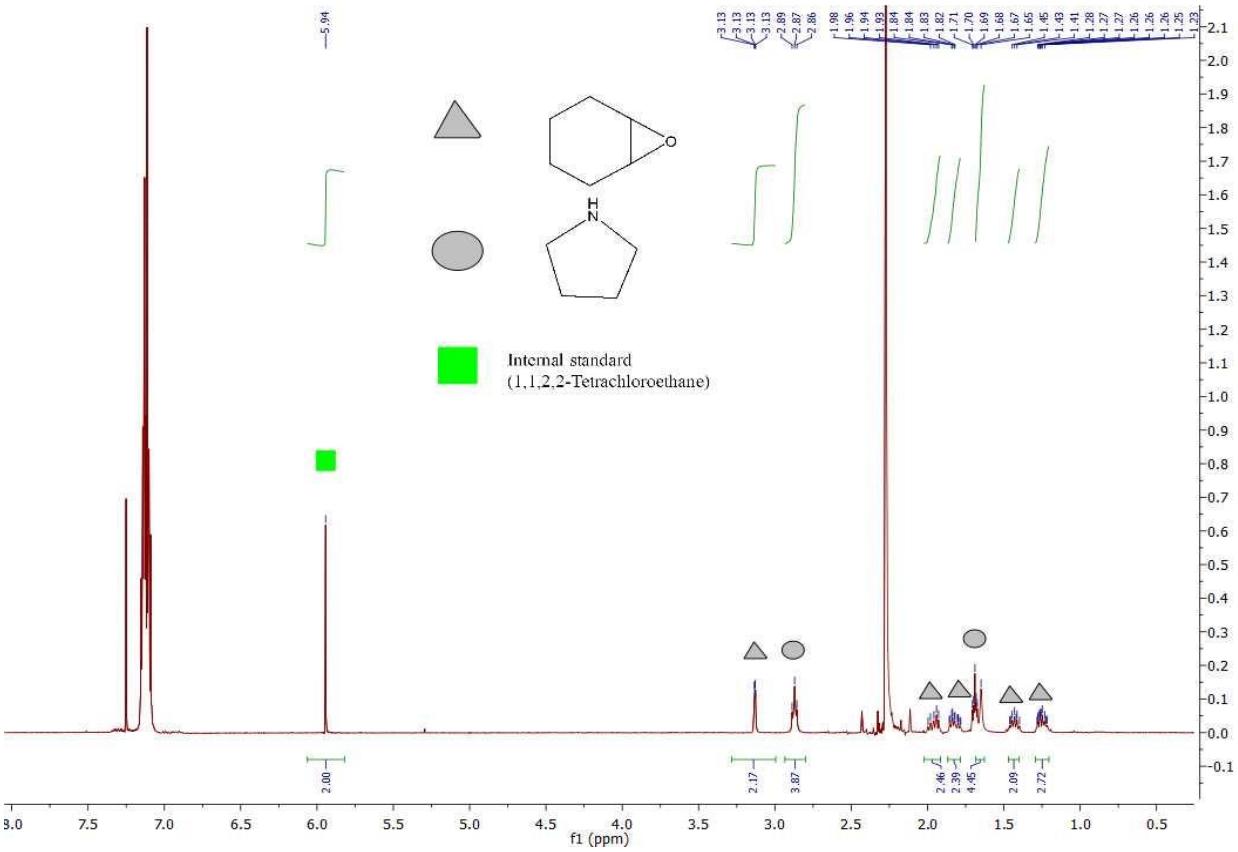

Figure S 9: ^{1}H NMR spectrum for entry 2[a] in table 2

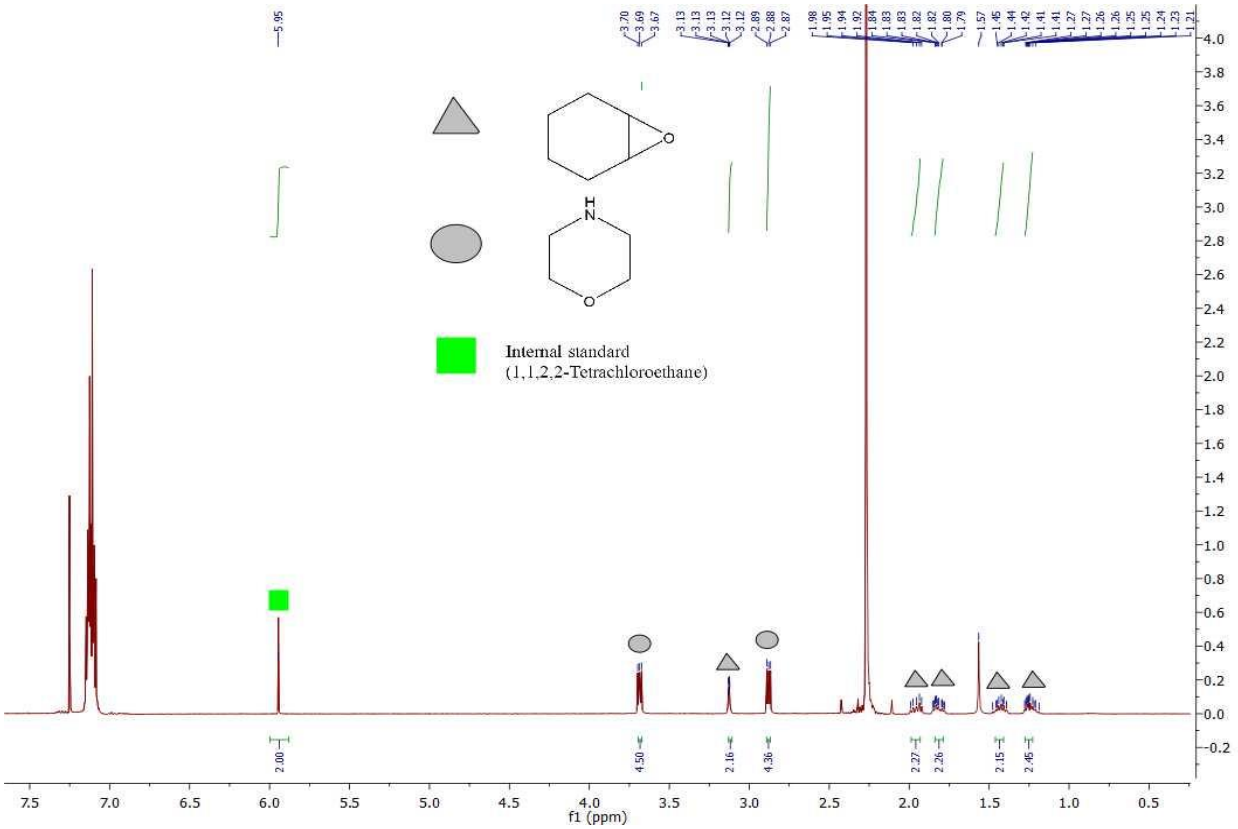

Figure S 10: ^{1}H NMR spectrum for entry 3[a] in table 2

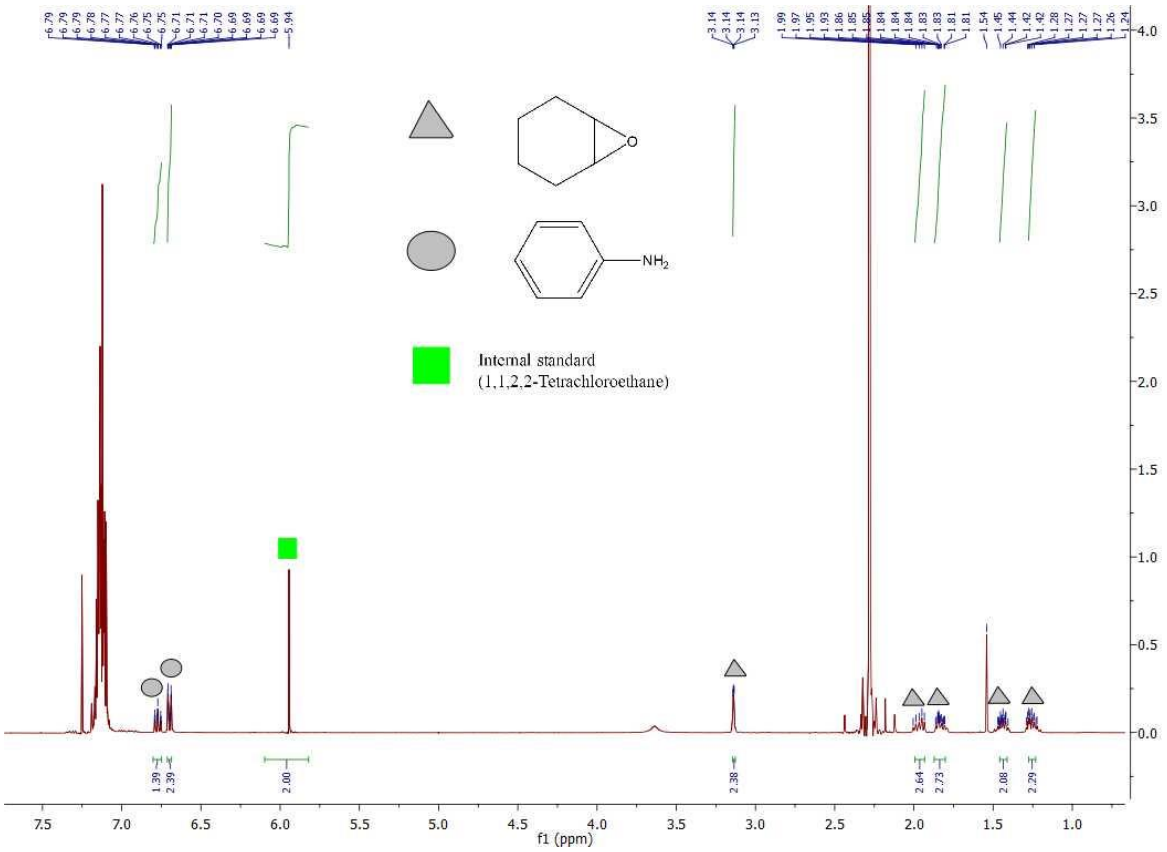

Figure S 11: ^{1}H NMR spectrum for entry 4[a] in table 2

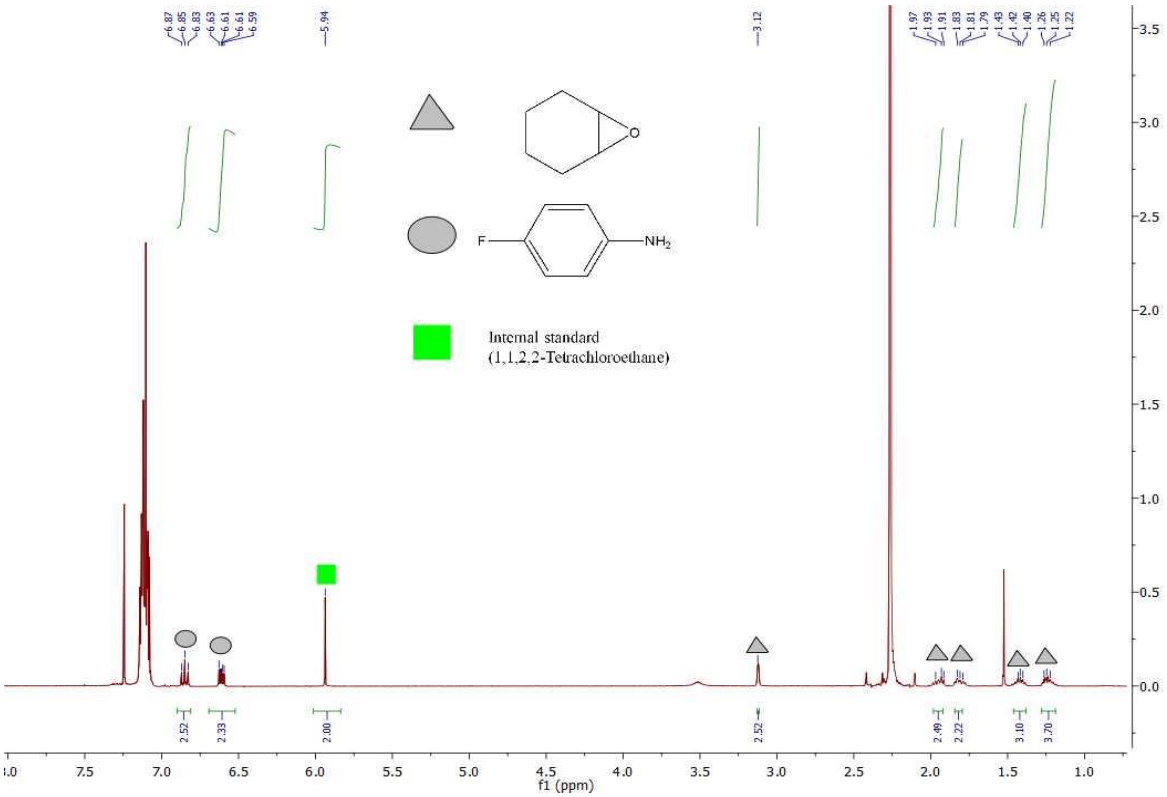

Figure S 12: ^{1}H NMR spectrum for entry 5[a] in table 2

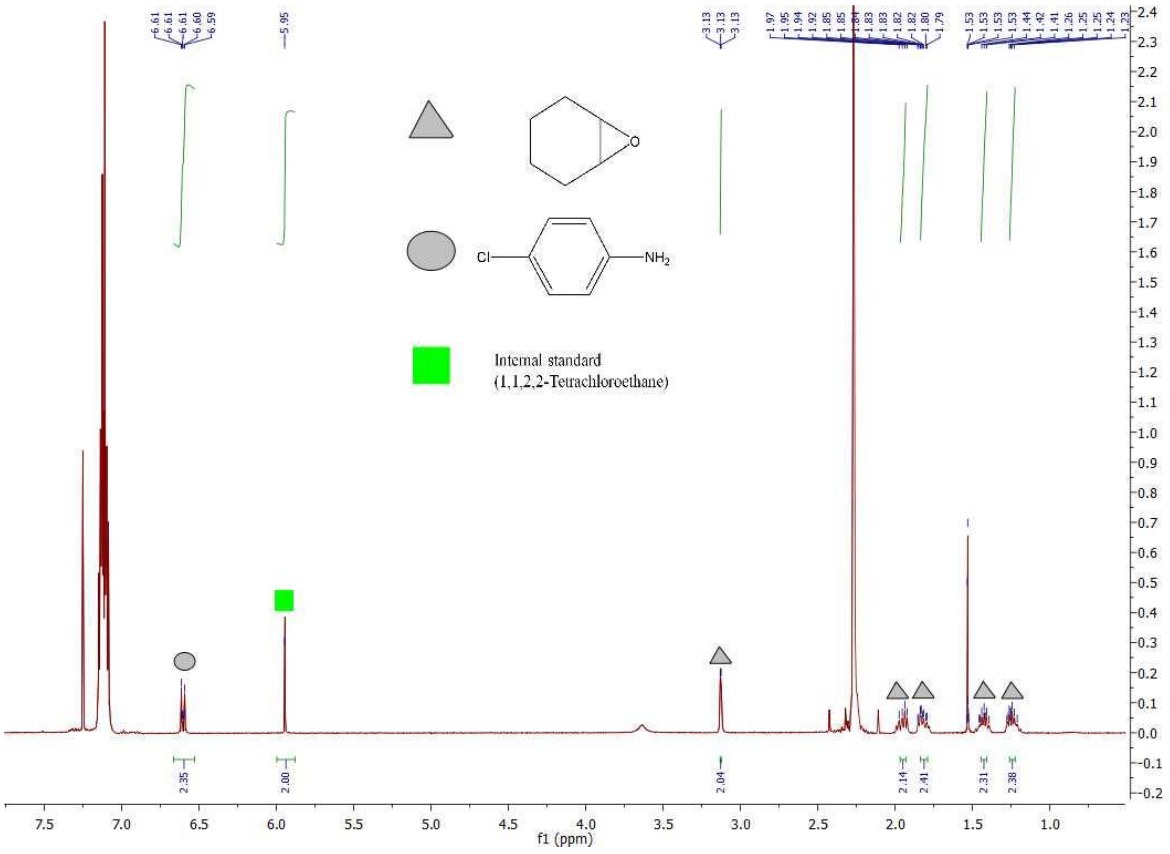

Figure S 13: ^{1}H NMR spectrum for entry 6[a] in table 2

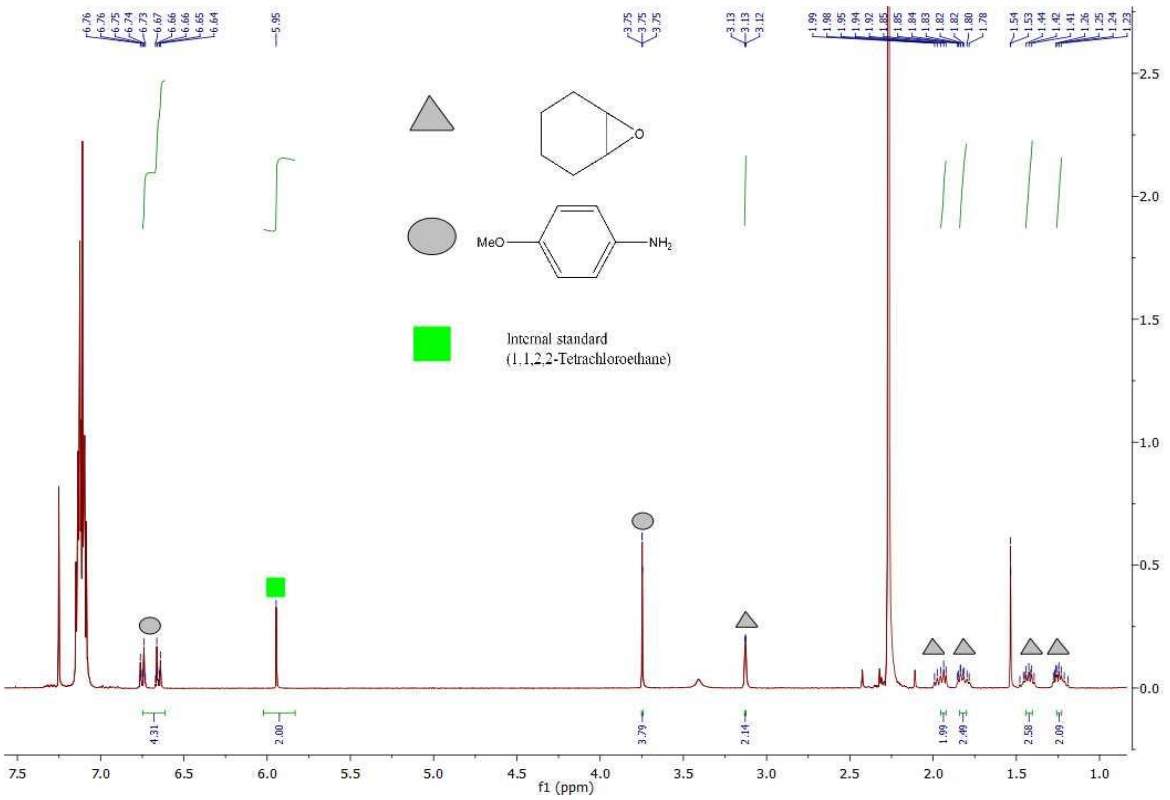

Figure S 14: ^{1}H NMR spectrum for entry 7[a] in table 2

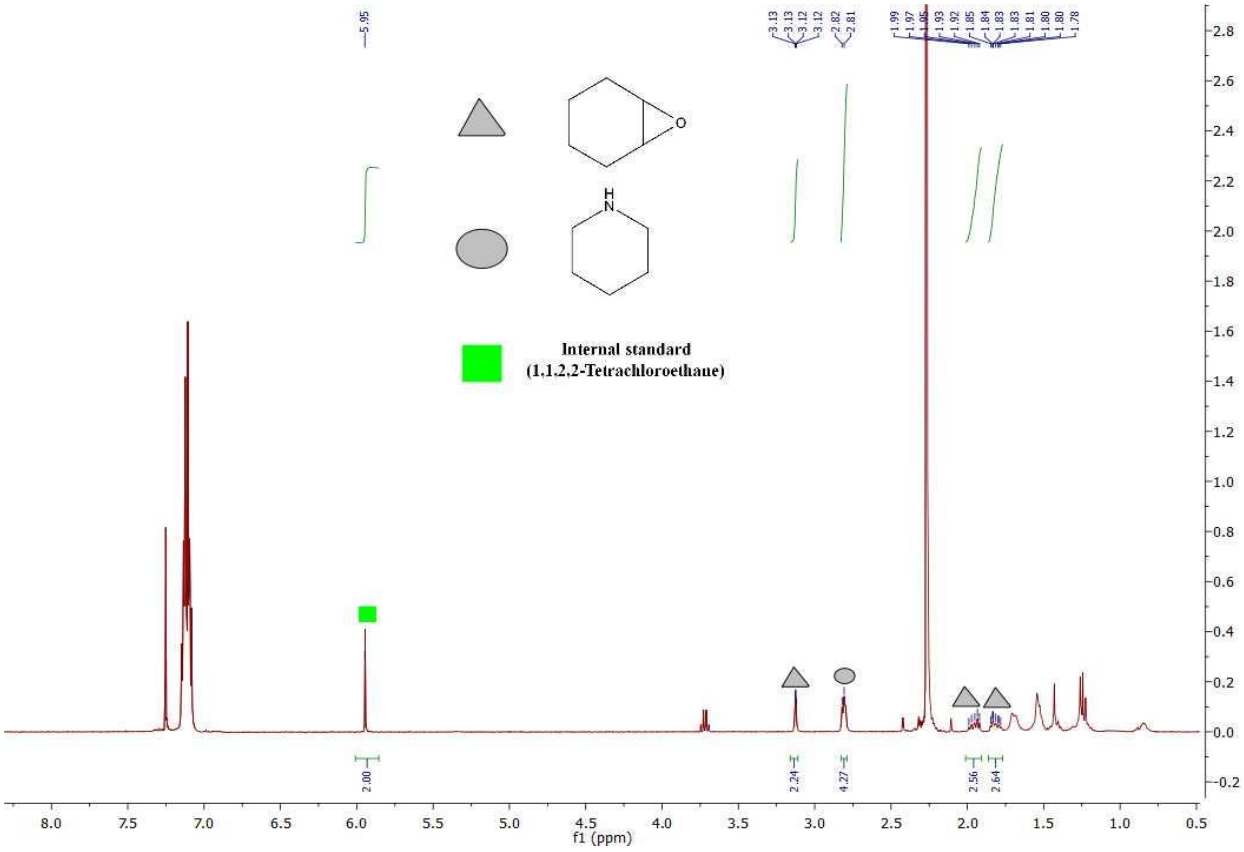

Figure S 15: ^{1}H NMR spectrum for entry 1^{b} in table 2

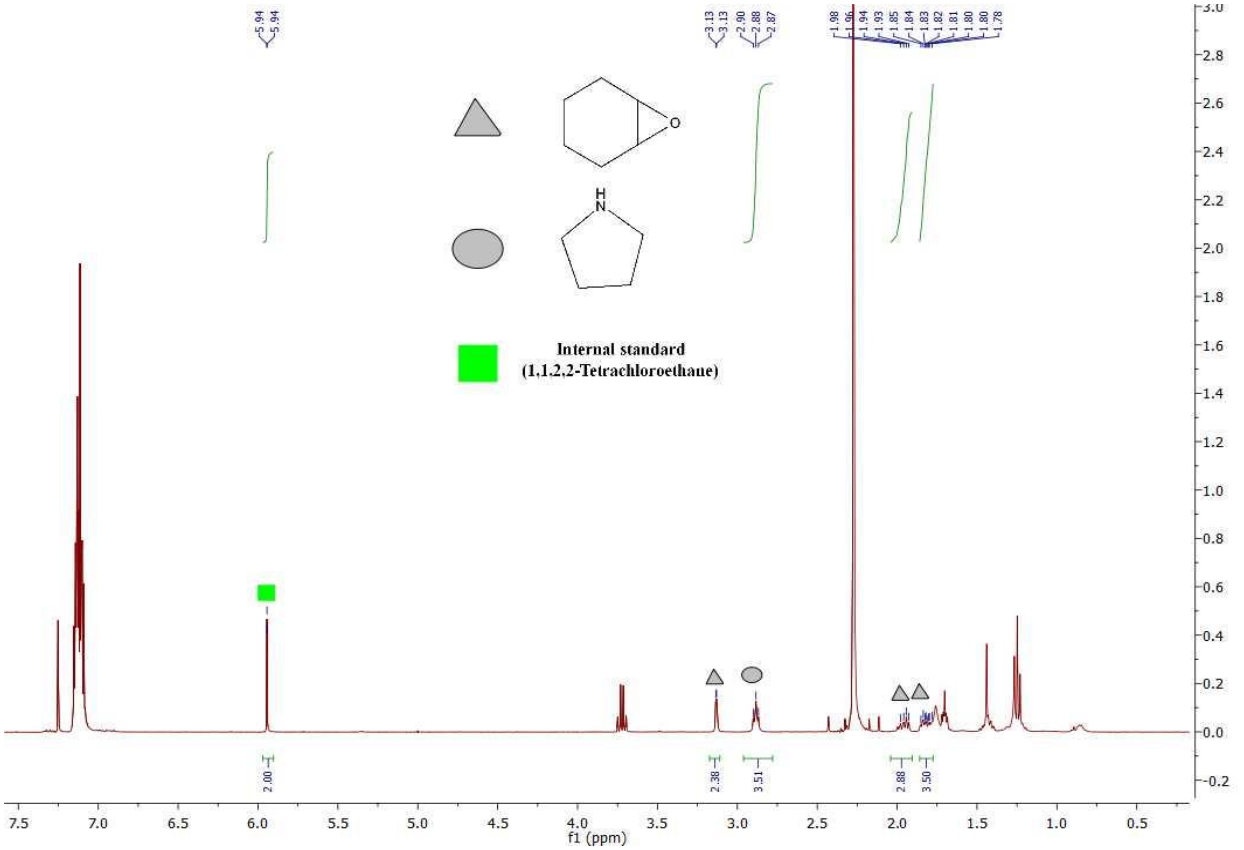

Figure S 16: ^{1}H NMR spectrum for entry 2^{b} in table 2

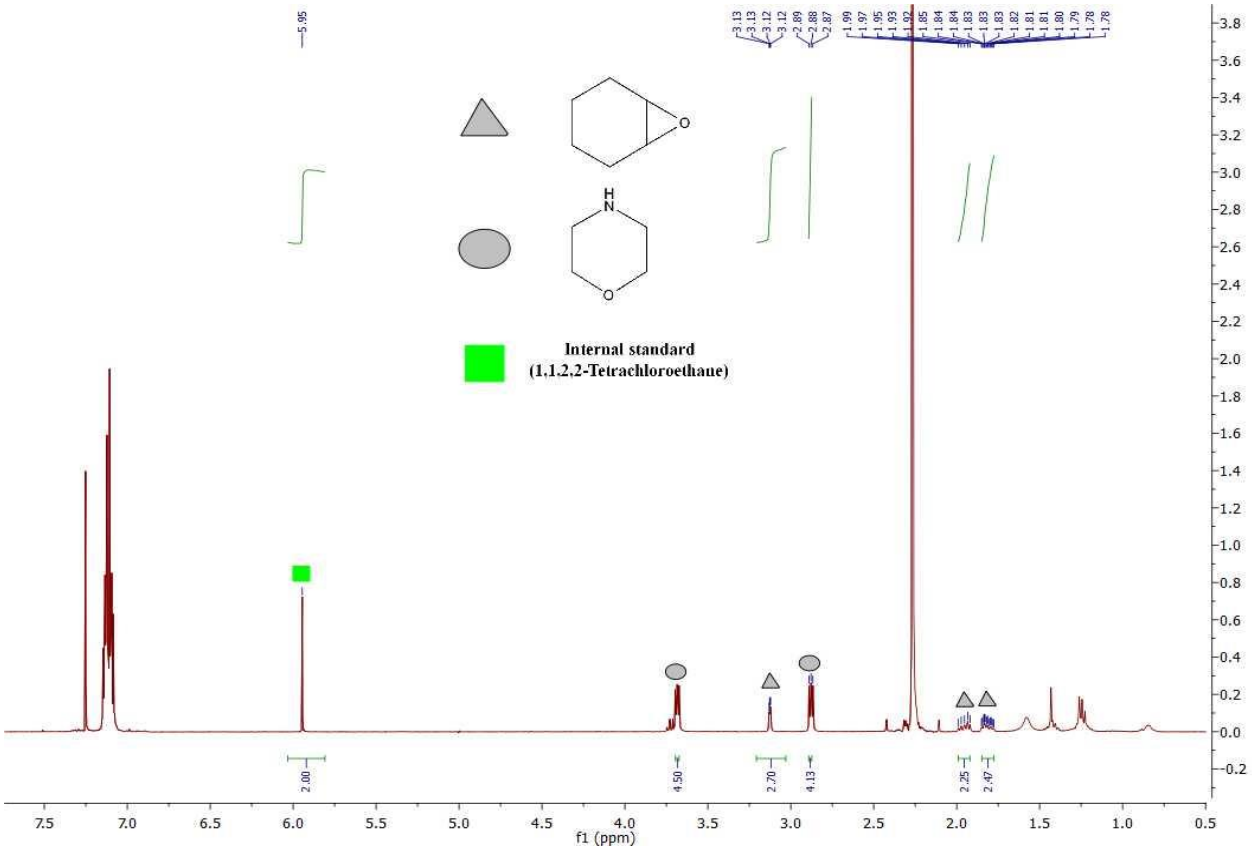

Figure S 17: ^{1}H NMR spectrum for entry 3^{b} in table 2

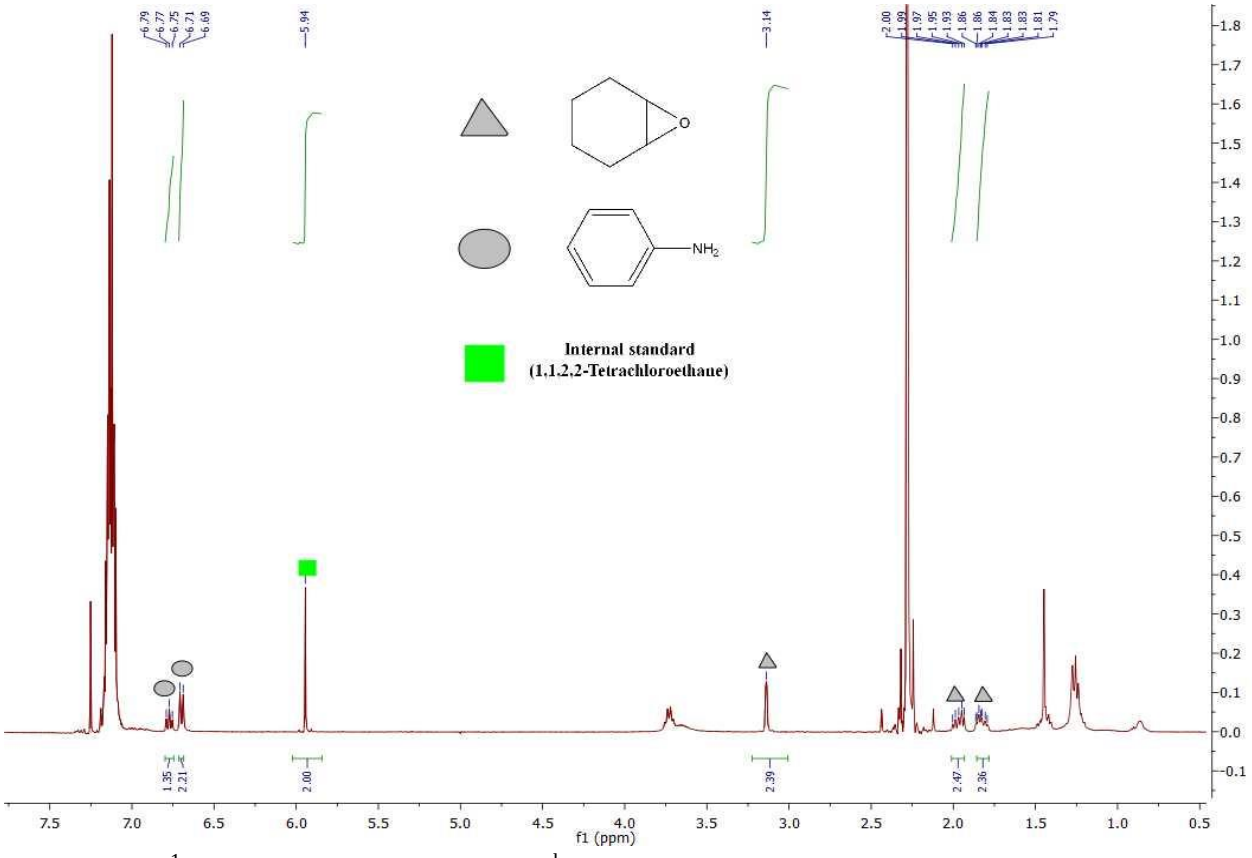

Figure S 18: ^{1}H NMR spectrum for entry 4^{b} in table 2

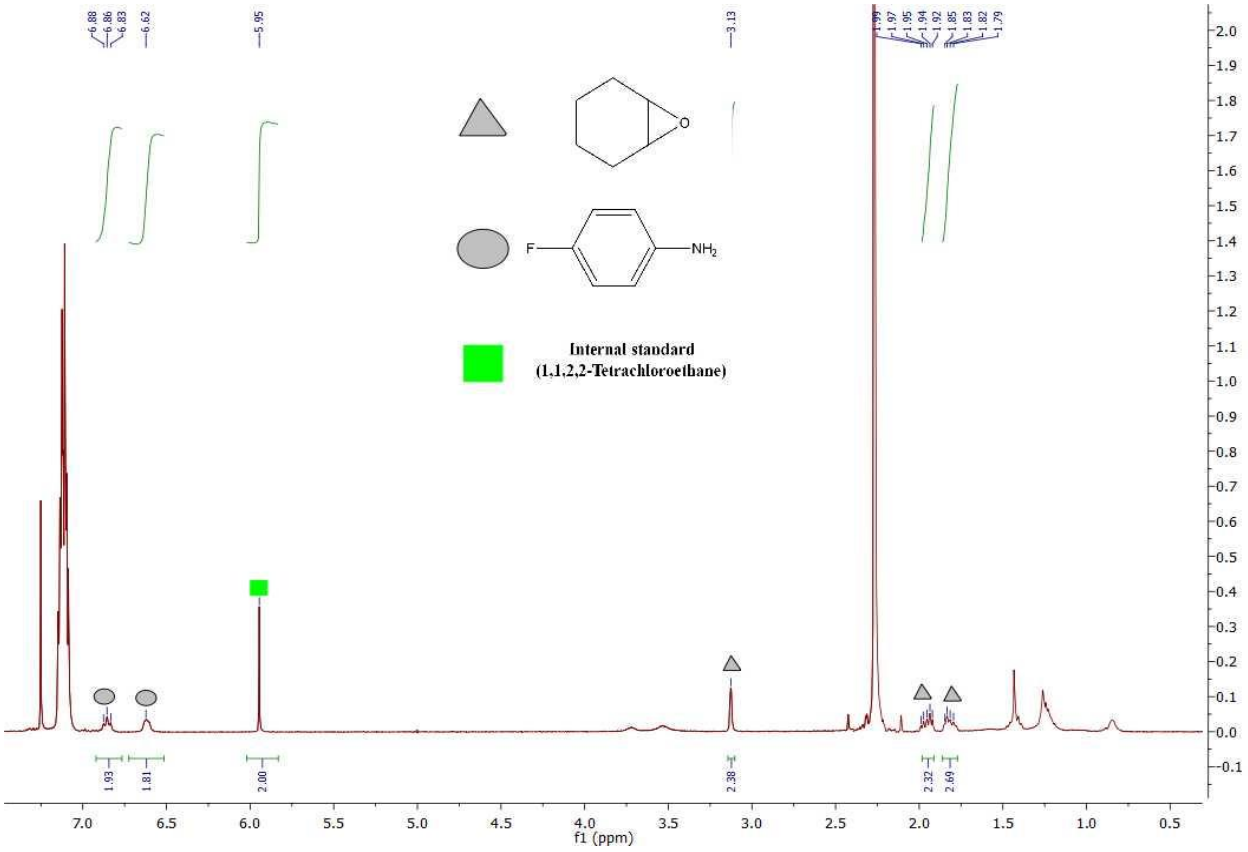

Figure S 19: ^{1}H NMR spectrum for entry 5^{b} in table 2

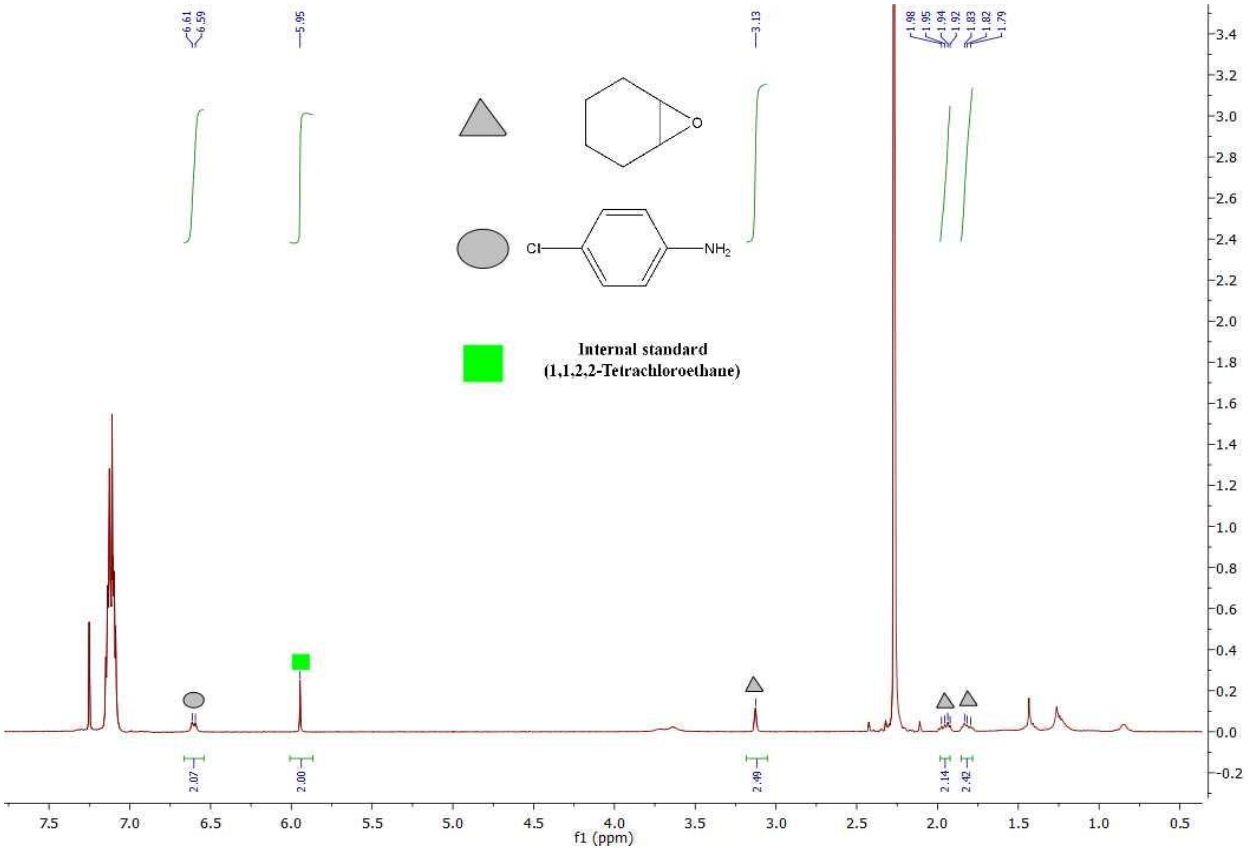

Figure S 20: ^{1}H NMR spectrum for entry 6^{b} in table 2

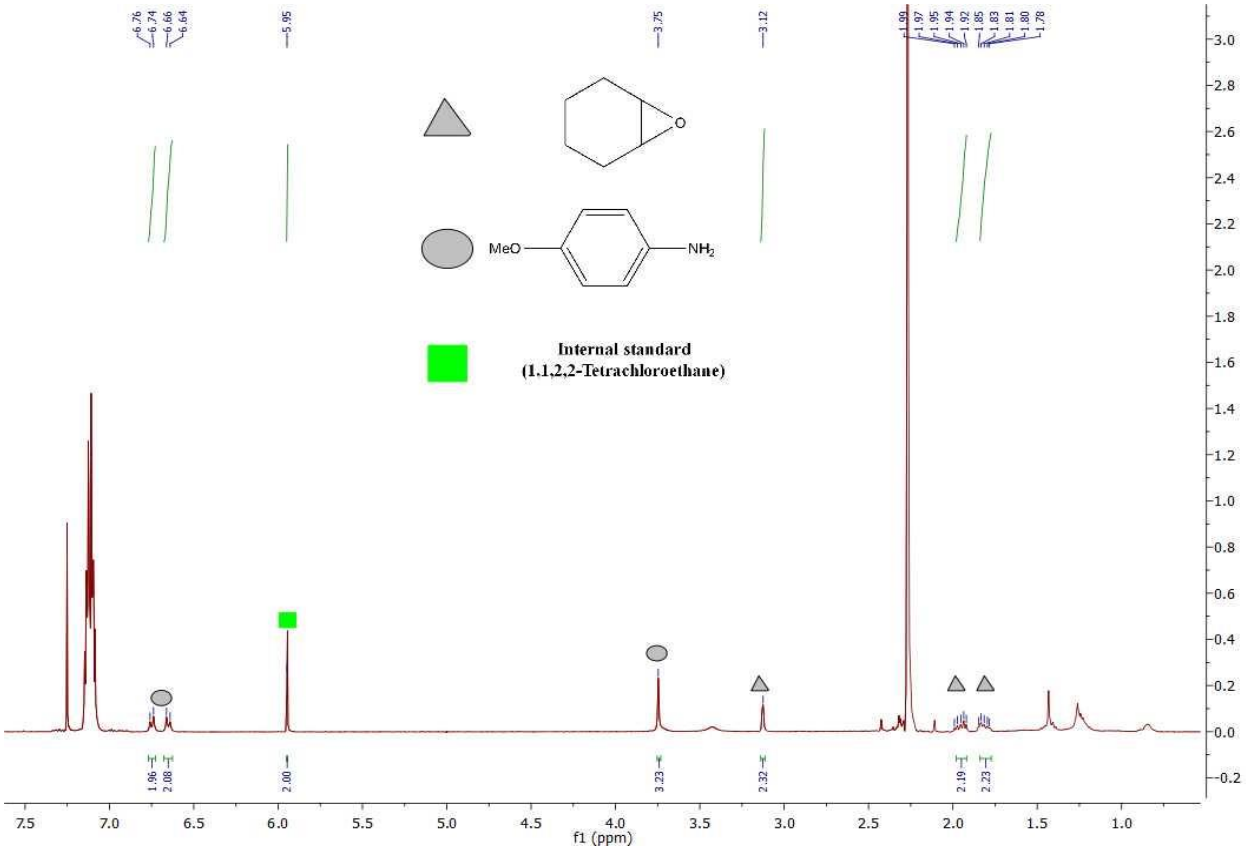

Figure S 21: ^{1}H NMR spectrum for entry 7^{b} in table 2

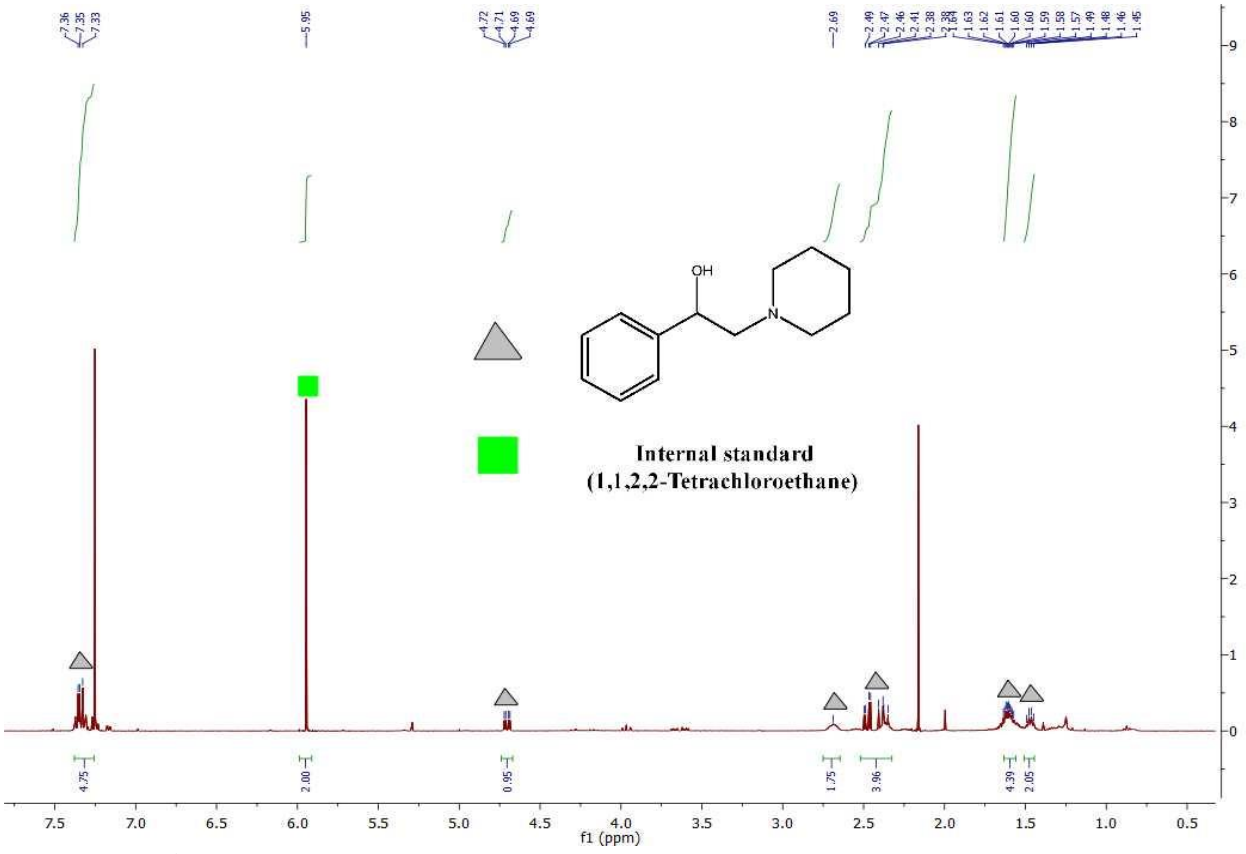

Figure S 22: ^{1}H NMR spectrum for entry 1 in table 3

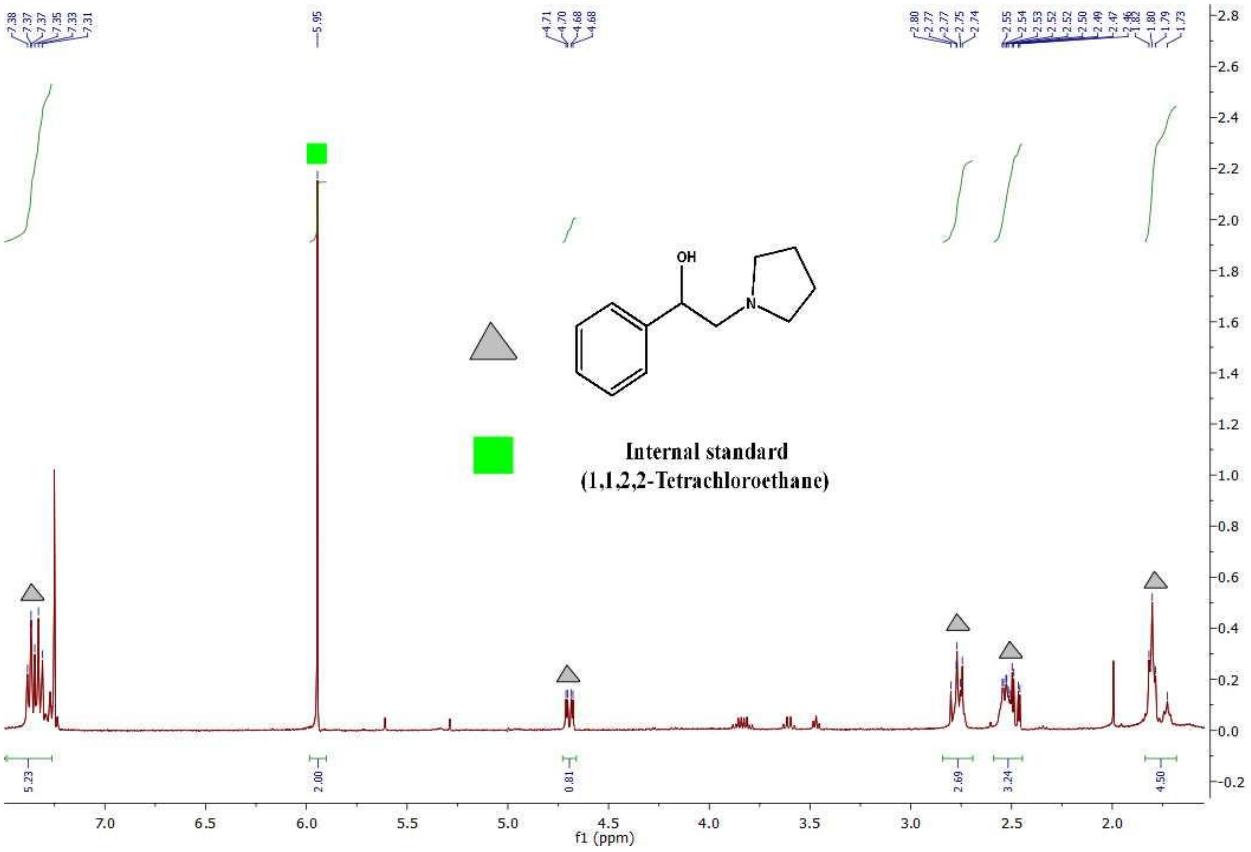

Figure S 23: ^{1}H NMR spectrum for entry 2 in table 3.

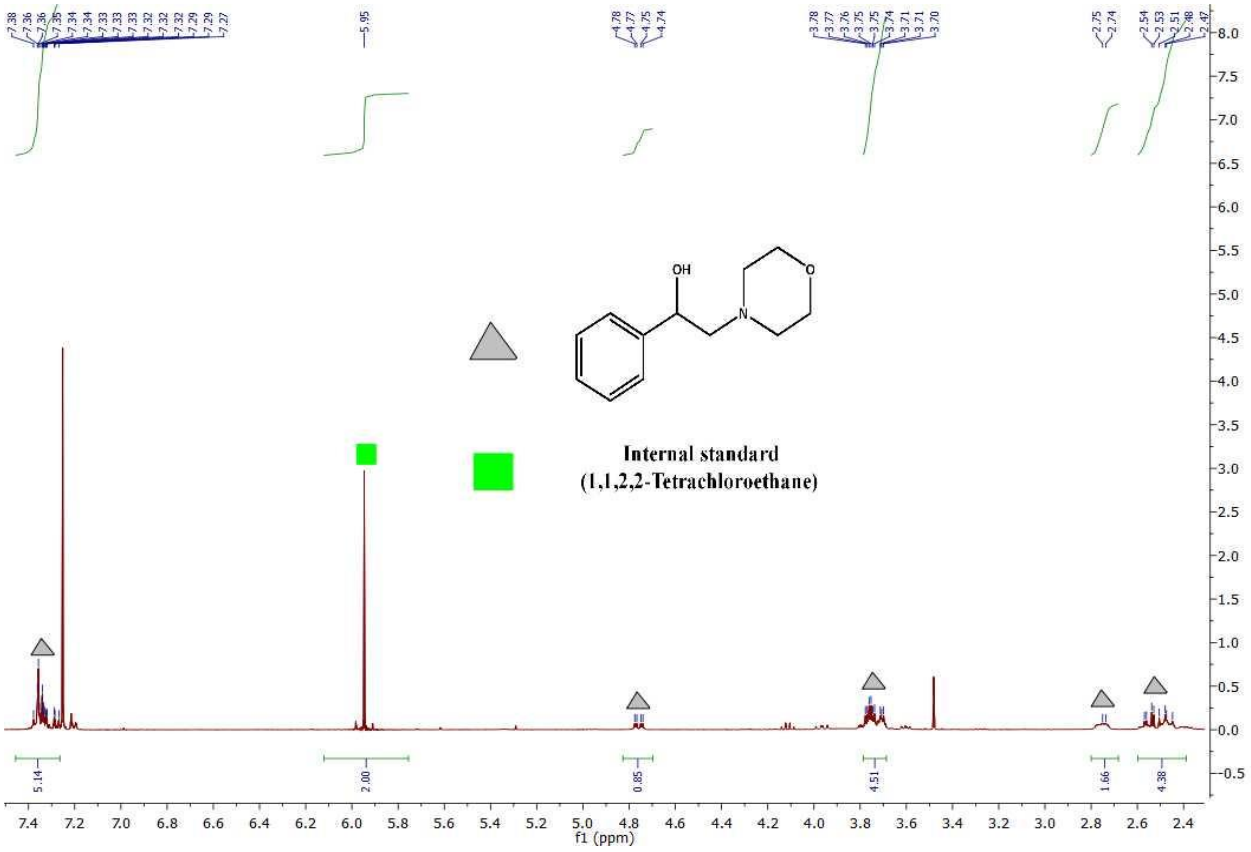

Figure S 24: ^{1}H NMR spectrum for entry 3 in table 3.

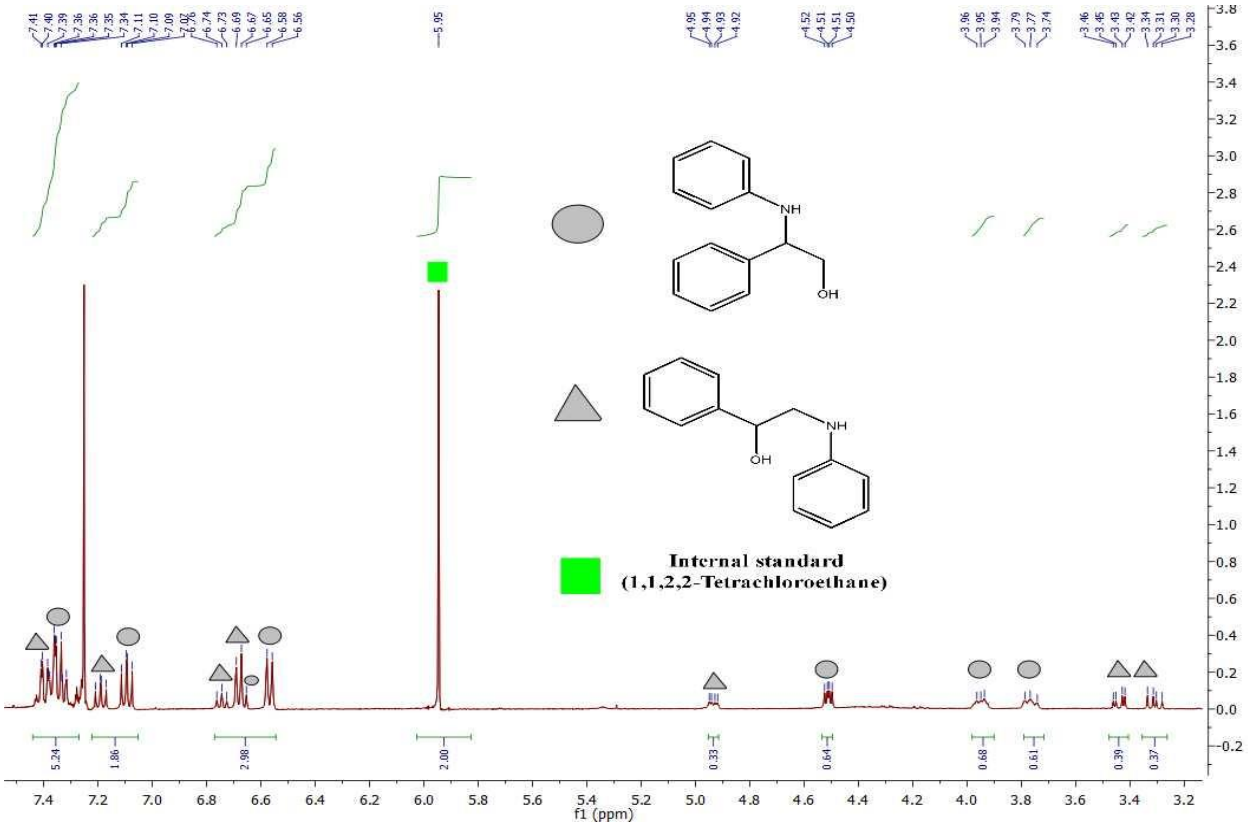

Figure S 25: ^{1}H NMR spectrum for entry 4 in table 3

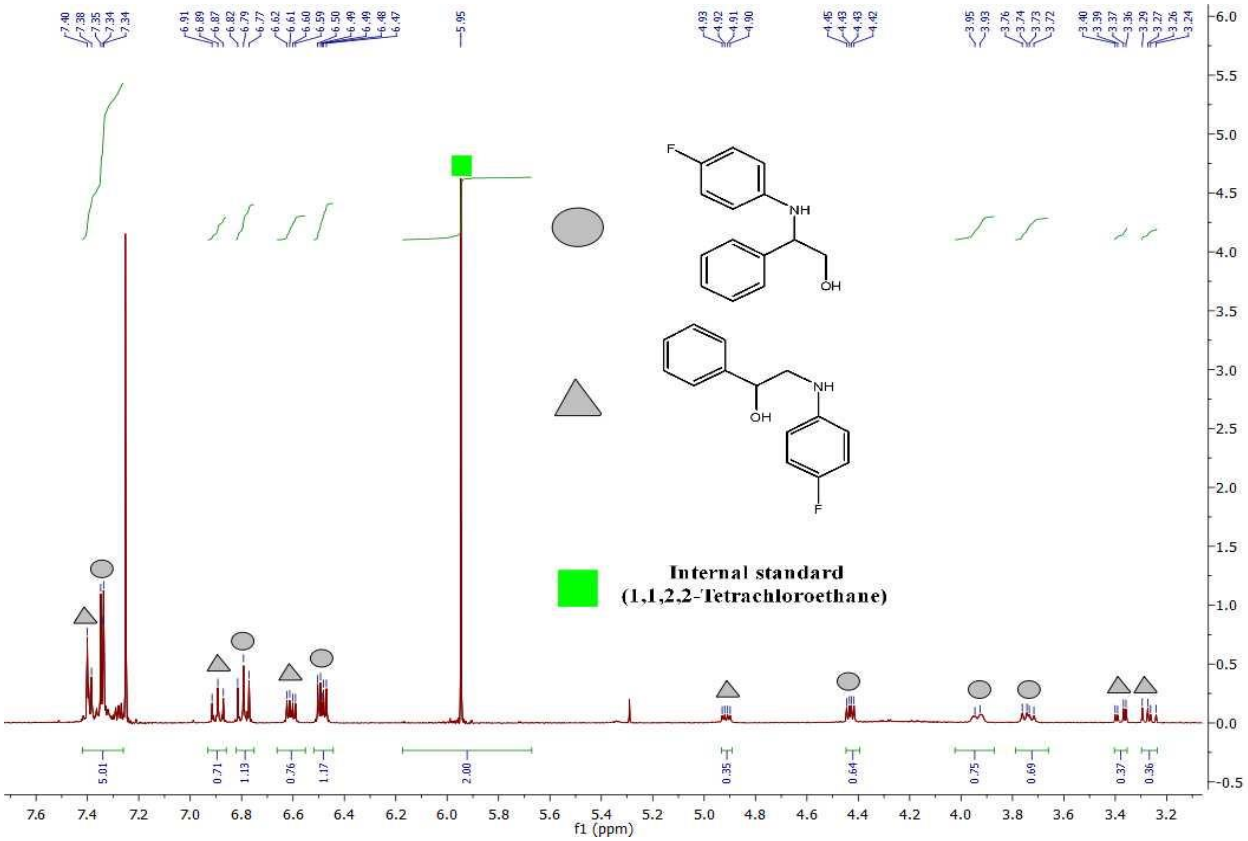

Figure S 26: ^{1}H NMR spectrum for entry 5 in table 3

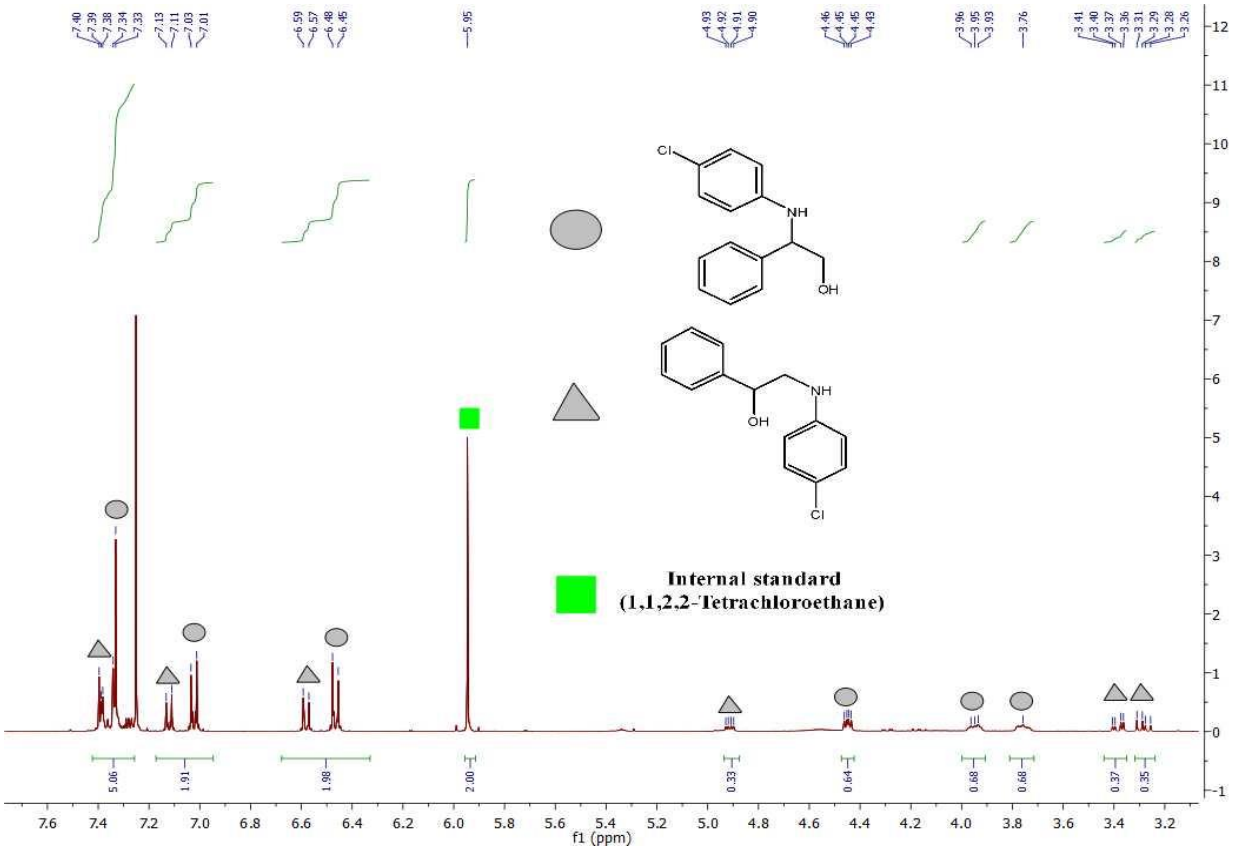

Figure S 27: ^{1}H NMR spectrum for entry 6 in table 3

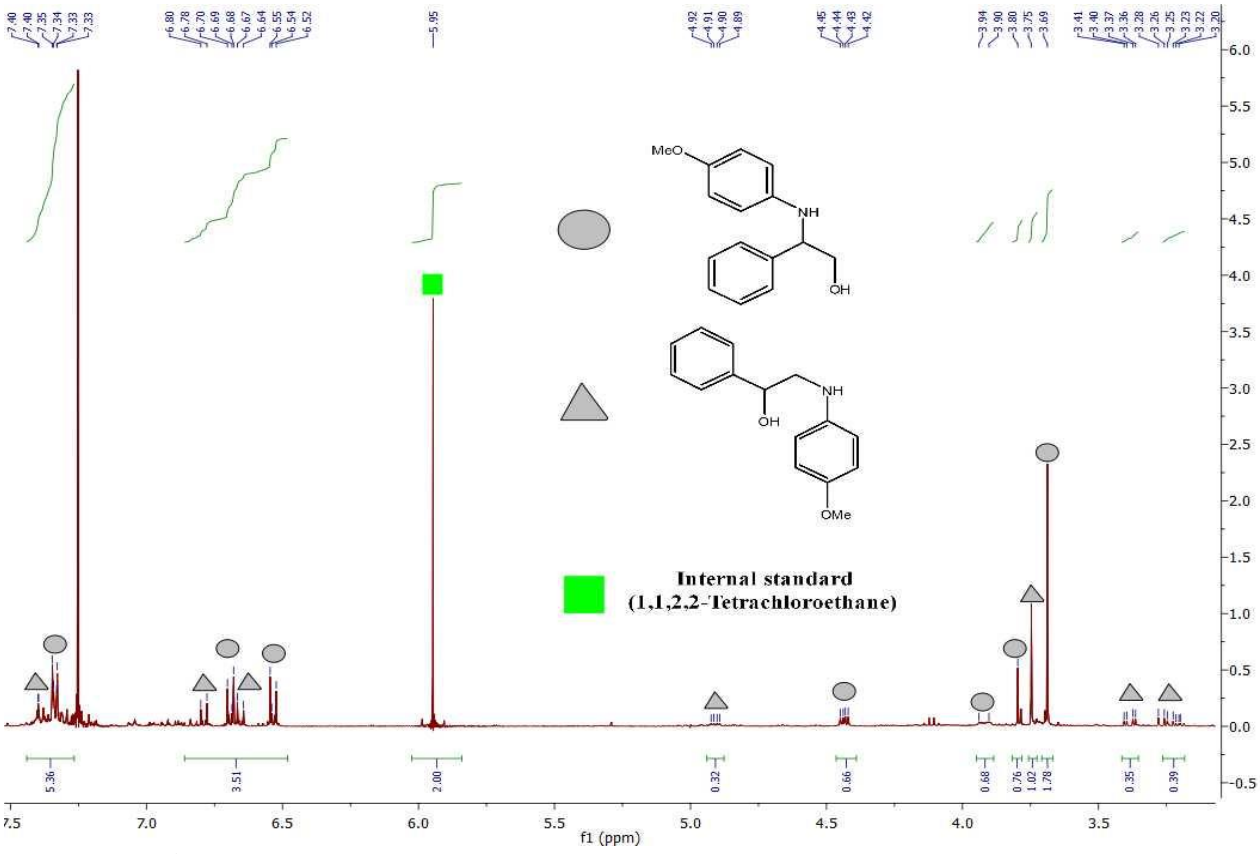

Figure S 28: ^{1}H NMR spectrum for entry 7 in table 3

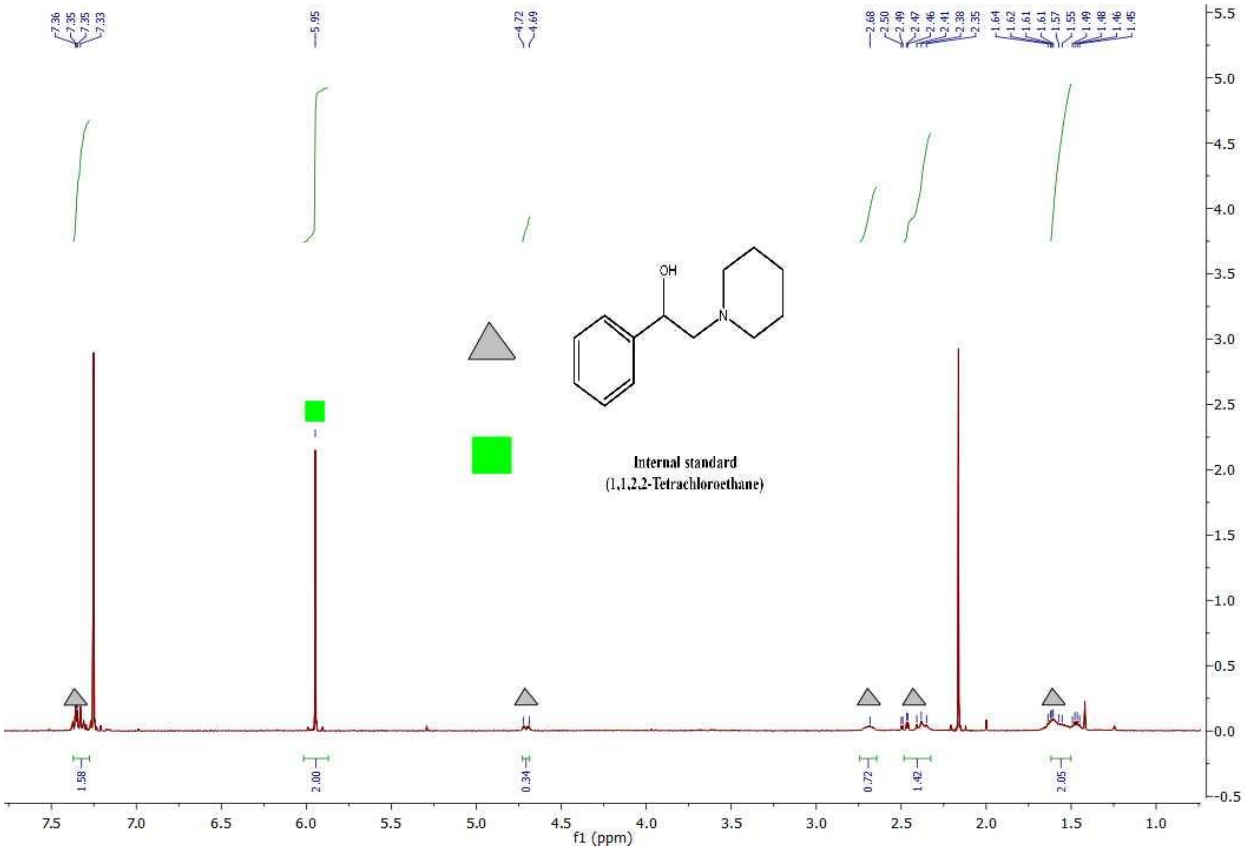

Figure S 29: ^{1}H NMR spectrum for entry 1[a] in table 4

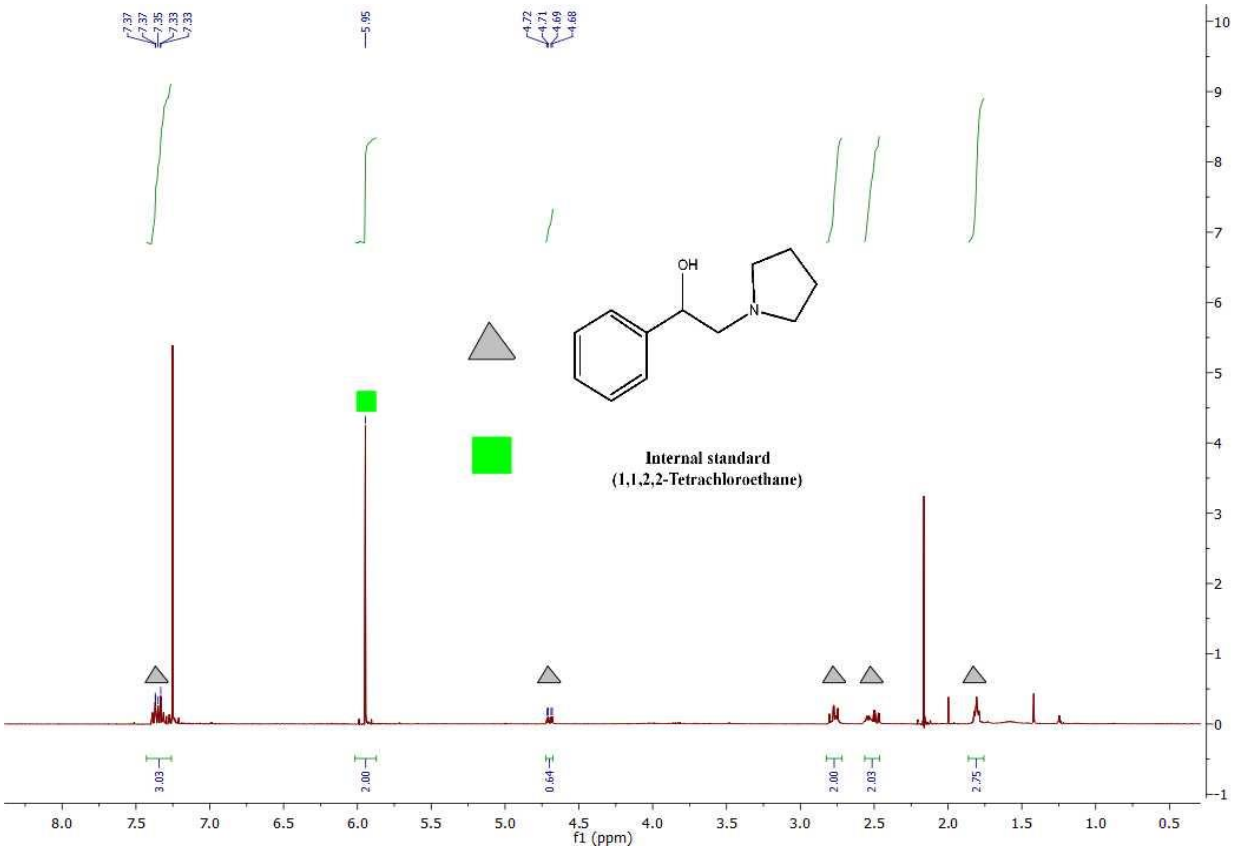

Figure S 30: ^{1}H NMR spectrum for entry 2[a] in table 4

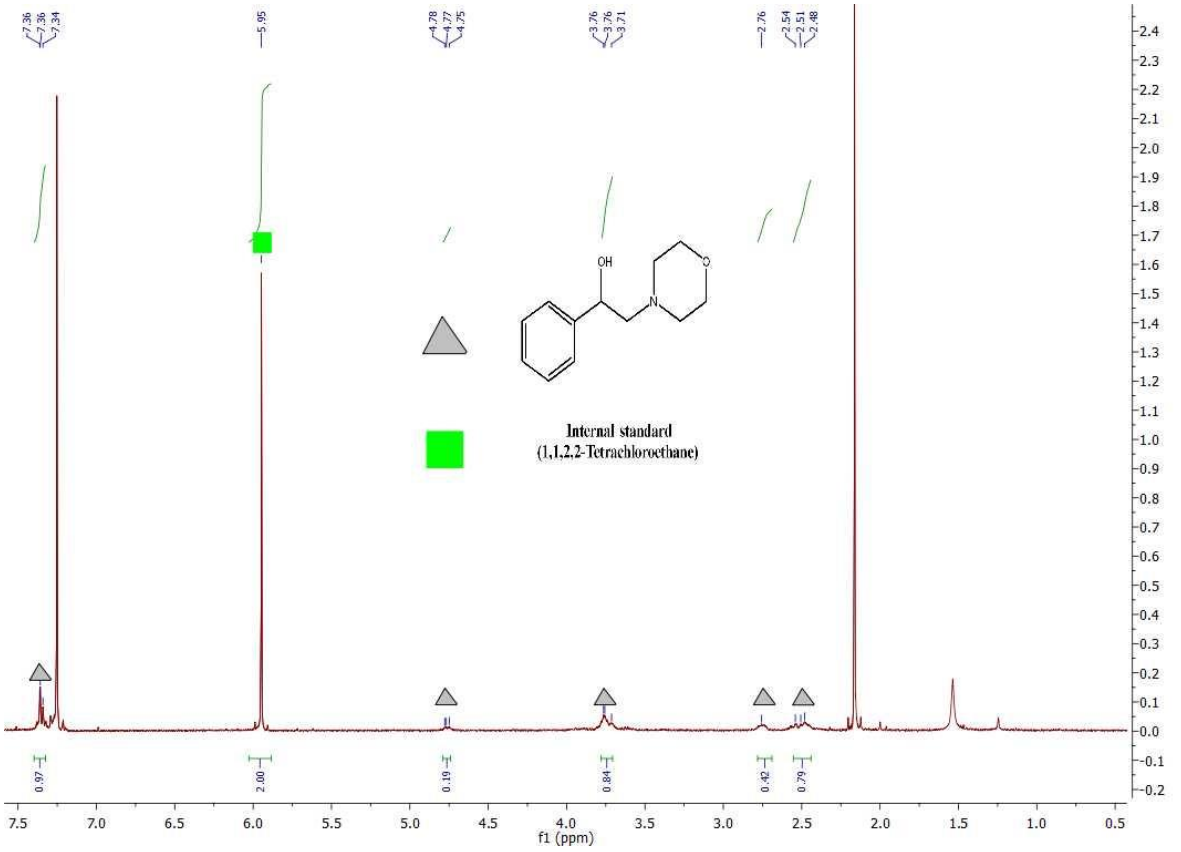

Figure S 31: ^{1}H NMR spectrum for entry 3[a] in table 4

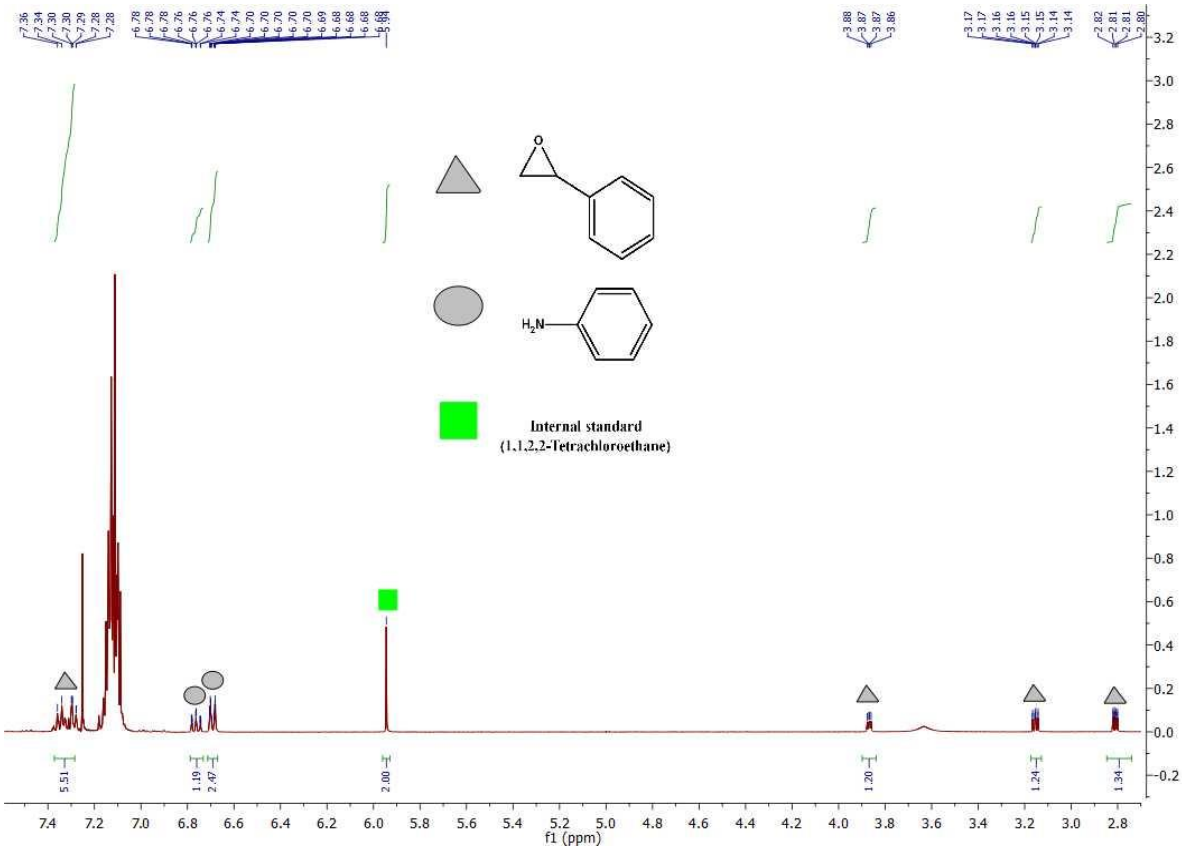

Figure S 32: ^{1}H NMR spectrum for entry 4[a] in table 4

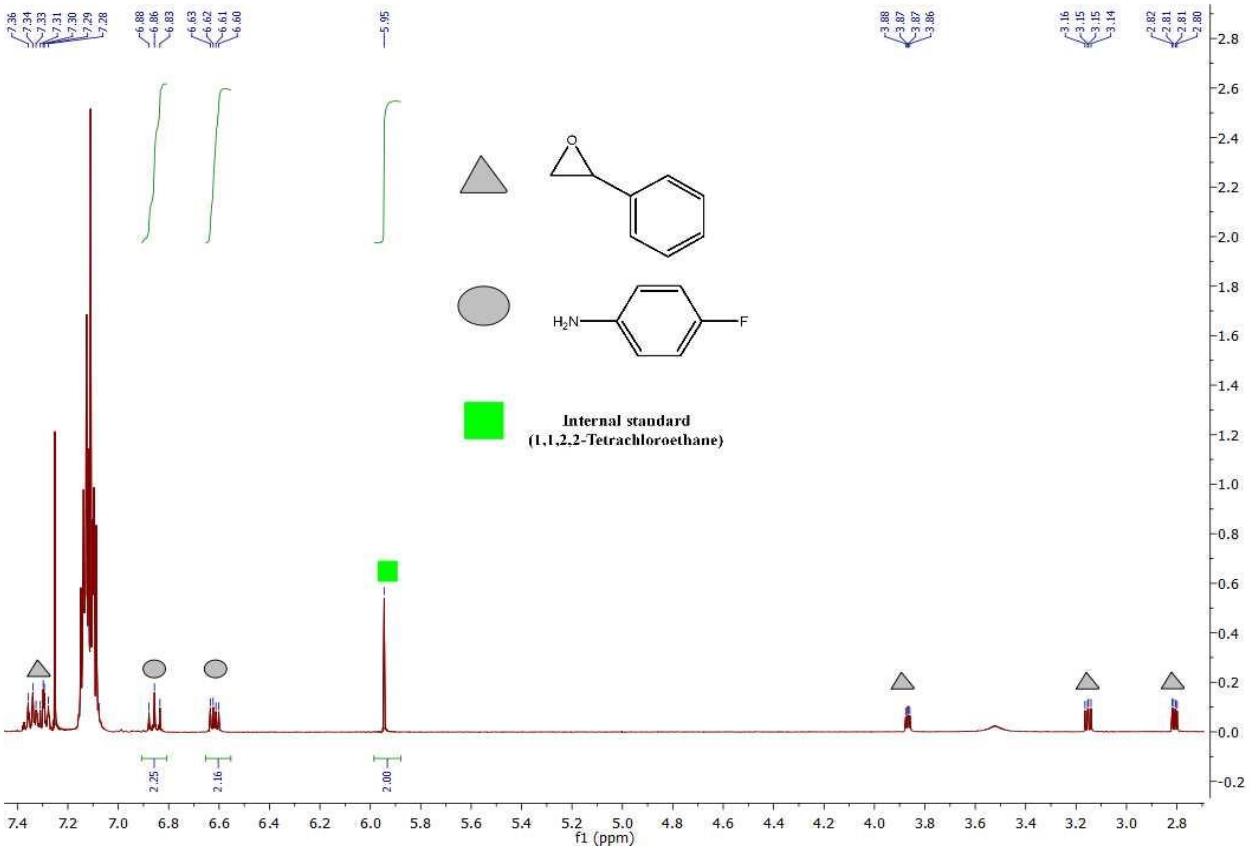

Figure S 33: ^{1}H NMR spectrum for entry 5[a] in table 4

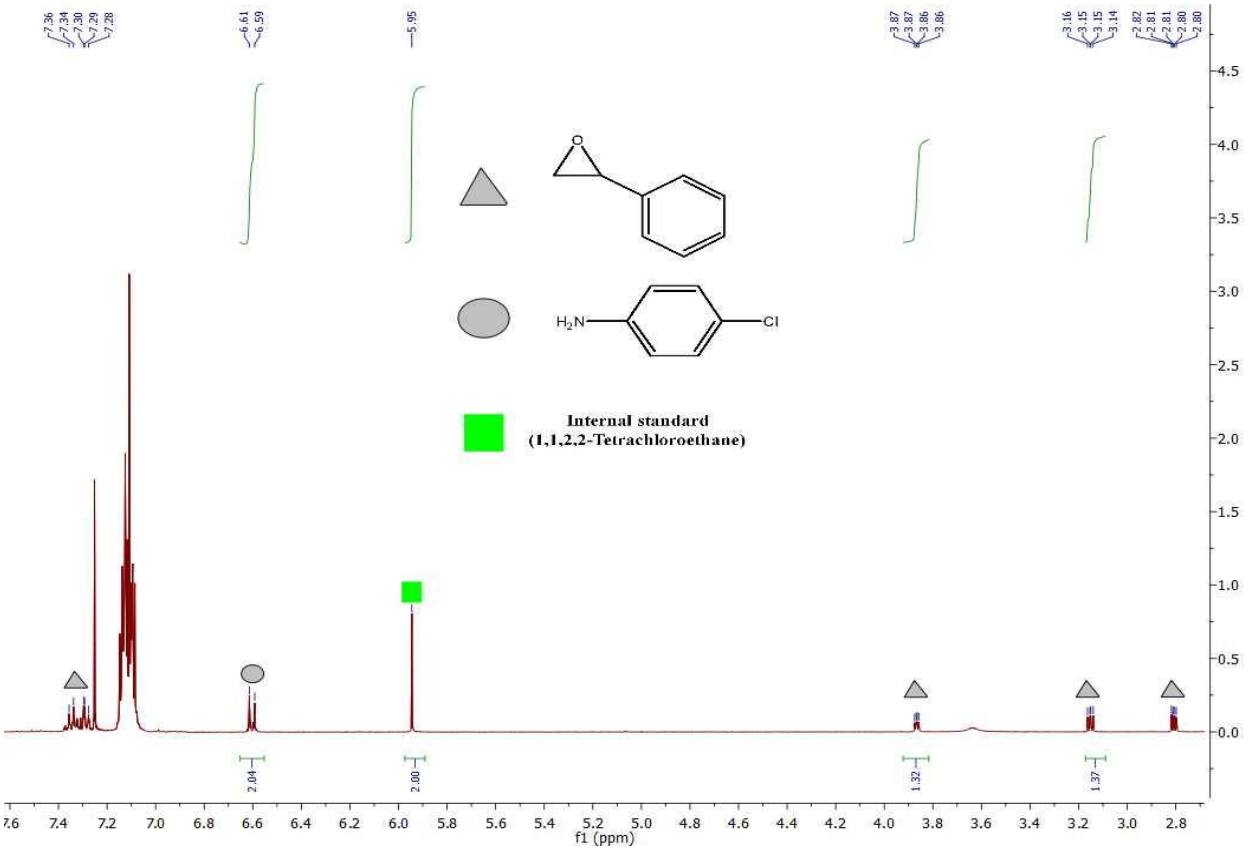

Figure S 34: ^{1}H NMR spectrum for entry 6[a] in table 4

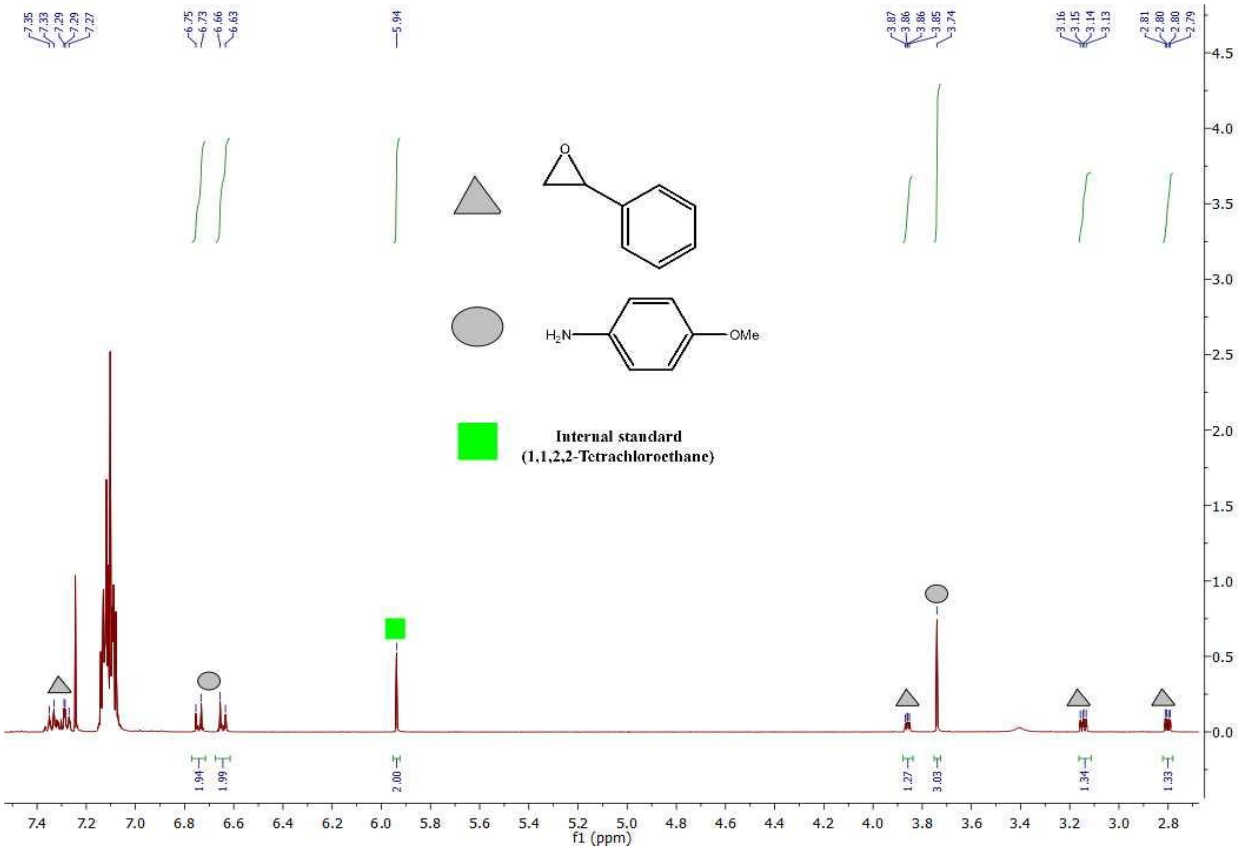

Figure S 35: ^{1}H NMR spectrum for entry 7[a] in table 4

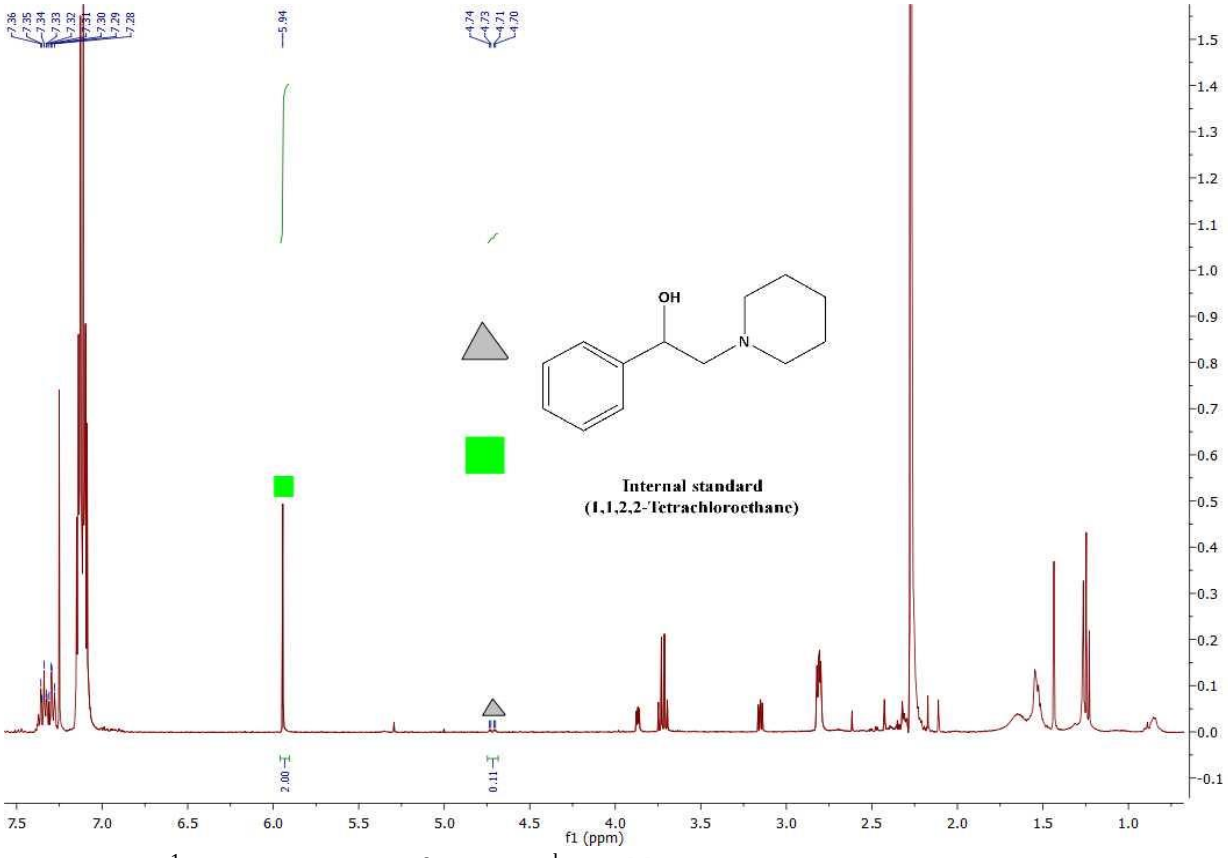

Figure S 36: ^{1}H NMR spectrum for entry 1[b] in table 4

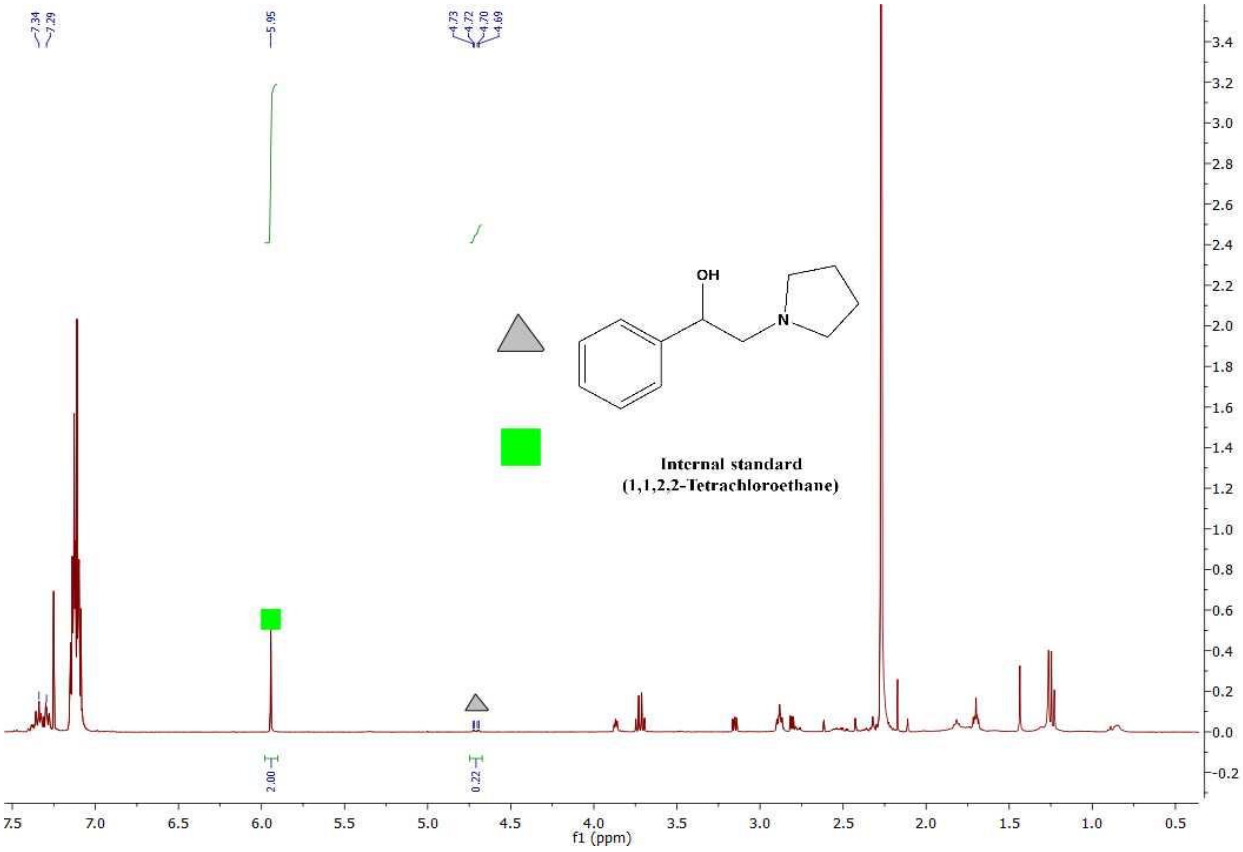

Figure S 37: ^{1}H NMR spectrum for entry 2^{b} in table 4

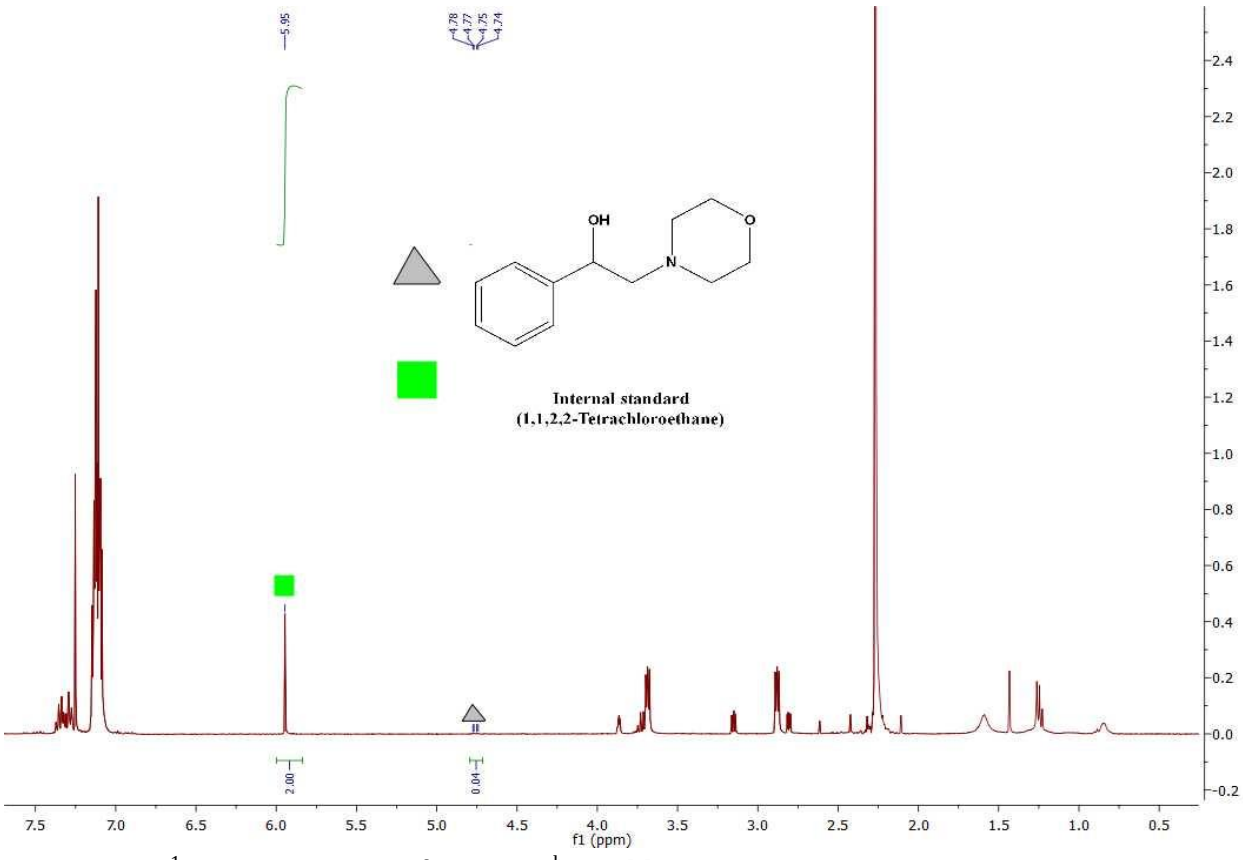

Figure S 38: ^{1}H NMR spectrum for entry 3^{b} in table 4

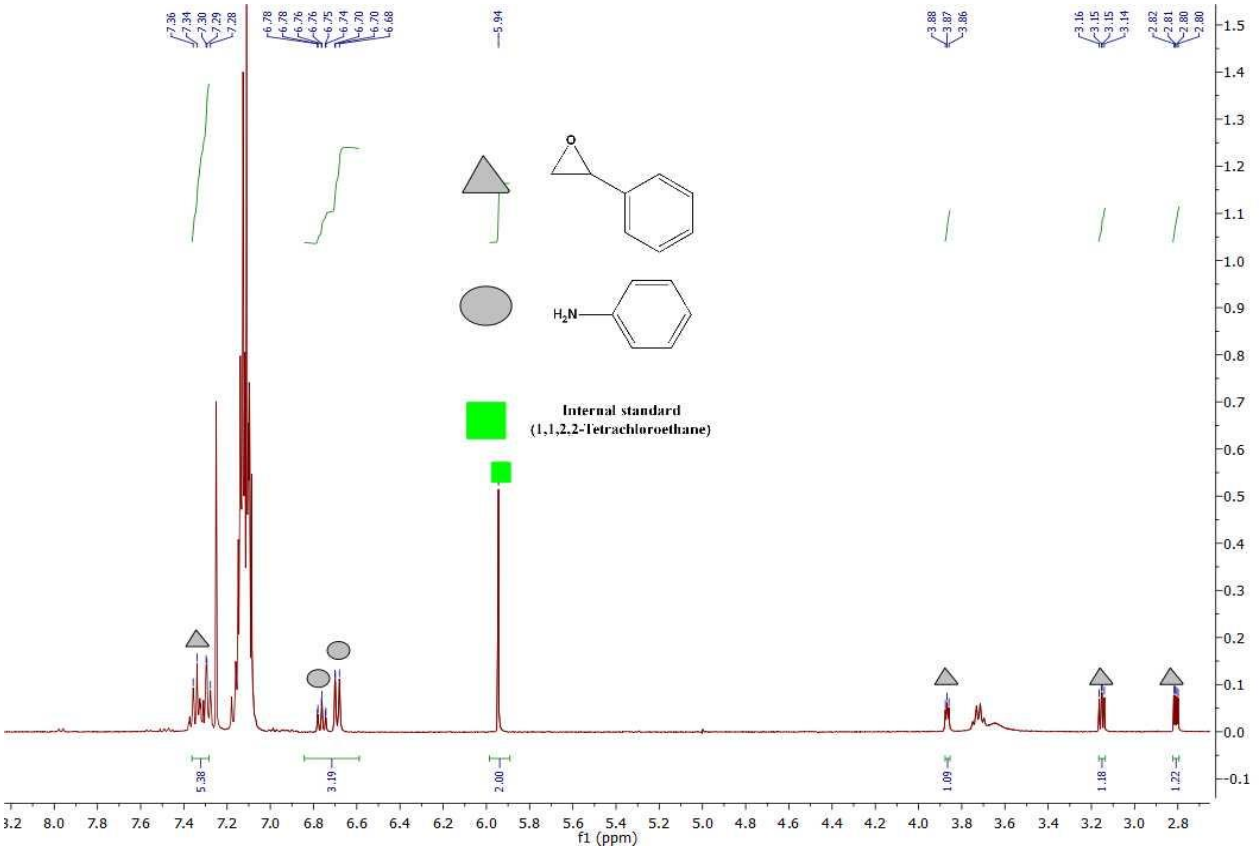

Figure S 39: ^{1}H NMR spectrum for entry 4^{b} in table 4

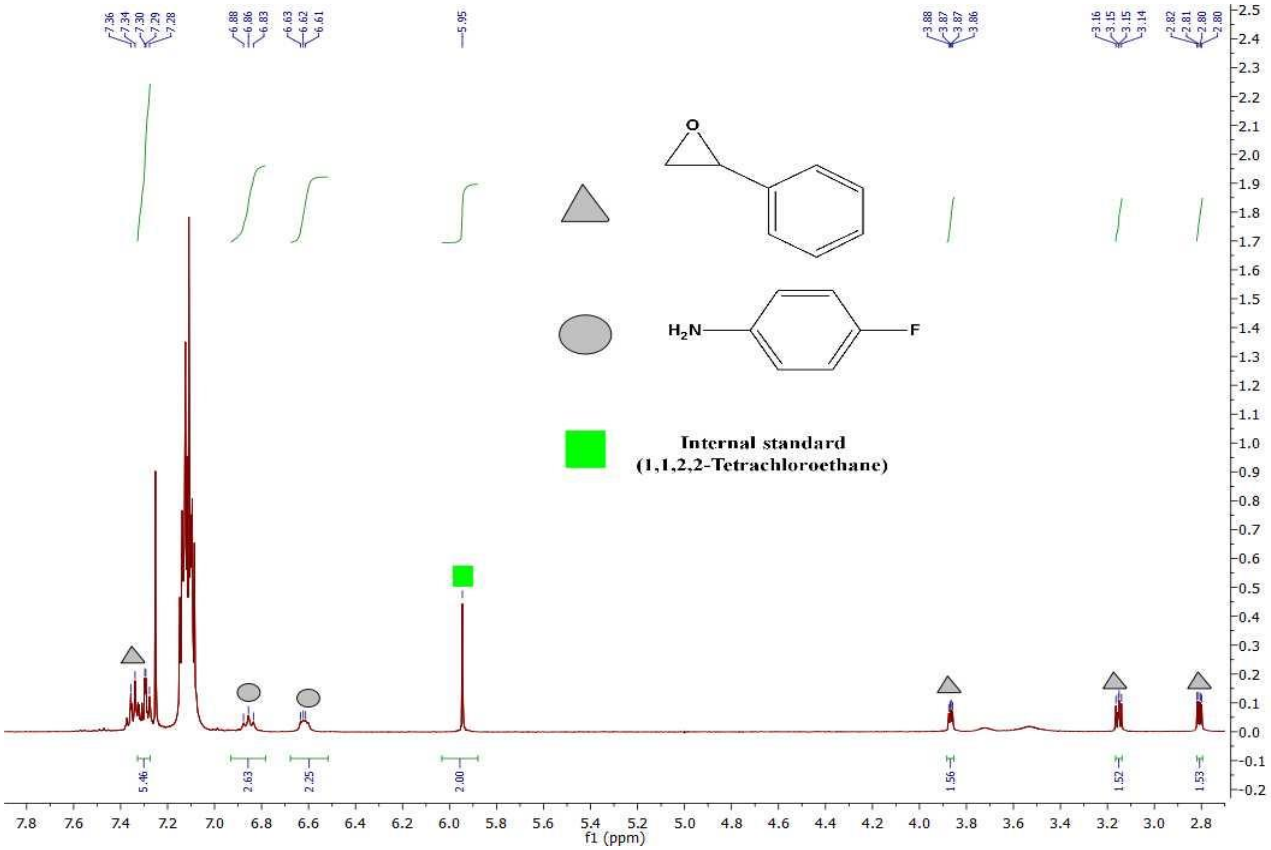

Figure S 40: ^{1}H NMR spectrum for entry 5^{b} in table 4

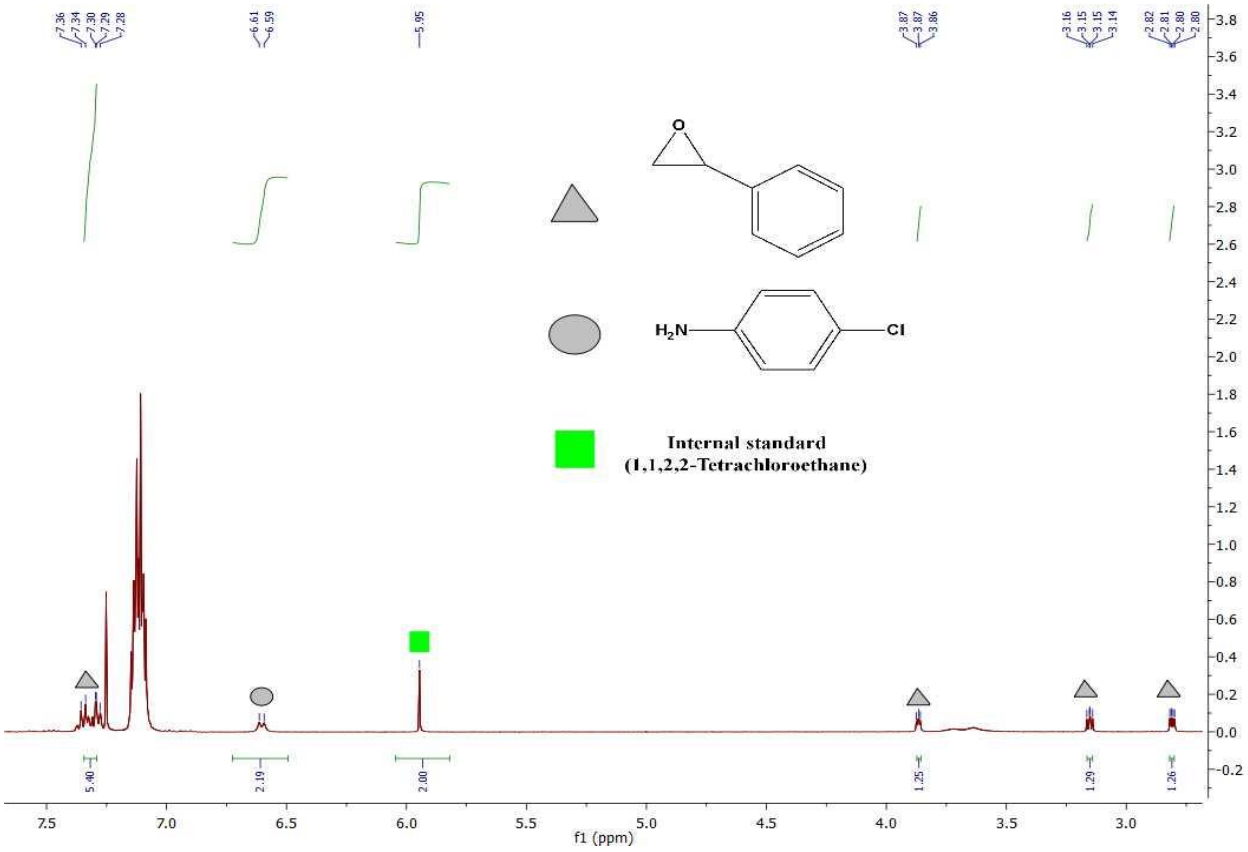

Figure S 41: ^{1}H NMR spectrum for entry 6^{b} in table 4

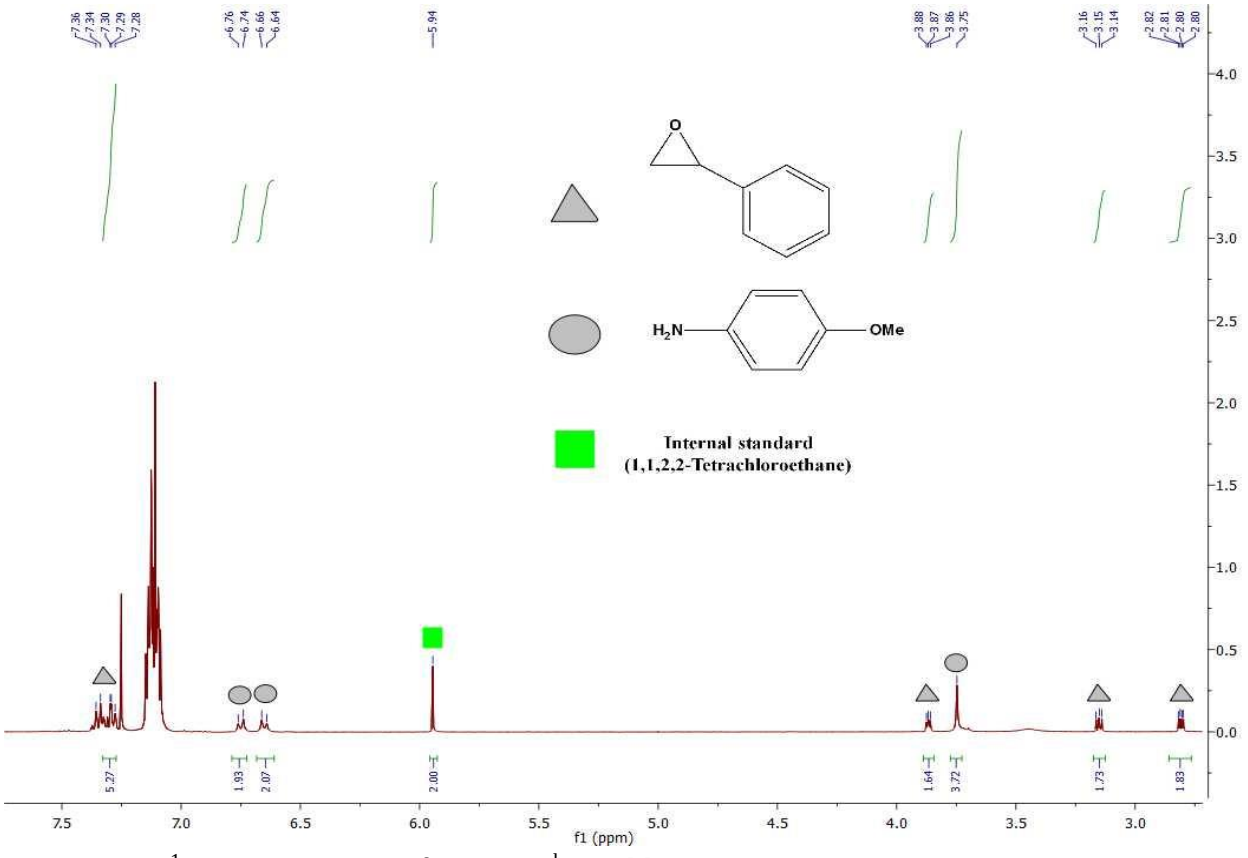

Figure S 42: ^{1}H NMR spectrum for entry 6^{b} in table 4

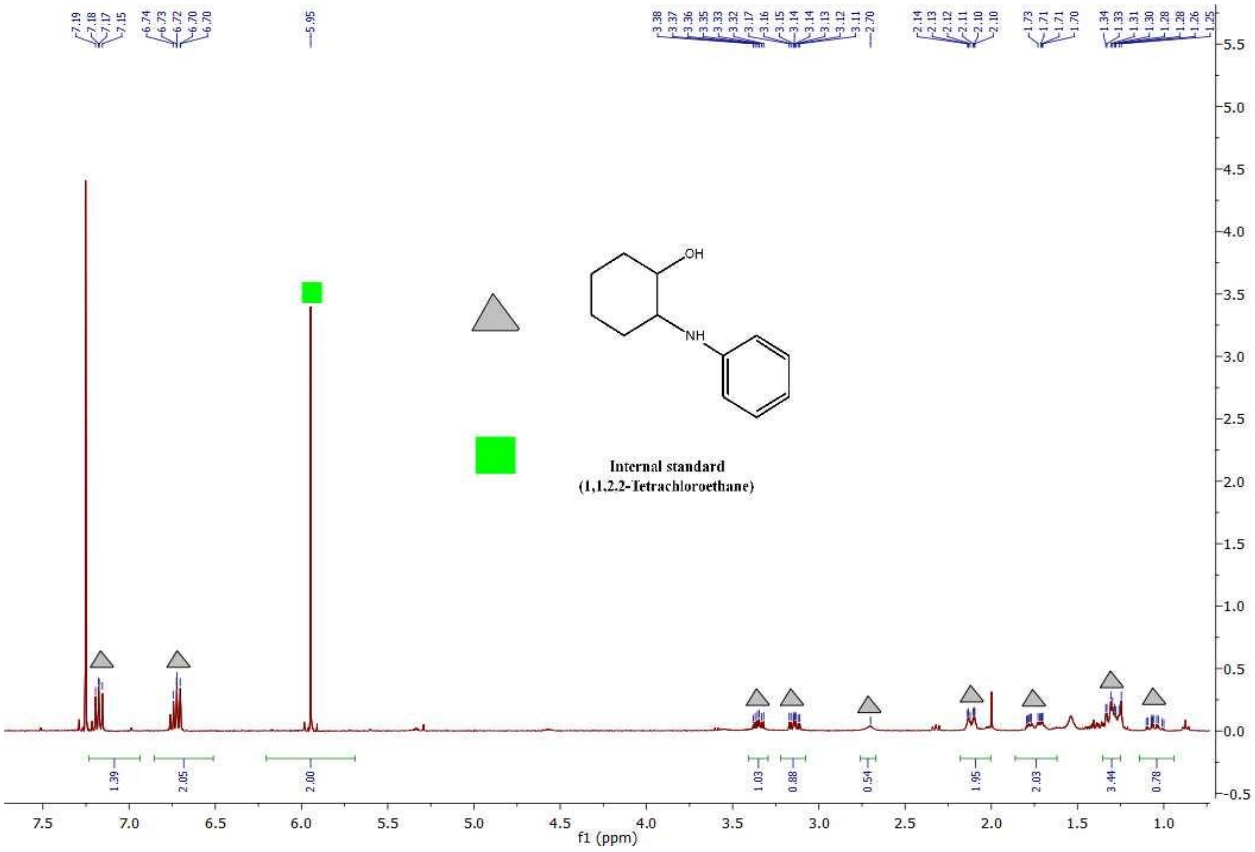

Figure S 43: ^{1}H NMR spectrum for entry 1 in table 5

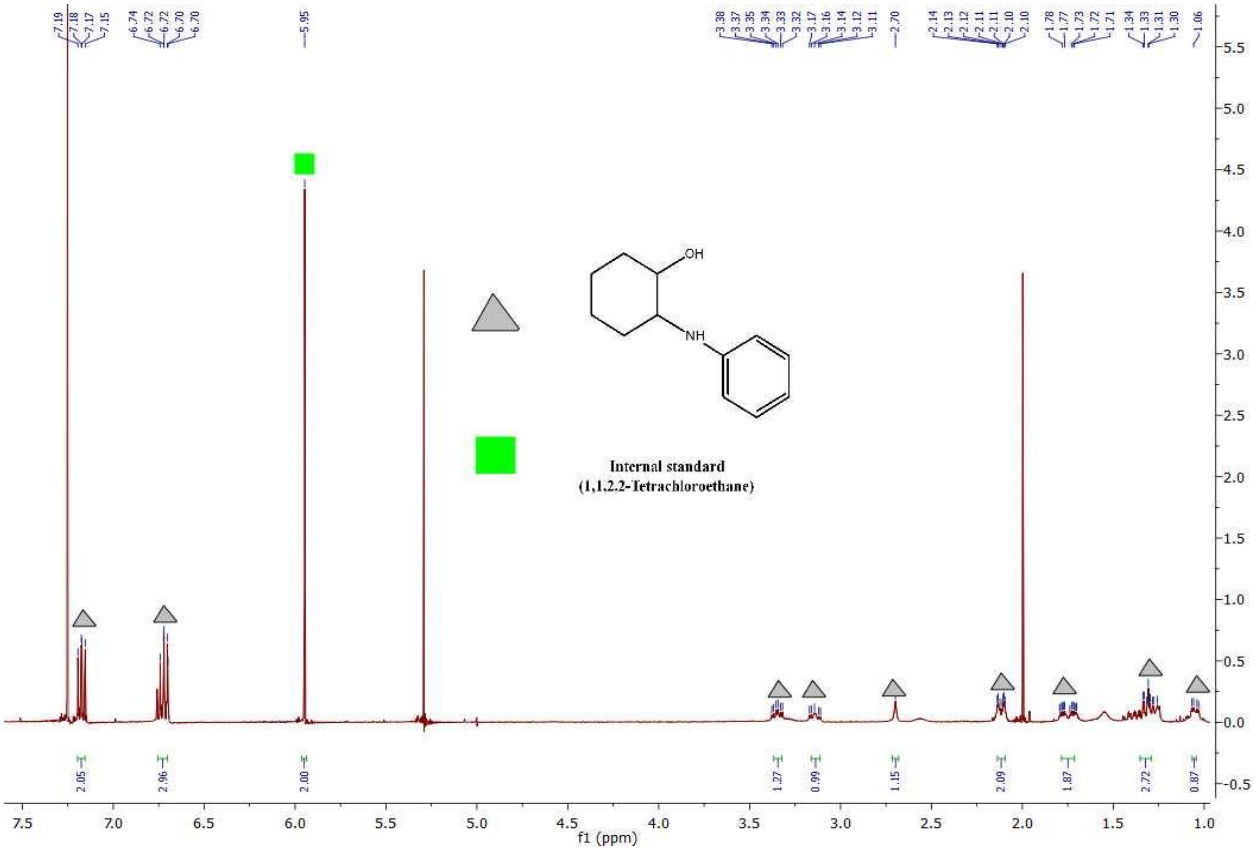

Figure S 44: ^{1}H NMR spectrum for entry 2 in table 5

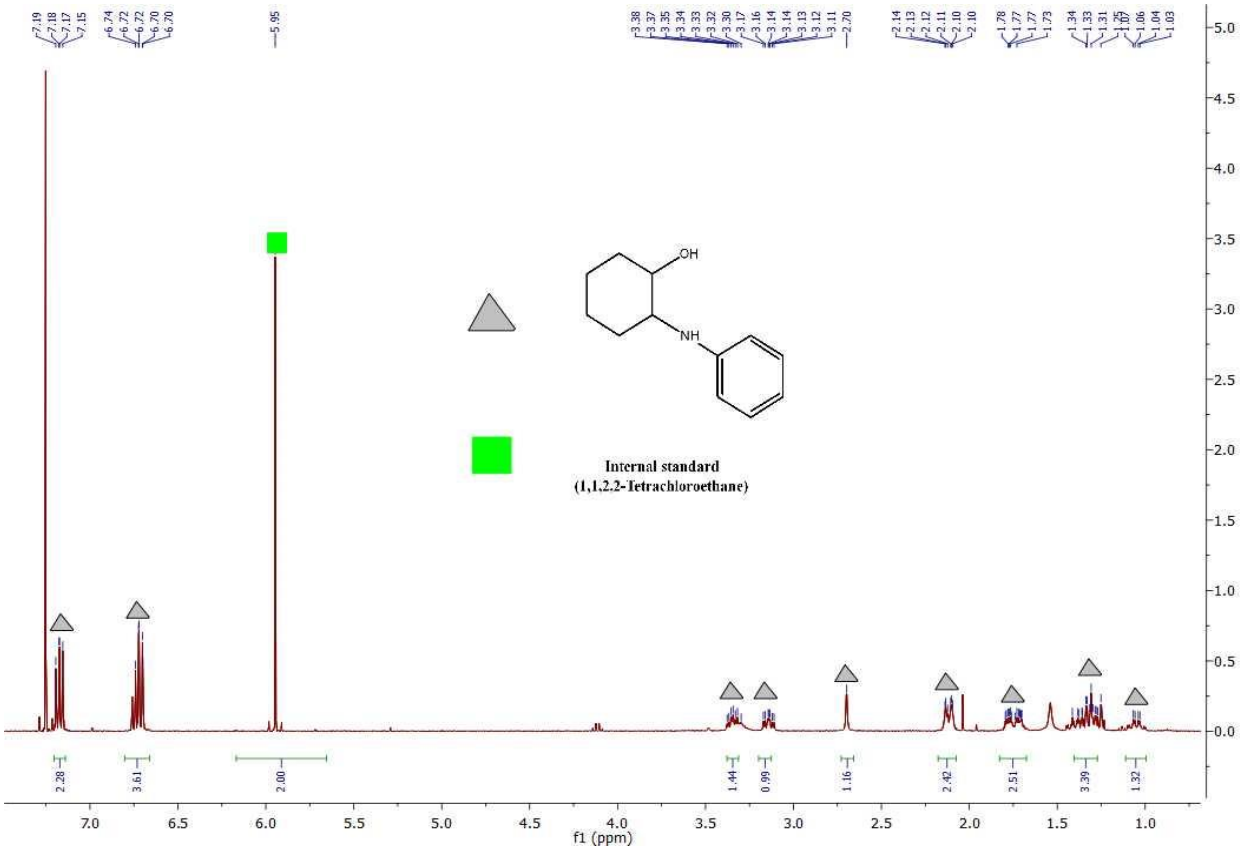

Figure S 45: ^{1}H NMR spectrum for entry 3 in table 5

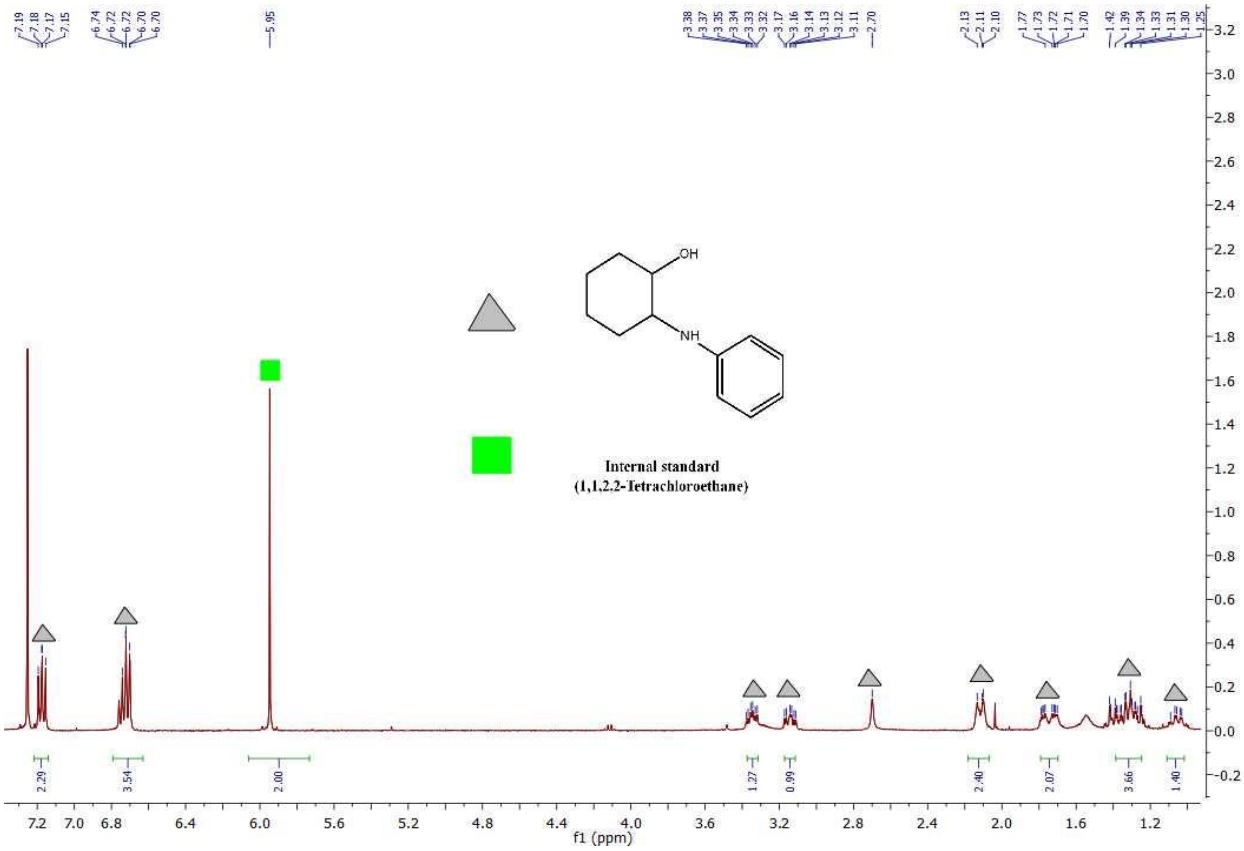

Figure S 46: ^{1}H NMR spectrum for entry 4 in table 5

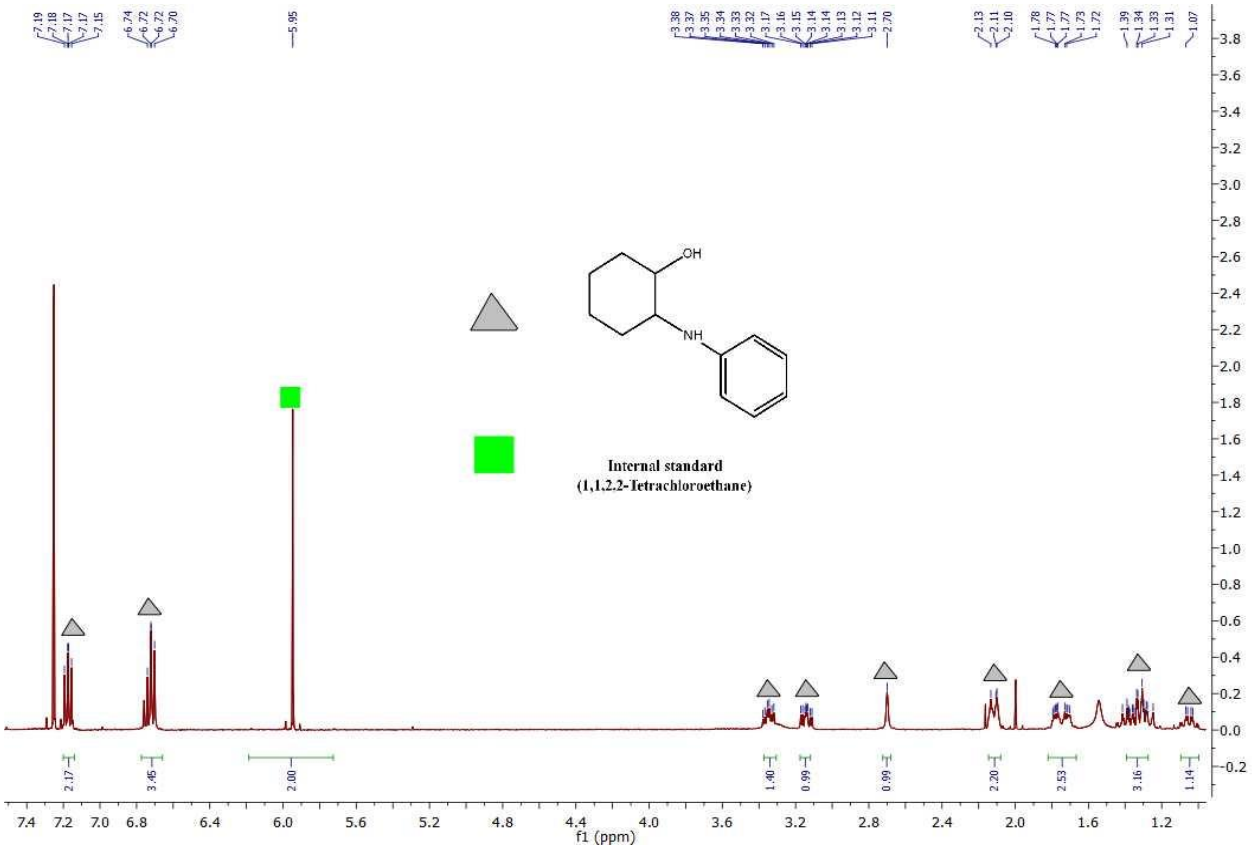

Figure S 47: ^{1}H NMR spectrum for entry 5 in table 5

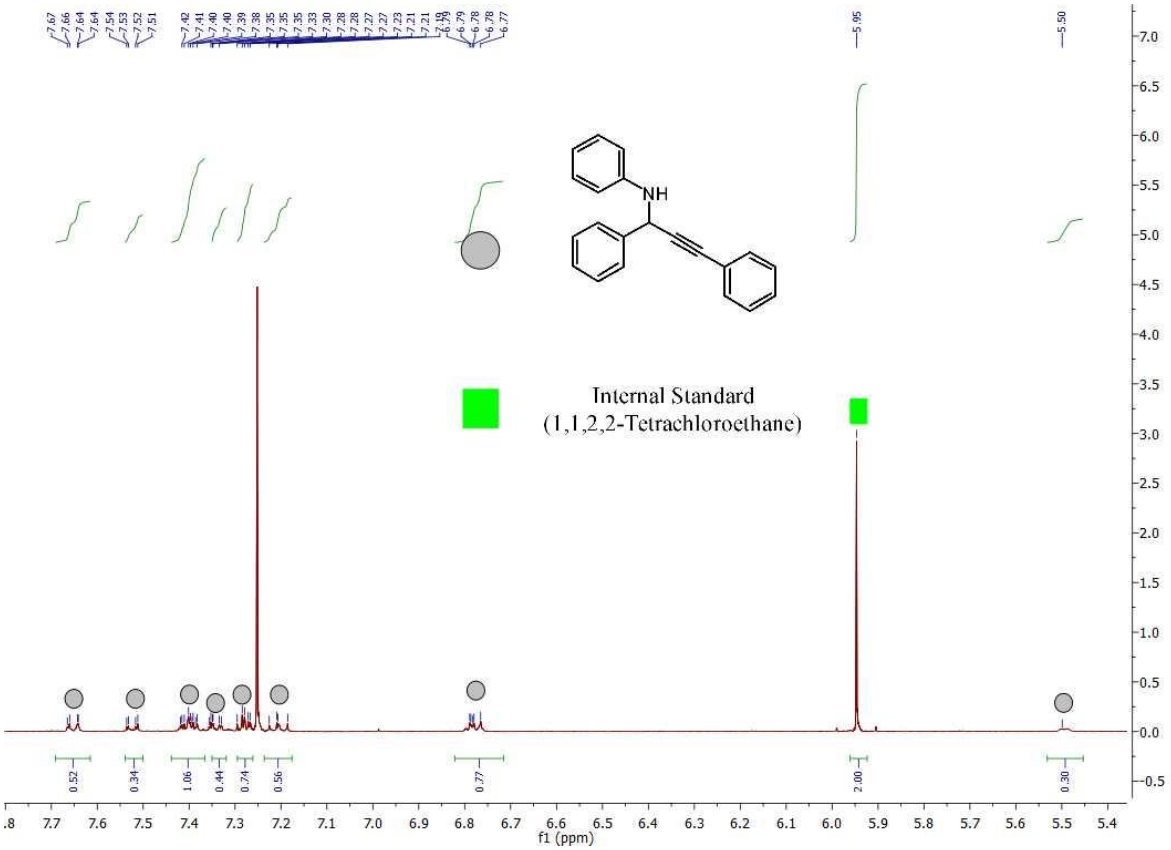

Figure S 48: ^{1}H NMR spectrum for reaction depicted in figure 21.

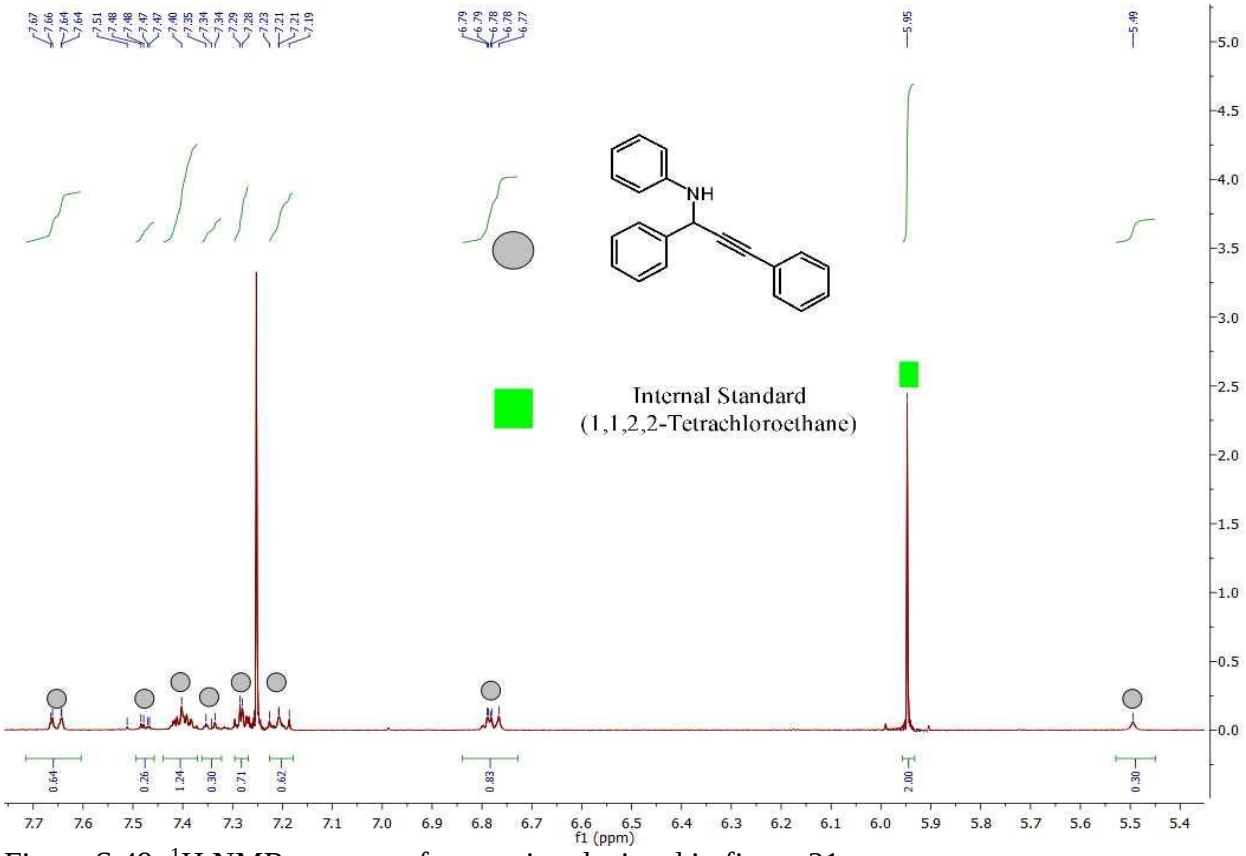

Figure S 49: ^{1}H NMR spectrum for reaction depicted in figure 21.

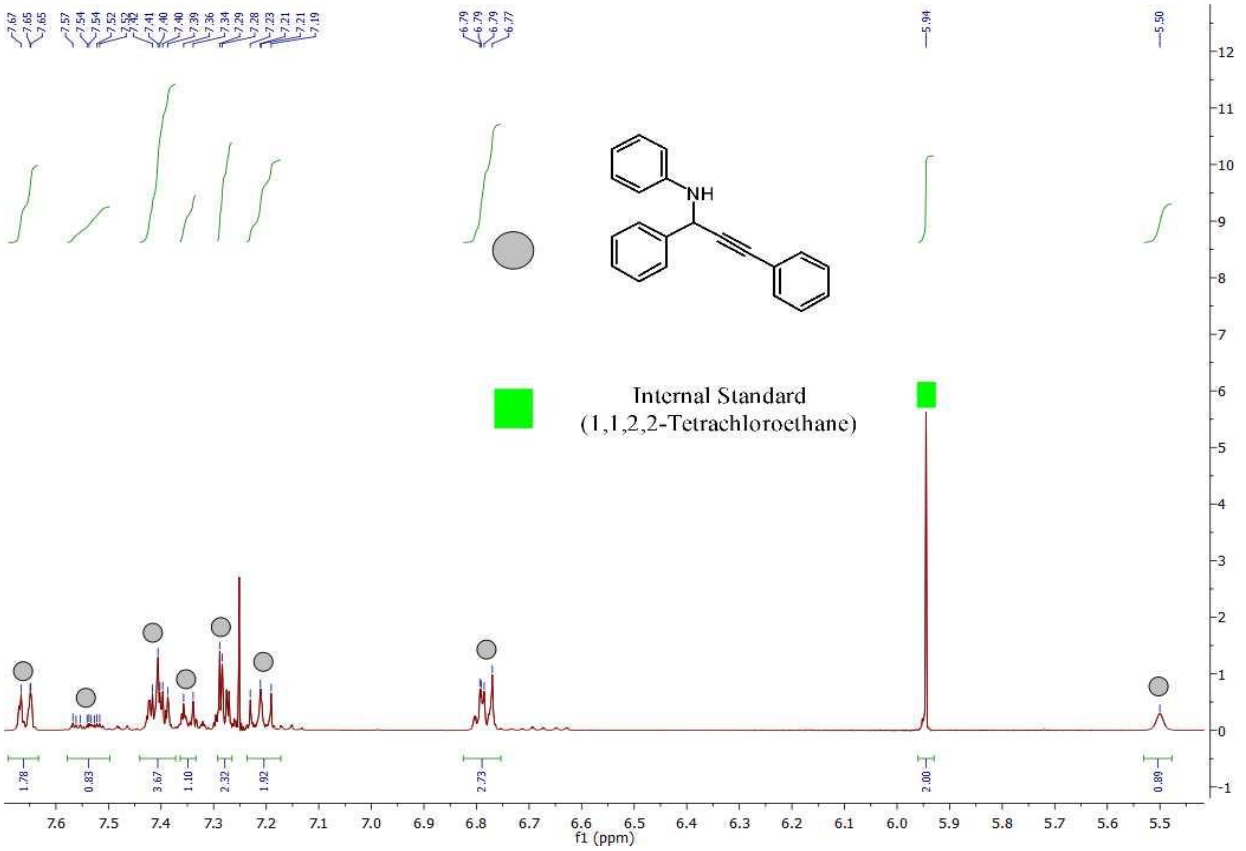

Figure S 50: ^{1}H NMR spectrum for entry 1 in table 6

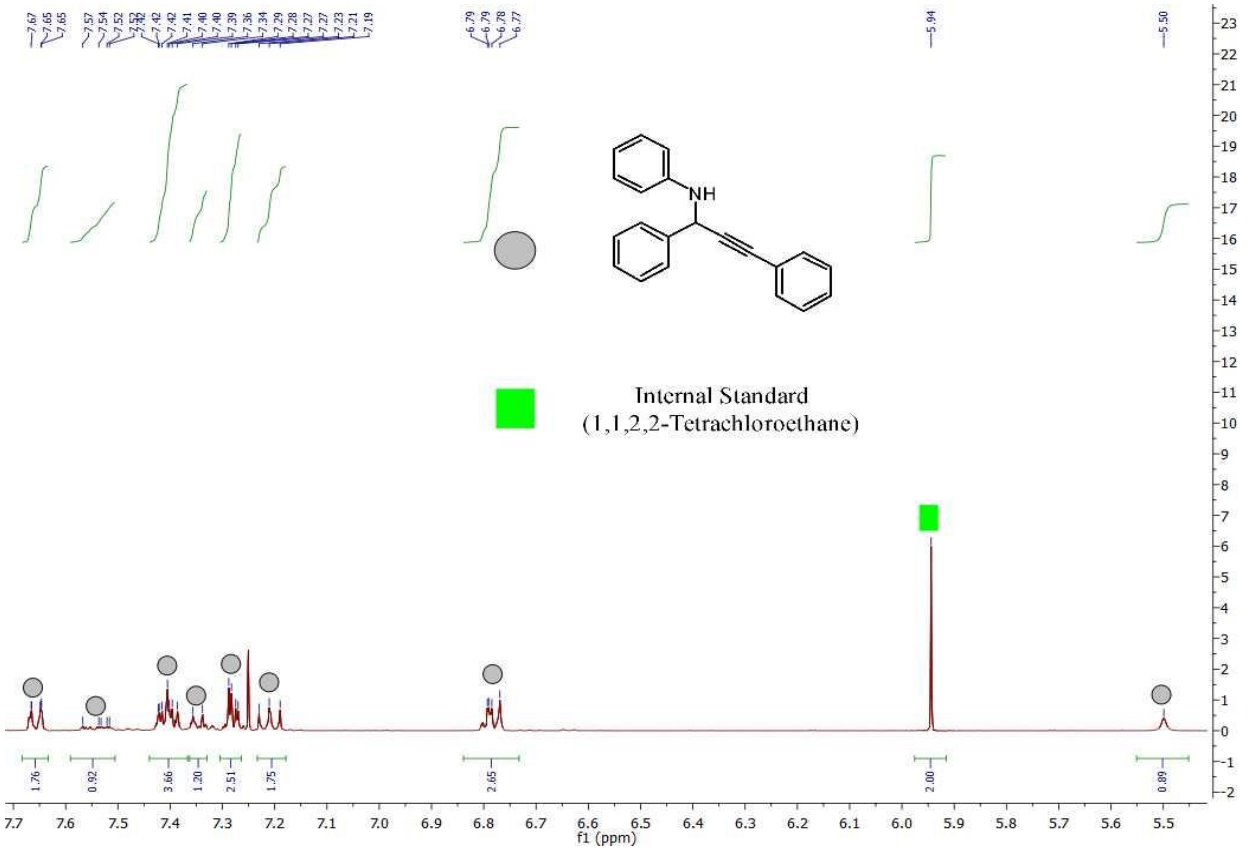

Figure S 51: ^{1}H NMR spectrum for entry 2 in table 6

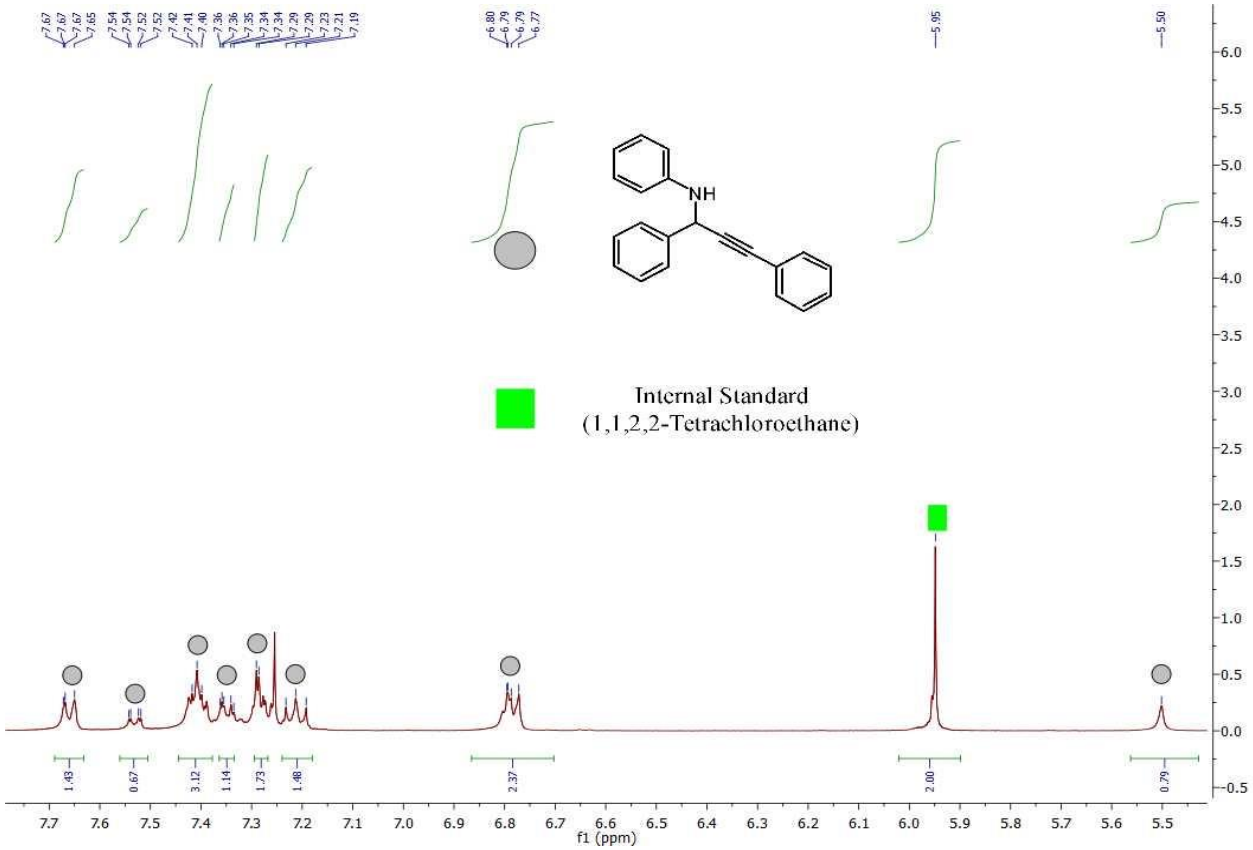

Figure S 52: ^{1}H NMR spectrum for entry 3 in table 6

References

1. Schlögl, R., Heterogeneous Catalysis. *Angewandte Chemie International Edition* **2015,** *54* (11), 3465-3520.
2. Corma, A.; García, H., Lewis Acids: From Conventional Homogeneous to Green Homogeneous and Heterogeneous Catalysis. *Chemical Reviews* **2003,** *103* (11), 4307-4366.
3. Dang, D.; Bai, Y.; He, C.; Wang, J.; Duan, C.; Niu, J., Structural and catalytic performance of a polyoxometalate-based metal-organic framework having a lanthanide nanocage as a secondary building block. *Inorg Chem* **2010,** *49* (4), 1280-2.
4. Jian, W.; Qian, B.; Bao, H.; Li, D., AlCl3 catalyzed oxa-Diels-Alder reaction of aromatic aldehydes with simple dienes. *Tetrahedron* **2017,** *73* (29), 4039-4044.
5. Kobayashi, S.; Sugiura, M.; Kitagawa, H.; Lam, W. W. L., Rare-Earth Metal Triflates in Organic Synthesis. *Chemical Reviews* **2002,** *102* (6), 2227-2302.
6. Cotruvo, J. A., The Chemistry of Lanthanides in Biology: Recent Discoveries, Emerging Principles, and Technological Applications. *ACS Central Science* **2019,** *5* (9), 1496-1506.
7. Procopio, A.; Gaspari, M.; Nardi, M.; Oliverio, M.; Rosati, O., Highly efficient and versatile chemoselective addition of amines to epoxides in water catalyzed by erbium(III) triflate. *Tetrahedron Letters* **2008,** *49* (14), 2289-2293.
8. Breuer, M.; Ditrich, K.; Habicher, T.; Hauer, B.; Kesseler, M.; Stürmer, R.; Zelinski, T., Industrial methods for the production of optically active intermediates. *Angew Chem Int Ed Engl* **2004,** *43* (7), 788-824.
9. Natongchai, W.; Khan, R. A.; Alsalme, A.; Shaikh, R. R., YCl3-Catalyzed Highly Selective Ring Opening of Epoxides by Amines at Room Temperature and under Solvent-Free Conditions. *Catalysts* **2017,** *7* (11), 340.
10. Kawada, A.; Mitamura, S.; Kobayashi, S., Lanthanide trifluoromethanesulfonates as reusable catalysts: catalytic Friedel-Crafts acylation. *Journal of the Chemical Society, Chemical Communications* **1993,** (14), 1157-1158.
11. Wang, M.; Abbineni, G.; Clevenger, A.; Mao, C.; Xu, S., Upconversion nanoparticles: synthesis, surface modification and biological applications. *Nanomedicine: Nanotechnology, Biology and Medicine* **2011,** *7* (6), 710-729.
12. López-Peña, G.; Hamraoui, K.; Horchani-Naifer, K.; Gerke, C.; Ortgies, D. H.; Martín Rodríguez, E.; Chen, G.; Jaque, D.; Rubio Retama, J., Lanthanide doped nanoheaters with reliable and absolute temperature feedback. *Physica B: Condensed Matter* **2022,** *631*, 413652.
13. Wu, X.; Yeow, E. K. L., Ultrathin Near-Infrared Light Activated Nano-Hotplate Catalyst. *Small* **2020,** *16* (40), 2002698.
14. Zhao, X.; Suo, H.; Zhang, Z.; Guo, C., Upconverting CeO2: Yb3+/Tm3+ hollow nanospheres for photo-thermal sterilization and deep-tissue imaging in the first biological window. *Ceramics International* **2019,** *45* (17, Part A), 21910-21916.
15. Haas, K. M.; Lear, B. J., Billion-fold rate enhancement of urethane polymerization via the photothermal effect of plasmonic gold nanoparticles. *Chemical Science* **2015,** *6* (11), 6462-6467.
16. Aitken, R. A.; Kilényi, S. N., *Asymmetric synthesis / edited by R.A. Aitken and S.N. Kilényi*. 1st ed. ed.; Blackie Academic & Professional: London ;, 1992.
17. Blaser, H.-U., Chirality and its implications for the pharmaceutical industry. *Rendiconti Lincei* **2013,** *24* (3), 213-216.

18. Aspinall, H. C.; Greeves, N.; Smith, P. M., Catalytic, asymmetric cyanohydrin synthesis mediated by lanthanide(III) chloride pybox complexes. *Tetrahedron Letters* **1999,** *40* (9), 1763-1766.
19. Jönsson, C.; Lundgren, S.; Haswell, S. J.; Moberg, C., Asymmetric catalysis in a micro reactor—Ce, Yb and Lu catalysed enantioselective addition of trimethylsilyl cyanide to benzaldehyde. *Tetrahedron* **2004,** *60* (46), 10515-10520.
20. Zeng, T.; Yang, L.; Hudson, R.; Song, G.; Moores, A. R.; Li, C.-J., Fe3O4 Nanoparticle-Supported Copper(I) Pybox Catalyst: Magnetically Recoverable Catalyst for Enantioselective Direct-Addition of Terminal Alkynes to Imines. *Organic Letters* **2011,** *13* (3), 442-445.
21. Liu, J.-N.; Bu, W.-B.; Shi, J.-L., Silica Coated Upconversion Nanoparticles: A Versatile Platform for the Development of Efficient Theranostics. *Accounts of Chemical Research* **2015,** *48* (7), 1797-1805.
22. Paściak, A.; Misiak, M.; Trejgis, K.; Elżbieciak-Piecka, K.; Bezkrovnyi, O.; Marciniak, Ł.; Bednarkiewicz, A., Highly-doped lanthanide nanomaterials for efficient photothermal conversion – selection of the most promising ions and matrices. *Journal of Alloys and Compounds* **2023,** *934*, 167900.
23. Wu, X.; Yeow, E. K. L., Exploiting the upconversion luminescence, Lewis acid catalytic and photothermal properties of lanthanide-based nanomaterials for chemical and polymerization reactions. *Physical Chemistry Chemical Physics* **2022,** *24* (19), 11455-11470.
24. Aspinall, H. C.; Dwyer, J. L. M.; Greeves, N.; Smith, P. M., Lanthanide complexes with C2 symmetric ligands for use in enantioselective organic synthesis. *Journal of Alloys and Compounds* **2000,** *303-304*, 173-177.